

Technische Universität München

Max-Planck-Institut für Biochemie

Development of new approaches for kinase-centric proteomics

Felix Sebastian Oppermann

Vollständiger Abdruck der von der Fakultät für Chemie der Technischen Universität München zur Erlangung des akademischen Grades eines Doktors der Naturwissenschaften genehmigten Dissertation.

Vorsitzender:

Univ.-Prof. Dr. Michael Groll

Prüfer der Dissertation:

1. Priv.-Doz. Dr. Henrik Daub

2. Univ.-Prof. Dr. Johannes Buchner

Die Dissertation wurde am 23.08.2010 bei der Technischen Universität München eingereicht und durch die Fakultät für Chemie am 01.12.2010 angenommen.

for my parents

Content

I.	Introduction	1
1.1	Protein kinases in health and disease.....	1
1.1.1	Protein kinases and phosphorylation-based signaling.....	1
1.1.2	Control of substrate specificity	2
1.1.3	Protein kinases and human cancer	3
1.1.4	Inhibiting protein kinase activity.....	4
1.2	Chronic myeloid leukemia and Bcr-Abl	5
1.2.1	Chronic myeloid leukemia	5
1.2.2	Protein domains of Bcr-Abl and leukemogenic signaling	7
1.2.3	Therapeutic strategies for treating chronic myeloid leukemia	9
1.2.4	Imatinib and resistance formation	10
1.3	Polo-like kinase 1, a mitotic Serine/Threonine kinase	12
1.3.1	Structural properties and activity control of Polo-like kinase 1	12
1.3.2	Mitotic functions of Polo-like kinase 1	13
1.3.3	Polo like kinase 1 and human cancer	16
1.4	Mass spectrometry-based proteomics	17
1.4.1	Mass spectrometry applied to protein research	17
1.4.2	Quantitative proteomics	19
1.4.3	Phosphoproteomics	21
1.5	Characterizing protein kinase inhibitors and kinase signaling.....	22
1.5.1	Chemical proteomics	22
1.5.2	Chemical genetics	24
II.	Aims of the thesis	26
III.	Materials and Methods	28
3.1	Material sources	28
3.1.1	Laboratory chemicals and biochemicals	28
3.1.2	Chemicals for SILAC and MS-analysis	28
3.1.3	Other materials	29
3.2	Cell culture Media.....	29

3.3 Stock solutions and commonly used buffers	29
3.4 Cells.....	30
3.5 Antibodies	31
3.5.1 Primary antibodies.....	31
3.5.2 Secondary antibodies.....	31
3.6 Cell culture	32
3.7 Protein analytical methods	32
3.7.1 Determination of protein concentration in cell lysates.....	32
3.7.2 SDS-polyacrylamide-gel electrophoresis (SDS-PAGE)	32
3.7.3 Transfer of proteins onto nitrocellulose membranes	32
3.7.4 Immunoblot detection	32
3.8 SILAC labeling, cell lysis and anti-pTyr immunoprecipitation	33
3.8.1 Cell culture in SILAC medium	33
3.8.2 Cell lysis with Triton X-100	34
3.8.3 Cell lysis with NP-40 and anti-pTyr immunoprecipitation	34
3.8.4 Cell lysis with 8M Urea	35
3.9 Generation of kinase inhibitor resins and kinase-affinity enrichment	35
3.9.1 Study for the quantitative comparison of kinase inhibitor resins.....	35
3.9.2 Study for the quantitative comparison of relative kinase expression levels	36
3.9.3 Study for the qualitative comparison of phospho-kinomes.....	36
3.9.4 Study for the identification of cellular imatinib targets and imatinib-sensitive phosphorylation sites.....	36
3.10 Mass spectrometry sample preparation	37
3.10.1 In-solution protein digest	37
3.10.2 In-gel protein digest	38
3.10.3 Titanium dioxide microsphere-based enrichment of phosphopeptides....	38
3.10.4 Immobilized metal affinity chromatography for phosphopeptide enrichment.....	39
3.10.5 Strong cation exchange chromatography for phosphopeptide separation (ResourceS column)	39

3.10.5 Strong cation exchange chromatography for phosphopeptide separation (polySULFOETHYL A column)	39
3.10.6 Sample processing for the comparison of inhibitor-resins, kinase expression levels and the phospho-kinome analysis	40
3.10.7 Sample processing for the identification of imatinib targets and imatinib-sensitive phosphorylation events.....	40
3.10.8 Sample processing for the cellular substrate identification for Polo-like-kinase 1	40
3.11 MS analysis and data processing.....	41
3.11.1 MS analysis on the LTQ-Orbitrap.....	41
3.11.2 Peptide identification, quantification and data analysis (MSQuant).....	41
3.11.3 Peptide identification and quantification (MaxQuant).....	43
3.11.4 Determine Ratio similarity coefficient curves (RSC)	43
3.11.5 Gene ontology analysis	44
3.11.6 Phosphorylation site overlap between technical and biological replicates.	44
IV. Results.....	45
4.1 Large-scale Proteomics Analysis of the Human Kinome.....	46
4.1.1 Comparative profiling for kinase-selective pre-fractionation reagents.....	46
4.1.2 Comparative Kinase Expression Analysis in Different Cancer Cell Lines	54
4.1.3 Benchmark analysis of the PTM scoring algorithm.....	59
4.1.4 Kinase-centric phosphoproteomics analysis of cancer cell lines	61
4.2 Identification of cellular imatinib targets and imatinib-sensitive phosphorylation sites.....	69
4.2.1 Multicolumn-based protein kinase affinity chromatography	69
4.2.2 Parallel, batch-wise processing for protein kinase enrichment	73
4.2.3 Analysis of the phosphotyrosine-containing sub-proteome upon imatinib treatment.....	80
4.3 Identification of Plk1 cellular substrates	84
4.3.1 Implementation of an efficient phosphopeptide enrichment strategy	84
4.3.2 New strategy for the identification of cellular substrates of Plk1	86

4.3.3 Characterization of the identified cellular substrates of Plk1	91
V. Discussion	94
5.1. Large-scale proteomics analysis of the human kinome	94
5.1.1 Pyrido[2,3-d]pyrimidin-based affinity resins are efficient protein kinase pre-fractionation tools	94
5.1.2 Comparative analysis of kinase expression in three cancer cell lines	96
5.1.3 Benchmark analysis for the precision in automated phosphorylation site localization	97
5.1.4 In-depth survey of kinase phosphorylations	98
5.2 Identification of cellular kinase inhibitor targets and interconnected mediators of downstream signaling cascades	99
5.2.1 Identification of direct kinase inhibitor targets without prior compound immobilization	99
5.2.2 Identification of mediators in Bcr-Abl signaling cascades	102
5.3 New strategy for the analysis of cellular kinase-substrate relationships	106
5.3.1 Establishment of an optimized phosphoproteomics workflow	106
5.3.2 Identification of cellular substrates of Plk1	107
VI. Summary	111
VII. Literature	112
VIII. Appendix	126

I. Introduction

1.1 Protein kinases in health and disease

Every cell of a multi-cellular organism interacts with its environment. This requires highly complex molecular networks for the appropriate regulation of both inter- and intracellular signaling. In case of humans the underlying machinery needs to be exceedingly sophisticated as an estimated total number of 100 trillion cells have to act coordinately to ensure homeostasis of the whole organism. An important mechanism in cellular signal transduction is based on the binding of external ligands to cellular receptors. This triggers a response at their cytoplasmic site which typically initiates various cellular signaling cascades. By employing a multitude of different effector proteins these signal transduction pathways modify protein functions to induce major cellular changes such as altered gene expression patterns. The highly conserved code of eukaryotic signal transduction pathways is based on post-translational modifications (PTM) of proteins. The most common and intensely studied PTM is the reversible protein phosphorylation on serine, threonine and tyrosine residues catalyzed by members of the human protein kinase superfamily of enzymes.

1.1.1 Protein kinases and phosphorylation-based signaling

The first example of phosphorylation-dependent activity control of proteins was described for glycogen phosphorylase in 1955¹⁻². Thereafter, the term kinase was coined for proteins that transfer a phosphate group to an amino acid residue of a substrate protein. In 1979, the group of Tony Hunter discovered that, in addition to serine and threonine, protein phosphorylation also occurred on tyrosine residues³. Furthermore, seminal studies with tumor viruses revealed the existence of specific protein tyrosine kinases, in particular the Src

protein from rous sarcoma virus (RSV)⁴ and the Abl protein from Abelson leukemia virus⁵. In addition, it was demonstrated that the human epidermal growth factor receptor (EGFR) is homologous to the protein encoded by the v-Erb-B oncogene from avian erythroblastosis virus⁶.

Today it is firmly established that reversible protein phosphorylation represents the most common type of PTM in eukaryotic organisms and is evolutionary conserved from yeast to man⁷. The importance for accurate regulation of cellular signaling cascades is underscored by the fact that about two percent of the human genome encode for protein kinases⁸. Therefore, protein kinases present one of the largest protein families. Moreover, it is estimated that about one third of all cellular proteins are modified through reversible protein phosphorylation⁹. The human genome project revealed the existence of a total of 518 distinct PKs⁸. These are classified into two major groups consisting of about 400 serine/threonine and 90 tyrosine directed kinases which can further be subdivided into families and subfamilies based on sequence similarities, and the other constituted by atypical protein kinases⁸.

1.1.2 Control of substrate specificity

As there is an estimated number of about 700.000 potential phosphorylation sites per cell multiple mechanism have evolved that endow PKs with high substrate specificity¹⁰. The majority of PKs possess a conserved catalytic kinase domain that consists of an N-terminal lobe, which is rich in β -sheet structures, and a larger C-terminal lobe comprising mainly α -helices. ATP is coordinately bound in the cleft between these two main lobes. Conserved residues in the phosphate binding loop (P-loop) of the C-terminal lobe ensure the correct spatial orientation as a premise for the transfer of the γ -phosphate group from an ATP molecule to a substrate protein¹¹. In general, specificity is determined by the amino acid composition and size of the substrate binding site, which is generally more spacious in case of tyrosine directed PKs compared to serine/threonine kinases. Moreover, PK activity can be controlled through phosphorylation events in the centrally located activation segment¹².

The particular modification state of a protein can not only modify its function but in addition also recruit other proteins. Thus, substrate specificity can also be controlled by binding of a

respective PK, or an associated protein, to substrate proteins through specific binding motifs¹³⁻¹⁴. To decode the state of modification, specialized modular protein interaction domains that function in localization and assembly of multiprotein complexes have evolved. The most common protein domains that recognize phosphorylated tyrosine residues are the Src-homology 2 domain (SH2) and the phosphotyrosine binding domain (PTB). In case of the growth factor receptor-bound protein 2 (Grb2) and SH2 domain-containing transforming protein (SHC) these domains mediate binding to the epidermal growth factor receptor (EGFR) at phosphorylated tyrosine residues of its cytoplasmic region. Phosphorylation-dependent interactions can also be mediated by phosphoserine/threonine-binding domains such as 14-3-3 domains, WD40-repeat domain (WD40) and the polo-box domain (PBD)¹³. Besides proteins also other entities such as sugars and lipids are modified by specific phosphorylation. In case of lipids phosphoinositides represent common docking sites for other signaling proteins or act as second messengers, respectively. The pleckstrin homology domain (PH) typically interacts with phosphoinositides, thereby recruiting proteins to the cell membrane and bringing them into proximity to transmembrane proteins such as receptor tyrosine kinases (RTKs). Aside from protein phosphorylation a diverse set of additional PTMs fulfils important regulatory functions in signal transmission, e.g. the methylation of arginine (Arg), the acetylation, methylation, ubiquitylation or sumoylation of lysine (Lys) and hydroxylation of proline (Pro) residues among others¹⁵. Taken together, substrate specificity is determined not only by the amino acid sequence of the catalytic groove of the PK and its cognate substrate peptide but instead occurs on multiple levels in a concerted manner. In addition, alterations in the expression level, e.g. in a cell cycle dependent manner, and protein interaction domains influencing the local PK-substrate ratio create mechanisms for space- and time-dependent regulation.

1.1.3 Protein kinases and human cancer

Deregulated tyrosine phosphorylation in the context of cancer was first postulated in 1976 by the later Nobel laureates Bishop and Varmus who discovered the transforming capacity of the Rous sarcoma virus (RSV)¹⁶. Since then numerous PKs including the EGFR and Abl

have been proven to be such homologs of viral oncogenes⁵⁻⁶. Notably, in many cancers of epithelial origin like breast and lung cancers, members of the EGFR family show aberrant activity¹⁷.

Nearly all cellular processes like metabolism, cell growth, differentiation, cell cycle control and apoptosis are regulated by phosphorylation-based signal transmission. In particular, aberrant protein kinase expression or constitutive kinase activity, often due to gene amplification or mutational changes, are involved in pathological processes leading to cellular transformation and tumor development¹⁸⁻¹⁹, immunodeficiencies²⁰, diabetes²¹ and cardiovascular diseases. Besides, genetic rearrangements resulting in the expression of fusion proteins with significantly altered activity, as it is the case for the Bcr-Abl oncoprotein²², account for a significant subset of known oncogenes.

Today it is known that the human genome encodes at least 350 proto-oncogenes among which protein kinases are particularly prominent²³. Therefore, PKs have emerged as a major class of drug targets for therapeutic intervention and after G-protein coupled receptors, represent the most pursued target class in current drug development²⁴⁻²⁶.

1.1.4 Inhibiting protein kinase activity

Groundbreaking discoveries by Paul Ehrlich and his coworkers at the beginning of the 20th century established the concept of targeted therapeutic intervention. Ehrlich postulated his 'magic bullet' concept to fight human diseases through the targeted elimination of a 'pathogen' with chemical drugs which should be without adverse effects in healthy body cells²⁴. Today's strategies for the targeted inhibition of PKs with chemical compounds are based on the identification of naturally occurring small molecules that interfere with PK activity. In 1977, a screen for microbial alkaloids resulted in the identification and purification of the indolocarbazole staurosporine from *Streptomyces staurosporeus*. Staurosporine was shown to inhibit multiple PKs, including protein kinase C (PKC), at nanomolar concentrations²⁷⁻²⁸. The first described evidence for a natural product affecting the tyrosine kinase activity of PKs was described in 1983 for the bioflavonoid quercetin, which was shown to inhibit the phosphorylation activity of v-Src²⁹. In 1984, Hiroyoshi Hidaka demonstrated the feasibility of synthesizing specific inhibitors for serine kinases that

were ATP-competitive and, most importantly, also cell-permeable³⁰. This paved the way for further studies towards the rational design of small molecule inhibitors. Tyrphostins, the first class of designed protein tyrosine kinase inhibitors, interfered with the EGFR. Importantly, these compounds exhibited a anti-proliferative potential as initially demonstrated in A431 cells³¹.

Today, antibodies and small molecule-based approaches represent the major therapeutic strategies targeting disease-relevant PKs. For the rational development of such PK-directed drugs comprehensive insights into the mechanisms of PK-mediated cellular signaling is of outstanding importance.

1.2 Chronic myeloid leukemia and Bcr-Abl

1.2.1 Chronic myeloid leukemia

In 1845, two reports showed that hypertrophy of the spleen and liver is associated with leukocytosis³²⁻³³. Later this chronic hyperproliferative disease of hematopoietic progenitor cells was termed chronic myeloid leukemia (CML). The course of CML can be subdivided into three distinct stages, namely a chronic, an accelerated and a blast phase, which is also known as blast crisis. The progression from a single hematopoietic stem cell expressing the *BCR-ABL* fusion gene, which initiates the chronic phase of CML, to the blast phase, is depicted in Figure 1.

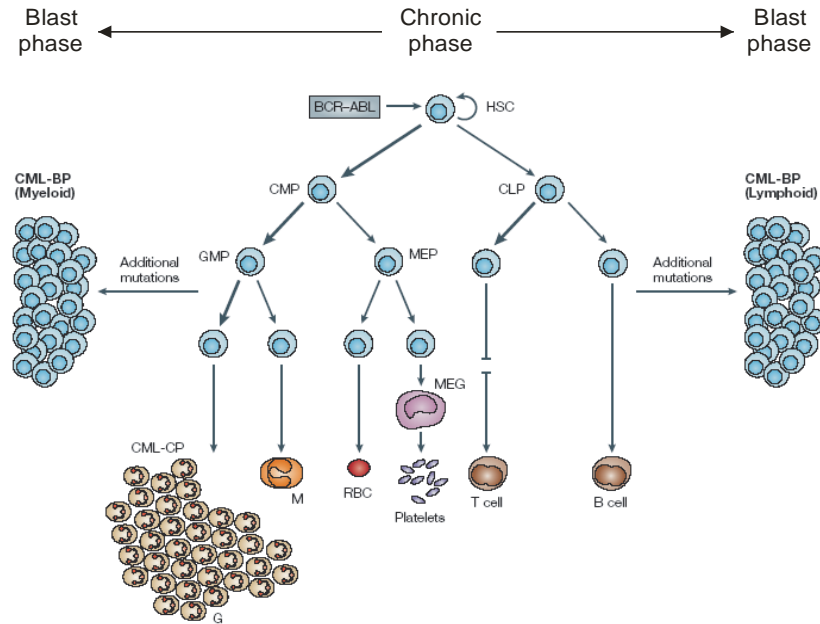


Figure 1: Development of chronic myeloid leukemia. CML is defined by three different stages of disease progression, the chronic, accelerated (not depicted) and blast phase. Initiated by the occurrence of the *BCR-ABL* fusion gene, hematopoietic stem cells (HSC) over time lose their differentiation potential into common myeloid- and lymphoid progenitor cells (CMP and CLP). The chronic phase of CML is characterized by an excessive production of mature granulocytes (CML-CP). At this stage progenitor cells remain capable of differentiating into granulocyte/macrophage progenitors (GMP) and megacaryocyte/erythrocyte progenitors (MEP), the progenitors of granulocytes (G) and macrophages (M) as well as red blood cells (RBC) and platelets, respectively. The later blast phase is denoted after the accumulation of undifferentiated, immature hematopoietic cells. Adapted from Ruibao Ren, Nature Reviews Cancer, 2005.

Most patients are diagnosed during the initial chronic phase when they show symptoms such as an enlarged spleen, fatigue and weight loss as well as an increased white blood cell (WBC) count of about $150 \times 10^9/L$ containing $< 2\%$ immature, undifferentiated cells, called blasts. At that stage the bulk of the hematopoietic stem cells (HSC) are still capable of differentiating into mature granulocytes. The advanced stages of CML are characterized by increased numbers of undifferentiated and non-functional granulocytes. Disease progression is driven by the accumulation of mutations in various genes including TP53, retinoblastoma 1, $p16^{\text{INK4A}}$ or aberrant expression of oncogenes like *MYC*³⁴. Blasts counts between 10-19% of all WBCs associated with thrombocytopenia define the accelerated phase. During the fatal blast phase the blast count exceeds 20% and, in addition to thrombocytopenia, anemia

occurs. About two thirds of all patients develop blasts of myeloid origin, the other one-third from lymphoid origin.

Important insights into the underlying molecular mechanism were obtained in 1960 by Nowell and Hungerford who detected distinct chromosomal abnormalities when performing karyotyping experiments with blood cells derived from CML patients³⁵. Later, this was termed Philadelphia (Ph) chromosome and its abnormality was demonstrated to result from a reciprocal translocation involving chromosome 9 and 22³⁶. This translocation generates the *BCR-ABL* fusion gene consisting of the 3' sequence of the *ABL* gene on chromosome 9 juxtaposed to the 5' sequence of the breakpoint cluster region (*BCR*) gene on a shortened chromosome 22. Due to varying breakpoints in the *ABL* gene at 9q34 and three distinct breakpoint cluster regions within the *BCR* gene, different variants of the *BCR-ABL* fusion gene can occur. The majority of all CML patients express the chimeric 210 kDa protein (p210 BCR-ABL, named Bcr-Abl in the following)³⁷. In contrast, p190 BCR-ABL is associated with acute lymphoblastic leukemia (ALL)³⁸ and p230 BCR-ABL with neutrophilic-chronic myeloid leukemia (CML-N)³⁹.

The majority of cancers arise through the stepwise accumulation of genetic alterations⁴⁰, whereas the chronic phase of CML is believed to originate solely from the expression of the Bcr-Abl fusion protein in a pluripotent hematopoietic stem cell⁴¹. Besides the homology to the viral oncogene v-Abl suggesting its oncogenic potential the transforming capacity of Bcr-Abl was demonstrated *in vitro*⁴². Furthermore, the retroviral transduction of bone-marrow cells with the Bcr-Abl fusion protein caused a myeloproliferative disease in mice resembling the chronic stage of human CML⁴³.

1.2.2 Protein domains of Bcr-Abl and leukemogenic signaling

The mechanism of malignant transformation induced by Bcr-Abl is based on altered adhesion, constitutive mitogenic signaling and an reduced apoptosis rate⁴⁴. Due to structural features of Bcr-Abl distinct from the c-Abl protein, the Abl kinase domain in Bcr-Abl is constitutively active⁴⁵⁻⁴⁶. In further contrast to c-Abl, which shuttles between the nucleus and cytoplasm, Bcr-Abl is mainly localized in the cytoplasm. In addition, there are many other protein domains involved in modulating its kinase activity and linking Bcr-Abl to

downstream signaling pathways (Figure 2). Together, altered cellular localization, deregulated kinase activity and recruitment of an entire molecular machinery results into abnormal substrate phosphorylations that transduce the disease-promoting signals from Bcr-Abl.

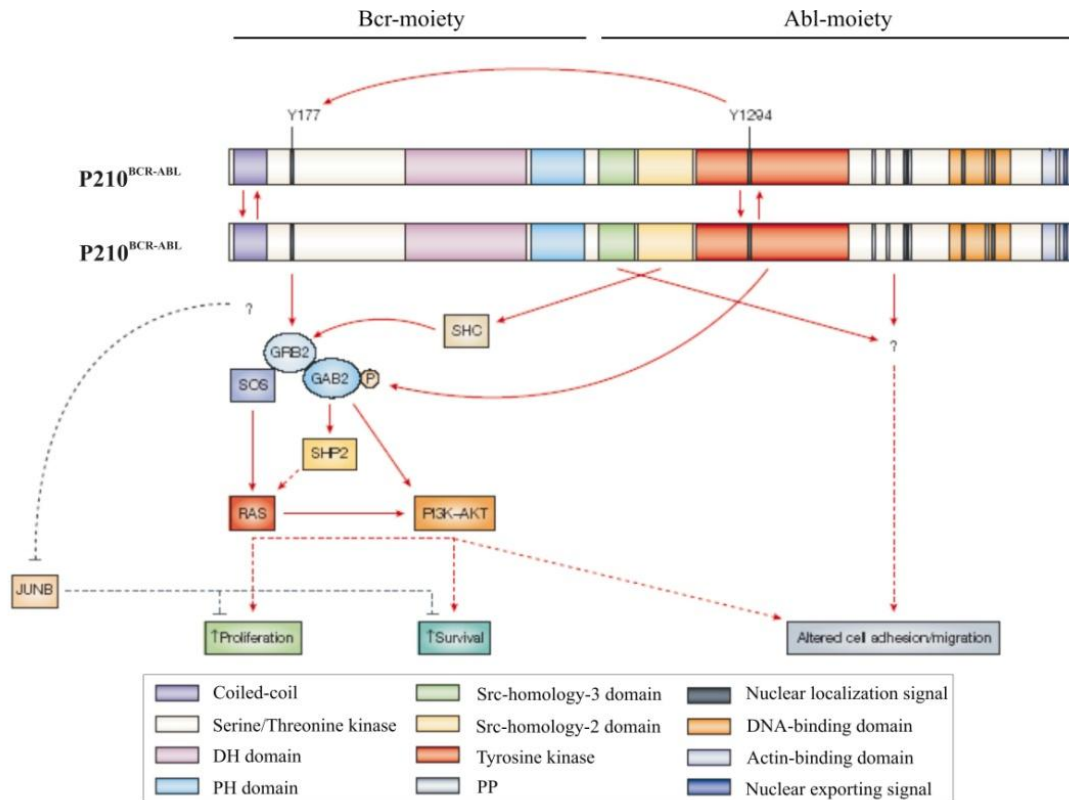


Figure 2: Protein domain organization and signaling of the Bcr-Abl fusion protein. In the Bcr-Abl fusion protein (p210BCR-ABL) the coiled-coil domain in the Bcr moiety enables the formation of dimers or tetramers facilitating trans-phosphorylation. The growth factor receptor-bound protein 2 (Grb2) binds phosphorylated tyrosine-177 through its SH2 domain. Grb2-associated proteins like son of sevenless (SOS) and Grb2-associated binding protein 2 (GAB2) are bound via the SH3 domain of Grb2. Grb2 can also be recruited by the Src homology and collagen (SHC) protein upon phosphorylation that is bound by the SH2 domain of Abl. In addition, the Abl SH3 domain can regulate cell adhesion and migration by mediating the interaction with different proteins. Proliferation and survival are promoted by Bcr-Abl through the activation of Ras- and PI3K/Akt-mediated signaling. Furthermore, junB, which inhibits proliferation and survival by counteracting the Ras target c-jun, is negatively regulated. Activation and/or direct interactions are indicated by red arrows, negative regulation by black arrows. Dashed lines indicate a multistep process. DH, Dbl/CDC24 guanine-nucleotide exchange factor homology; PP, proline-rich SH3 binding site. Adapted from Ruibao Ren, Nature Reviews Cancer, 2005.

Oligomerization of Bcr-Abl is mediated through the coiled-coil motif in the Bcr moiety and facilitates several auto- and/or trans-phosphorylation events⁴⁷⁻⁴⁸. These include the activation-loop phosphorylation of Tyr-1294 (corresponding to Tyr-412 in c-Abl) and Tyr-1127 (Tyr-245 in c-Abl) leading to increased catalytic activity⁴⁹. In addition, phosphorylation of Tyr177 in the Bcr-portion of the protein creates a binding site for the SH2 domain of the growth factor receptor bound protein 2 (Grb2)⁵⁰. Grb2 in turn acts as a docking protein for the son-of-sevenless (Sos) protein and Grb2-associated binding protein 2 (GAB2). Recruitment of the Sos protein, a guanine nucleotide exchange factor (GEF) that activates Ras, links Bcr-Abl to Ras-mediated signaling⁵¹. Ras signaling can further be activated by the adaptor molecules CrkL and Shc, which are also known substrates of Bcr-Abl⁵²⁻⁵³. Furthermore, Gab2 recruits the SH2 domain containing protein phosphatase (SHP2) that, besides activating Ras, was shown to activate phosphatidylinositol 3-kinase (PI3K)⁵⁴. The PI3K downstream effector Akt elicits anti-apoptotic signaling⁵⁵.

Over the past years, the list of reported cellular targets has kept growing with detection methods switching more and more to large-scale phosphoproteomics analyses⁵⁶⁻⁵⁷. Yet, for a comprehensive understanding of the cellular signaling cascades involved in Bcr-Abl mediated signaling, it is essential to identify all its substrates and gain further insights in associated downstream signaling events.

1.2.3 Therapeutic strategies for treating chronic myeloid leukemia

A therapeutic strategy to treat CML in the chronic phase is based on immune therapy using interferon alpha, often in combination with cytarabine, a chemotherapeutic agent. This can restore the WBC count to normal levels in up to 70 % of the patients but is often associated with adverse side effects⁵⁸.

The transforming capacity of Bcr-Abl is directly associated with its tyrosine kinase activity²². Consequently, this provided a rationale for direct inhibition of Bcr-Abl as a therapeutic strategy. The first compounds tested were natural products, isolated from fungal extracts, like the flavoid quercetin⁵⁹ and the isoflavonoid genistein⁶⁰. Notably, the set of 'tyrphostins' originally developed against the EGFR also contained molecules that selectively inhibited Bcr-Abl over c-Abl⁶¹⁻⁶².

Therefore, pharmaceutical kinase inhibitor screening programs were initiated and researchers at CIBA-Geigy (today part of Novartis) developed a series of molecules based on 2-phenylamidopyrimidines that included compound CGP57148, now typically referred to as STI571 or imatinib, which inhibited v-Abl, PDGFR, c-Kit and ARG⁶³⁻⁶⁵. Pre-clinical benefit was demonstrated by the ability of imatinib to inhibit the growth of Bcr-Abl positive cells as well as Bcr-Abl-induced tumors in mice⁶⁶⁻⁶⁷. These results were translated into clinical trials⁶⁸⁻⁶⁹ that eventually resulted into the FDA approval of imatinib for the treatment of chronic phase CML in May 2001.

2.4 Imatinib and resistance formation

In most malignant diseases the emergence of drug resistances is based on similar mechanisms. These include the expression of a drug-insensitive variant of the targeted protein, up-regulation of the target protein, the activation of alternate pathways, or increased drug-efflux through transporter proteins⁷⁰. Despite the remarkable initial response rates for imatinib prolonged treatment often results in the emergence of resistance⁷¹.

In the particular case of imatinib treatment of CML patients, which is remarkably efficient in the initial, chronic phase⁷², drug resistance in later disease stages is primarily caused by acquired mutations in the *BCR-ABL* gene^{71, 73}. Among those, frequently detected mutations are amino acid substitutions such as Tyr253His/Phe, Glu255Lys, the 'gatekeeper' residue substitution Thr315Ile and Met351Thr⁷⁴. Importantly, the Thr315Ile mutation sterically hinders access of imatinib to the hydrophobic pocket adjacent to the ATP-binding pocket which is crucial for imatinib binding, whereas binding of ATP and the catalytic activity of Bcr-Abl are not abrogated. Crystal structure analysis revealed a binding mechanism in which imatinib targets the ATP-binding pocket of catalytic inactive Bcr-Abl in the DFG-out confirmation (Figure 3)⁷⁵⁻⁷⁶. These structural analyses helped to understand how additional mutations in the *BCR-ABL* gene, also at sites distant to the ATP-binding pocket, can result in resistance against imatinib treatment.

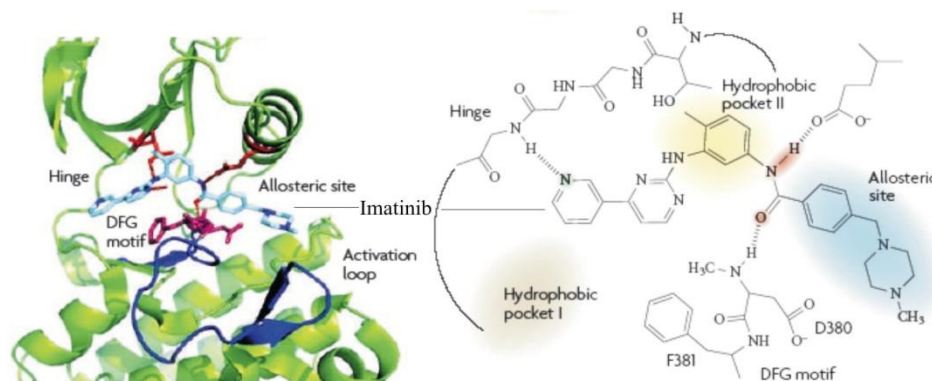


Figure 3: Ribbon- and chemical structure of the Abl-imatinib interaction. Imatinib binds to catalytic inactive Abl in the DFG-out conformation. The DFG motif resides at the start of the kinase activation loop (dark blue). The hinge region, the activation loop of Abl and imatinib (light blue) are indicated in the ribbon structure (left). Atoms of imatinib involved in binding to Abl are indicated in red. In the chemical structure (right), hydrogen bonds between imatinib and Abl are depicted in dashed lines and the hydrophobic regions I and II in shaded beige and yellow. Reproduced from Jianming Zhang, Priscilla L. Yang and Nathanael S. Gray, *Nature Reviews Cancer*, 2009.

Resistance formation by point mutations in the *BCR-ABL* gene gave insights into the molecular escape mechanism and provided evidence for the necessity of continued Bcr-Abl signaling. Notably, this also highlights the general validity of the PK inhibition approach in CML and confirmed Bcr-Abl variants as suitable targets for second-line treatment⁷⁰. Therefore, Bcr-Abl inhibitors that inhibit imatinib-resistant Bcr-Abl variants have been developed. This resulted in the FDA approval of the dual-specificity kinase inhibitor dasatinib (BMS-354825) and the imatinib analog nilotinib (AMN107) in 2006 and 2007 respectively⁷⁷⁻⁷⁸. Nonetheless, these compounds are not capable of inhibiting the Thr351Ile variant, which accounts for about 15 % of all cases of imatinib resistance in patients. However, compounds that demonstrated promising results in imatinib-resistant patients carrying the Thr315Ile mutation, such as MK-0457 (VX-680), have been reported recently⁷⁹⁻⁸⁰. Moreover, combined administration of the allosteric Bcr-Abl inhibitor GNF-2 and ATP-competitive inhibitors have been shown to efficiently inhibit the Thr315Ile Bcr-Abl variant *in vitro* and *in vivo*⁸¹.

However, as shown for dasatinib and nilotinib, resistance formation remains a major obstacle⁸² and appears to be an inevitable consequence of targeted therapeutic approaches. Therefore, an in-depth understanding of cellular signaling downstream of Bcr-Abl and the identification of additional targets could reveal alternative therapeutic strategies that might

eventually overcome cellular drug-escape mechanisms in case of CML and other hyperproliferative diseases.

1.3 Polo-like kinase 1, a mitotic Serine/Threonine kinase

One of the most fundamental cellular processes is mitotic cell division. Only through the precise regulation of this complex process error-free chromosome segregation is ensured and thereby genomic integrity maintained. This is of exceeding importance as genomic alterations are closely associated with disease progression in human cancer. Besides cycline-dependent kinases (Cdk), which are regarded as central regulators of cell proliferation, kinases of the Aurora, never in mitosis gene a (NIMA) as well as the Polo family are pivotally involved in regulating mitotic progression⁸³.

1.3.1 Structural properties and activity control of Polo-like kinase 1

The serine/threonine kinase Plk1 belongs to the family of polo-like kinases consisting of four members (Plk1-4) and is evolutionary conserved from yeast to man⁸⁴⁻⁸⁵. All human Plk family members share a common protein domain architecture (Figure 4). Their structure is divided into an amino-terminal serine/threonine kinase domain, a destruction-box involved in anaphase-promoting-complex (APC)-mediated degradation⁸⁶ and a carboxy-terminal polo-box domain (PBD)⁸⁴. The PBD is a phosphopeptide-binding motif involved in substrate recruitment through its ability to recognize a phosphorylated consensus sequence S-(pS/pT)-(P/X) on cellular Plk target proteins⁸⁷.

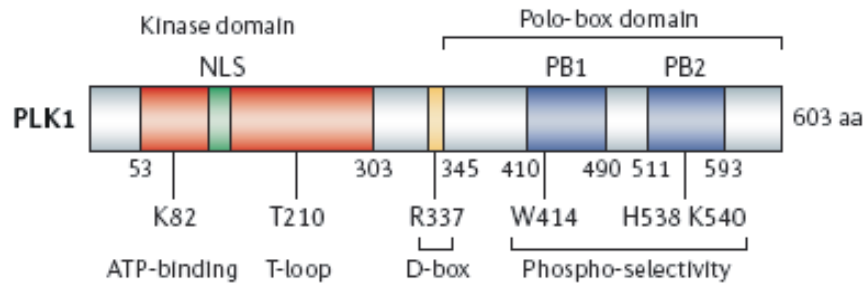


Figure 4: Plk1 protein domains and key residues. Located in the N-terminal kinase domain of Plk1, Lys82 and Thr210 are important residues involved in regulating catalytic activity. The destruction box (D-box) functions in Plk1 degradation. Within the C-terminal polo box (PB) domains Trp414, His538 and Lys540 mediate binding to the Plk1 consensus motif. Reproduced from Klaus Strebhardt and Axel Ullrich, Nature Reviews Cancer, 2006.

As Plk1 is a key regulator of centrosome assembly and mitosis its activity is tightly regulated in a cell cycle-dependent manner. Dynamic changes of protein expression, which peaks at the G2/M transition⁸⁸, as well as an activating phosphorylation of Thr-210 in the kinase domain⁸⁹⁻⁹⁰ carried out by Aurora A kinase in cooperation with bora⁹¹⁻⁹² allow for the spatio-temporal control of Plk1 activity in mitotic cells. In addition to conferring substrate specificity, phosphopeptide binding to the PBD relieves an autoinhibitory interaction of the PBD with the kinase domain which further results in increased catalytic activity⁹³⁻⁹⁴.

1.3.2 Mitotic functions of Polo-like kinase 1

Crucial involvement of Plk1 in establishing a bipolar spindle apparatus was experimentally indicated by antibody microinjections resulting in severe mitotic defects⁹⁵⁻⁹⁶. Based on discoveries revealing the dynamic localization of Plk1 during cell cycle progression to various cellular structures like centrosomes, the central spindle apparatus and the midbody⁹⁷ it was postulated that this behavior might correlate with a multitude of different Plk1 substrates.

The dual specificity phosphatase Cdc25 was the first reported cellular substrate of Plk1 and initially identified in *Xenopus* egg extracts⁹⁸. Later, Plk1-mediated phosphoregulation of Cdc25 was also shown in human cells. Here, increased Cdc25 phosphorylation correlated with increased phosphatase activity⁹⁹. In turn, Cdc25 activates cyclin-dependent kinase 1

(Cdk1) by counteracting Wee1 and Myt1 function through dephosphorylation of the Cdk1 residues Thr14 and Thr15¹⁰⁰. Dephosphorylated Cdk1 in complex with cyclin B1, a further substrate of Plk1¹⁰¹ then fulfils its key functions in mitotic progression. Notably, kinase activities of Wee1 and Myt1 are known to be inhibited by phosphorylation, and both are reported substrates for human Plk1¹⁰²⁻¹⁰³. Together, these examples indicate a tight regulation of the mitotic entry by Plk1 (Figure 5).

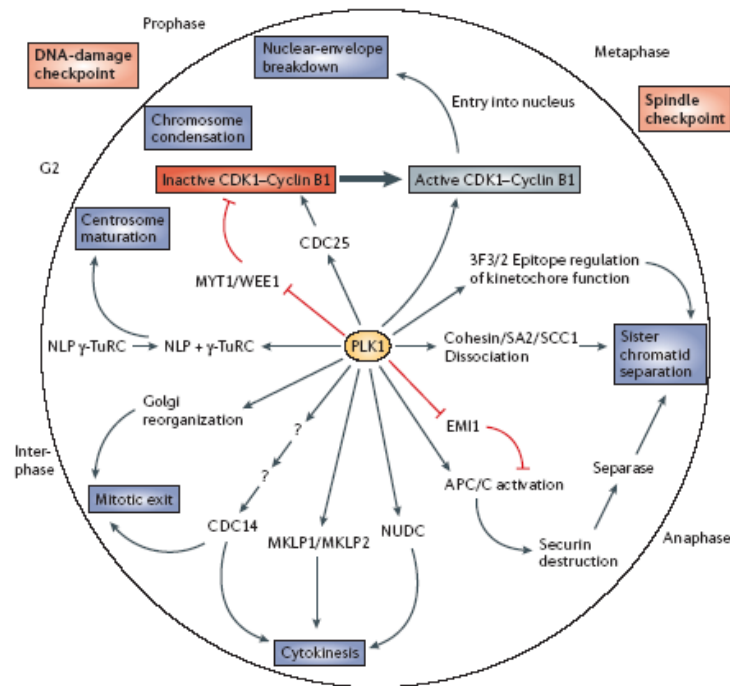


Figure 5: Mitotic functions of Plk1. Plk1 regulates mitotic progression by interacting with a multitude of different proteins. Shown are selected activating (black arrows) and inactivating (red blunt arrow) modifications of target proteins by Plk1. Abbreviations and protein names are described in the main text. Reproduced from Klaus Strebhardt and Axel Ullrich, *Nature Reviews Cancer*, 2006.

A second function of Plk1, the establishment of a functioning spindle apparatus, was discovered in *Drosophila melanogaster* mutants¹⁰⁴. Plk1 recruits the γ -tubulin-containing multiprotein ring complex (γ -TuRC), which is involved in microtubule nucleation, to the centrosome where it participates in the formation of a bipolar mitotic spindle¹⁰⁵. Another protein involved in microtubule organization is ninein-like protein (Nlp) that interacts with the γ -TuRC. Phosphorylation of Nlp by Plk1 at the G2/M-transition abolishes its interaction

with γ -TuRC and leads to its dissociation from the centrosomes, which might enable the recruitment of other γ -TuRC-binding proteins¹⁰⁶⁻¹⁰⁷. Cellular mislocalization of Plk1 has been shown to provoke defects in chromosome congression¹⁰⁸. Moreover, Plk1 is required for proper spindle assembly, microtubule-kinetochore attachment¹⁰⁹, and is also involved in the spindle assembly checkpoint (SAC). The SAC is a crucial surveillance mechanism that ensures the correct attachment of the two kinetochores of each chromosome to opposite spindle poles as a prerequisite of chromosome segregation. Plk1 recruits several proteins involved in the SAC such as BubR1, Cenp-E, Mad2 and Nurf2 by generating the so-called 3F3/2 phosphoepitope on tension-lacking kinetochores¹¹⁰⁻¹¹². Besides other cellular responses this causes the inactivation of the E3-ubiquitin ligase anaphase-promoting complex/cyclosome (APC/C), the main regulator of chromosome segregation¹¹³. Upon satisfaction of the SAC, Plk1 phosphorylates the APC/C inhibitor Emi2 thereby targeting it for degradation¹¹⁴⁻¹¹⁵. Once activated, APC/C ubiquitinates securin and thereby primes it for proteosomal degradation. This leads to the release of separase, which in turn cleaves the multi-protein complex cohesin that interconnects sister chromatids. As a result separation of sister chromatids at the onset of anaphase occurs¹¹⁶. A prerequisite for the dissociation of cohesin is the phosphorylation of its SA2 subunit that was also identified as a Plk1 substrate¹¹⁷. In addition, together with separase, Plk1 is also involved in centriole disengagement and duplication¹¹⁸.

In concordance with its localization at the midbody in late mitosis⁹⁵ Plk1 executes essential functions in cytokinesis. The Plk1-mediated phosphorylation of several proteins has been shown to be required for the initiation of cytokinesis, such as mitotic kinesin-like protein2 (Mklp2)¹¹⁹, nuclear distribution geneC (NudC)¹²⁰ and Nir2¹²¹. Important insights into the requirements for the initiation of cytokinesis came from studies utilizing the ‘chemical genetics’ approach developed by Kevan Shokat’s group¹²². Applied to Plk1, it was demonstrated that inhibition of human Plk1 at anaphase onset, after silencing the SAC, resulted in defective cytokinesis¹²³. This was accompanied by disordered localization of the RhoA GTPase and Ect2, the corresponding guanine nucleotide exchange factor (GEF) required for RhoA activity at the equatorial cortex, which resulted in the absence of cleavage furrow-inducing signals. Recently, it was shown that site-specific phosphorylation of HsCYK-4 by Plk1 creates the essential docking site for recruitment of Ect2¹²⁴.

1.3.3 *Polo like kinase 1 and human cancer*

The importance of accurate cell cycle regulation and surveillance mechanisms is obvious as errors in chromosome segregation will result in chromosomal instability which, in conjunction with other, yet unidentified factors, permits aneuploid cells to propagate¹²⁵. Chromosomal instability acts as a driving force for the eventual onset of oncogenic transformation¹²⁶⁻¹²⁷. Therefore, it is not surprising that deregulated expression levels of Plk1 have been reported in a variety of human cancer including non-small cell lung cancer, gastric carcinoma, melanoma, breast cancer, ovarian cancer, prostate cancer and glioblastoma and are often associated with poor prognosis¹²⁸⁻¹²⁹.

DNA damage checkpoints confer a cellular surveillance mechanism to detect DNA lesions and elicit the activation of repair or, in case of severe DNA damage, apoptotic pathways. Their proper functioning is of major importance to maintain homeostasis and guard against neoplastic transformation. Besides the ataxia-telangiectasia mutated (ATM) and ataxia-telangiectasia and Rad3-related (ATR) kinases, the retinoblastoma (RB) protein and the transcription factor p53 have emerged as key regulators of the DNA damage checkpoints¹³⁰. Increased Plk1 activity can counteract these effects by overriding DNA damage checkpoints¹³¹⁻¹³². Moreover, Plk1-mediated phosphorylation of p53 inhibits its pro-apoptotic function¹³³. Therefore, Plk1 is an attractive anti-cancer target as abrogation of Plk1 function can cause a prolonged mitotic arrest followed by apoptosis. Furthermore, it could be shown that transformed cells are more sensitive towards Plk1 depletion compared to normal cells¹³⁴⁻¹³⁵. Among the different approaches initiated to develop Plk1 inhibitors, promising ATP-competitive small molecules have emerged. Several compounds like BI 2536 or GSK461364 have entered clinical trials and as in case of BI 2536 demonstrated robust Plk1 inhibition and efficacy in xenograft models¹³⁶⁻¹³⁷. A hurdle for these ATP-competitive inhibitors is reasoned in their potential off-target effects towards other essential kinases. As the PBD is unique for Plks, targeting this domain might offer an alternative strategy for the development of Plk family-specific inhibitors. Recently, the first non-peptidic compound, poloxin, which interferes with PBD-mediated protein-protein interactions, has been described and shown to induce mitotic arrest and apoptosis in HeLa cells¹³⁸.

Since the initial discovery of Plk1 various cellular substrates have been identified. In addition, the consensus sequence of Plk1 substrate phosphorylation sites has been

determined¹⁰². However, a comprehensive knowledge of how Plk1 elicits its various mitotic functions through site-specific phosphorylation is needed to gain mechanistic insights into the overall mode of action of therapeutic Plk1 inhibition⁷⁰.

1.4 Mass spectrometry-based proteomics

The ultimate goal of proteomics is to study and analyze the entire proteome that encompasses all expressed proteins in a cell or organism¹³⁹. Mass spectrometry (MS) has tremendously advanced as a technique to study cellular biochemistry on a global scale and recently enabled the sequencing and quantification of an entire eukaryotic proteome as demonstrated for *S. cerevisiae*¹⁴⁰. The basic principle of MS is the measurement of mass/charge ratios (m/z) of ionized analytes. Therefore, a mass spectrometer consists of an ion source, which converts analytes into gas-phase ions, a mass analyzer, which resolves ions according to their m/z ratios, and a detector that measures the resulting ion signal intensities and records them in a mass spectrum.

1.4.1 Mass spectrometry applied to protein research

Compared to more classic techniques like one-dimensional (1D) gel electrophoresis followed by antibody-based immunoblot analysis, MS analysis upon proteolytic cleavage of proteins to peptides offers considerable advantages: First, MS allows for the unbiased analysis of complex protein mixtures of unknown composition derived from any organism characterized on the genome level¹⁴¹. Second, MS offers a way for high-throughput analysis of thousands of proteins in a single experiment. And third, the continued increase in the dynamic detection range, sophisticated separation methods and database search strategies combined with novel algorithms for automated quantification allow for high sensitivity and accuracy as well as the acquisition of trustworthy data. In addition, tandem MS (MS/MS) provides sequence information of analyzed peptide ions supporting unambiguous peptide identification as well as enabling site-specific analysis of PTMs.

Today's most widely used MS approach in protein research is the so called bottom-up or shotgun proteomics where, instead of whole proteins, peptides are analyzed. The analyzer used in all MS experiments reported in this thesis is the hybrid linear ion trap (LTQ)-Orbitrap mass spectrometer¹⁴². The LTQ-Orbitrap combines the high mass accuracy and wide dynamic range of the Orbitrap, a Fourier-transform ion cyclotron (FT-ICR) instrument, with the speed and sensitivity of the linear ion trap. The typical experimental workflow adopted in the experiments of the present study, is depicted in Figure 6. Extracted proteins, derived from a cell line, tissue or body fluid are usually proteolytically digested with trypsin that cleaves C-terminal to arginine and lysine residues¹⁴³. Various methods can be applied to reduce the sample complexity and thereby boost proteome coverage. Three different fractionation techniques were utilized in the present study: First, the separation of whole proteins according to their molecular weights via gel electrophoresis. Second, the immunoprecipitation of tyrosine phosphorylated proteins with modification-specific antibodies. And third, the fractionation of phosphopeptides by means of strong cation exchange chromatography (SCX). SCX utilizes differences between the capacity of phosphorylated and non-phosphorylated peptides to bind to the stationary phase of the SCX column. Furthermore, phosphopeptides are separated according to their net charge at an acidic pH¹⁴⁴. In the LC-MS/MS experiments following sample fractionation and preparation peptides are then separated by reversed-phase chromatography and the masses of eluting peptides are determined in an initial survey scan (MS scan) in the Orbitrap part of the mass spectrometer. Selected ions are then isolated and fragmented by collision-induced dissociation (CID) for the subsequent measurement of the resulting fragment ions (MS/MS or MS2 scan) in the linear ion trap. Taking advantage of search algorithms (e.g. Mascot) and the respective protein database as reference the generated mass lists are then matched to peptide sequences and assigned to proteins.

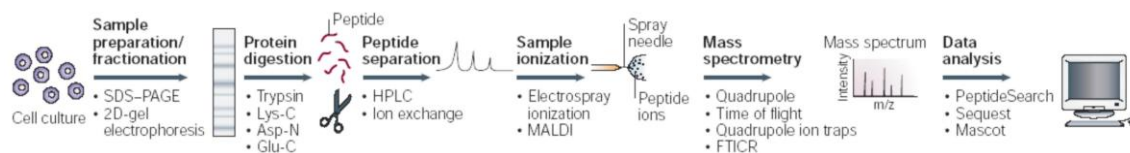


Figure 6: Workflow of a typical shotgun proteomic experiment. Cells are cultured and treated according to the individual biological question e.g. with a small molecule inhibitor or growth factor before protein digest. Proteins or peptides can be separated by, for example, gel electrophoresis or ion exchange chromatography (e.g. SCX). Typically, nanoscale reversed-phase liquid chromatography (LC) is coupled online to the mass spectrometer (e.g. an LTQ-orbitrap) via an electrospray ion source. The peaklists extracted from acquired MS and MS/MS spectra are used in subsequent database searches for peptide identification. Adapted from Hanno Steen and Mathias Mann, *Nature Reviews Molecular Cell Biology*, 2004.

1.4.2 Quantitative proteomics

A major challenge in proteomics is the quantitative analysis of two or more physiological states in a given biological system. As MS is not quantitative *per se* various approaches have been developed to overcome this limitation including approximations that take into account the sequence coverage or the number of peptide-spectrum matches¹⁴⁵⁻¹⁴⁶. However, these approaches are often rather inaccurate with respect to the quantitation of relative protein abundance.

Protein or peptide labeling with non-radioactive stable isotopes, either done metabolically or chemically, offers today's most accurate methods for relative quantitative proteomics¹⁴⁷. These techniques are based on the assumption that a mass difference introduced by isotope labeling will not alter the chemical properties of the peptides but enable their differential detection by MS. Stable isotope labeling by amino acids in cell culture (SILAC)¹⁴⁸ is the most commonly used method for metabolic labeling that uses heavy isotope variants of arginine and lysine which, combined with tryptic protein digestion, ensures the labeling of all peptides except the very C-terminal ones. Generally, SILAC allows comparing up to three cell populations or samples in a single experiment. Therefore, cells are grown in the presence of either the natural ("light") or isotopically labeled ("medium" and "heavy") amino acid analogues with substituted ¹³C, ¹⁵N or ²H atoms. Compared to the "light" peptide incorporation of "medium" and "heavy" amino acids results in a defined mass shift that is detectable in MS survey scans. As the only difference between the distinct SILAC states is the mass of newly synthesized proteins cell growth is usually not affected¹⁴⁹. Furthermore,

more complex comparisons such as time course analyses can be performed by combining different experiments that share one identically SILAC-encoded and treated cell population as a common reference ¹⁵⁰. Notably, as cell populations are mixed directly after cell lysis (Figure 7), no additional errors are introduced during the subsequent sample preparation and potential pooling errors can later be accounted for. Recently, the SILAC approach has been successfully applied also to mice, enabling quantitative MS experiments even in a mammalian organism ¹⁵¹.

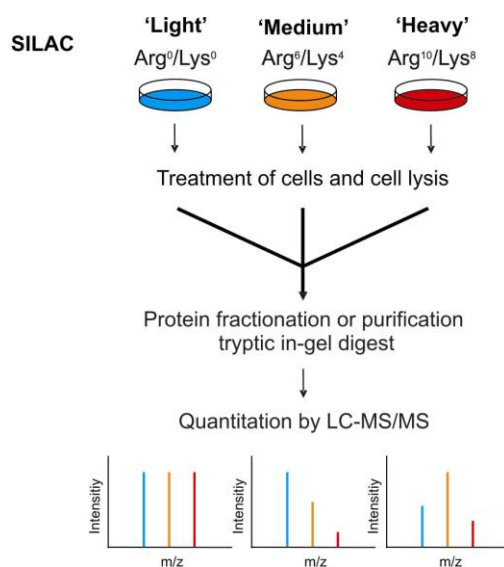


Figure 7: SILAC-based quantitative proteomics. Cells are grown in medium containing the respective 'light', 'medium' and 'heavy' amino acids. Upon complete labeling, cells can be stimulated with a growth factor or treated with a small molecule inhibitor in comparison to a control cell population. After optional sample fractionation or purification, proteins are digested and the relative intensities of the stable isotope-labeled peptides can be distinguished in the MS survey scan of an LC-MS/MS experiment. Relative quantification of identified peptides is done either software-aided (MSQuant) or fully automated (MaxQuant).

In cases where metabolic labeling is not applicable, for example when analyzing human body fluids or tissue samples, chemical modification with stable isotope-bearing reagents offers an alternative strategy for quantitative MS data acquisition. The first example for the chemical tagging of proteins was the cysteine-directed "isotope coded affinity tag" (ICAT) ¹⁵². Today's commonly used reagents for *in vitro* labeling are "isotope tags for relative and absolute quantification" (iTRAQ) ¹⁵³ and the "tandem affinity tag" (TMT) techniques ¹⁵⁴. Another approach that even allows for absolute quantification (AQUA) is based on the

addition of synthetic isotopically labeled peptides in known amounts prior to MS analysis¹⁵⁵.

1.4.3 Phosphoproteomics

Post-translational protein modification (PTM) is a common cellular mechanism that enables the fast modulation of protein function. The most widespread PTM is the reversible phosphorylation of serine, threonine and tyrosine residues catalyzed by protein kinases,¹⁵⁶. Until recently, common techniques applied in protein phosphorylation research were laborious and time-consuming and hence of only low throughput¹⁵⁷.

In contrast to serine and threonine, high-affinity antibodies directed against phosphorylated tyrosine residues have been generated like the 4G10 (Millipore) or p-Tyr-100 (Cell Signaling Technology) antibodies. These allow for an efficient enrichment of pTyr-containing proteins or peptides prior to MS analysis and enable the concurrent analysis of hundreds of pTyr residues in a single MS experiment¹⁵⁸. To enable the analysis of phosphorylation events all phosphorylatable residues including serines and threonines, general phosphopeptide enrichment methods have been developed¹⁵⁹⁻¹⁶⁰. The most frequently applied methods are based on the binding of phosphate groups to trivalent metal ions like Fe^{3+} or Ga^{3+} exploited in immobilized metal affinity chromatography (IMAC)¹⁶¹⁻¹⁶² and the adsorption of phosphate groups by titanium dioxide (TiO_2) microspheres through Lewis acid-base interactions¹⁶³⁻¹⁶⁴. TiO_2 -based phosphopeptide enrichment after prior one-dimensional gel electrophoresis allowed for the quantitative analysis of more than 6,000 phosphorylation events upon EGF stimulation in HeLa cells¹⁵⁰. More recently, a combination of phosphopeptide separation by means of SCX followed by IMAC-based phosphopeptide enrichment identified more than 13,000 phosphosites in *Drosophila melanogaster* embryos¹⁶⁵.

In conclusion, the development of powerful methods for phosphopeptide enrichment combined with MS-based identification and quantification resulted in a drastic increase in the number of phosphorylation events that can be analyzed in a single proteomics experiment. Thus, today's global phosphoproteomics studies often monitor thousands of phosphorylation sites in cellular systems¹⁶⁶⁻¹⁶⁸.

1.5 Characterizing protein kinase inhibitors and kinase signaling

Small molecule inhibitors of PK activity are often directed against the conserved ATP-binding pocket. Thus, the question of the actual specificity of these compounds is evident. In the process of drug development, the identification of ideally all cellular targets of a drug is of crucial importance, as this might allow the prediction of potential target-related toxicities. Moreover, detailed knowledge of all cellular drug targets can be advantageous to exploit the full therapeutic potential and reveal alternative targets of potential therapeutic relevance in additional medical indications. Besides, the identification of essential downstream mediators of the cellular signaling cascades that are controlled by drug-targeted PKs can reveal candidate proteins for the development of novel therapeutics.

The field of MS-based chemical proteomics is more and more emerging as a powerful technique to study proteome-wide small molecule-protein interactions and has proven to be a suitable tool for efficient PK pre-fractionation. In addition, novel chemical genetics approaches allow for the targeted functional analysis of a single PK.

1.5.1 Chemical proteomics

Chemical proteomics techniques can be divided into three major experimental concepts. First, and of particular interest regarding the scope of this thesis, are approaches based on immobilized small molecule inhibitors that are utilized as affinity capture reagents. Second, global proteomic approaches to study cellular effects upon small molecule interference can be employed. And third, activity-based protein profiling strategies allow for the identification of proteins that interact with a small molecule probe consisting of a reactive part fused to an affinity tag for subsequent purification¹⁶⁹⁻¹⁷⁰.

Already about forty years ago the general concept of employing an immobilized drug for affinity chromatography to enrich and identify interacting proteins was developed¹⁷¹. Recent combination with modern MS-based protein analysis has markedly increased the

possibilities of this technique. Ideally, for the most comprehensive analysis possible, this analysis should take place in the presence of all potential interacting proteins. In contrast to kinase activity assays that allow quantitative selectivity testing against a panel of recombinant enzymes¹⁷², chemical proteomics enables the unbiased analysis in the context of the entire expressed proteome. Furthermore, chemical proteomics enables to study naturally occurring, un-engineered proteins at their endogenous expression levels, harboring physiological PTMs, and interacting with their cellular binding partners¹⁶⁹⁻¹⁷⁰.

Seminal studies employing immobilized small molecule PK inhibitors as affinity capture reagents were conducted with the CDK inhibitor purvalanol B and paved the way for the further exploration of this strategy¹⁷³⁻¹⁷⁴. By introducing a suitable linker, which contains an amino-, carboxy- or hydroxyl group and can be used for immobilization on a matrix while maintaining the biological activity of the small molecule, this approach can theoretically be applied to any given chemical compound. The capabilities of this approach have been demonstrated in a study to unambiguously identify the cellular interaction profile for an analog of the p38 inhibitor SB 203580¹⁷⁵. In addition to the known target p38 α also cyclin-G associated kinase (GAK), casein kinase 1 (CK1) and Rip-like interacting caspase-like apoptosis-regulatory protein kinase (RICK), among others, were identified as novel targets. Similar studies were performed with bisindolylmaleimide derivatives targeting protein kinase C¹⁷⁶, the pyrido[2,3-*d*]pyrimidine based compound PP58¹⁷⁷, the gefitinib analog AX14596¹⁷⁸ and an derivative of the angiogenesis inhibitor SU6668¹⁷⁹. Besides an often broad cellular protein interaction profile of the tested compounds these studies also revealed specific interactions with non-PK proteins. In many cases these are other nucleotide-utilizing enzymes like adenosine kinase and quinone reductase type 2 (NQO2)¹⁷⁶.

The importance of PKs in the regulation of cellular signaling cascades and their involvement in pathological processes¹⁸ create the rationale for their comprehensive and global analysis. However, even in large-scale proteomics analysis, the information gained about PKs is often limited due to their comparatively low cellular expression levels. In addition, the targeted analysis of PKs is often hindered by the lack of high-affinity antibodies. To overcome these limitations, experimental strategies utilizing different, immobilized, and rather promiscuous small molecule PK inhibitors for combined affinity chromatography have been reported⁵⁷.

¹⁸⁰. Furthermore, the effectiveness of this approach was underscored in a SILAC-based quantitative study on cell cycle-dependent changes in the phosphorylation state of PKs ¹⁶⁶. Employing their ‘kinobeads’ approach in combination with iTRAQ-based quantitative MS, Bantscheff and colleagues studied dose-dependent competitive protein binding for the clinical Bcr-Abl inhibitors imatinib, bosutinib and dasatinib ⁵⁷. In addition they presented a strategy to estimate target-specific IC₅₀ concentrations at which half-maximal binding competition for a respective PK inhibitor is observed. The quantitative inaccuracy inherent to this approach, which assumes binding of only a small fraction of the total amount of a given protein to the ‘kinobeads’, is evident from comparison with other data derived from *in vitro* kinase activity assays, which in some cases differed by up to three orders of magnitude. Recently, our group reported an optimized approach which allows for the unambiguous identification of cellular target proteins as well as rather accurate affinity measurements for small molecule inhibitors, peptides and proteins and showed good agreement with *in vitro* kinase activity assays ¹⁸¹.

1.5.2 Chemical genetics

In addition to global phosphoproteomics analyses the accurate and comprehensive identification of the direct cellular substrates of an individual PK is of paramount interest. This can be achieved by mutating a bulky residue in the ATP binding pocket of a PK, usually to a comparatively small glycine, thereby enabling the catalytic usage of an N⁶-modified radioactive ATP analogs ¹⁸². The resulting γ -³²P-labeled substrates can then be detected also in the presence of other PKs. However, a general limitation is the inefficient delivery of the highly charged ATP molecules into the cell as well as hydrolysis of the ATP analog.

Another approach is based on interfering with the catalytic activity of the PK of interest. Importantly, this needs to be accurately controlled with high temporal resolution. Thus, methods like genetic knock-out or transient depletion of proteins by RNA interference, which often cause additional secondary changes, are only of limited value ¹⁸³. In contrast, small molecule kinase inhibitors meet these requirements and allow fast and effective inhibition of targeted PKs. However, although used in innumerable studies for elucidating

cellular functions of PKs, many PK inhibitors are far from being truly specific¹⁸⁴⁻¹⁸⁵. Ideally, monoselective inhibition of the kinase of interest is sought to be achieved in a tightly controlled manner.

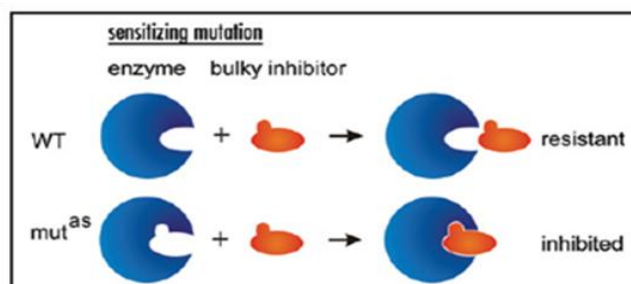


Figure 8: Principle of protein kinase inhibition by analog-sensitizing mutations. The bulky ATP- or purine analogs cannot be utilized by the wild-type PK (WT) that remains insensitive. In contrast, the mutated and thereby enlarged ATP binding pocket of the analog-sensitive PK variant (mut^{as}) is accessible to these analogs and can therefore be selectively inhibited. Adapted from Randall CL et al. Cell Cycle, 2007.

In theory, this is enabled by a powerful approach that was developed by the group of Kevan Shokat and is named ‘chemical genetics’ (Figure 8). This approach combines the features of small molecule inhibitors with the high accuracy achieved by introducing an analog-sensitizing mutation in the ATP binding pocket. Their initial report described the generation of a recombinant v-Src variant that proved to be selectively inhibited by N⁶-modified purine-based small molecule inhibitors *in vitro* and *in vivo*¹⁸⁶. In a subsequent study they generated a yeast strain expressing an inhibitor-sensitive variant of the human CDK1 which was selectively inhibited by a bulky analog of the kinase inhibitor PP1¹²². Recently, this technique has successfully been applied to the human cell cycle-regulatory kinase, Plk1¹²³. Moreover, another study utilizing the same Plk1 variant-expressing, analog-sensitive cell line identified the protein HsCYK, a subunit of centralspindlin, as a novel substrate of Plk1 adding further evidence to Plk1’s functioning in the initiation of cytokinesis¹²⁴.

Taken together, this approach presents a powerful technique to study the cellular function of PKs. However, its specificity has not yet been systematically analyzed. Besides, a limitation of the approach is that it cannot prove whether phosphoregulation is due direct substrate phosphorylation by the investigated PK. In addition, for some PKs it proved difficult to generate functional analog-sensitive PK variants.

II. Aims of the thesis

Post-translational protein modification by phosphorylation by members of the protein kinase superfamily is a central regulatory mechanism in eukaryotic signal transduction pathways. As the catalytic activity of protein kinases is itself controlled by reversible phosphorylation, detailed information about site-specific phosphorylation events on protein kinases and their cellular expression level can provide information on the activity status of connected signaling networks. Malfunctioning of various protein kinases has been associated with a variety of human cancers. Thus, protein kinases have emerged as major drug targets for therapeutic intervention. Among others, small molecule inhibitors that interfere with the protein kinase activity have successfully been introduced as therapeutic drugs. In addition, immobilized inhibitors with a broad spectrum of interacting kinases have been developed as enrichment tools enabling mass spectrometry-based kinase-centric studies. However, so far no systematic *in vivo* approaches for the identification of cellular substrates of human protein kinases have been developed.

This thesis comprises three projects with the common goal of advancing proteomics strategies for comprehensive kinase and kinase signaling analysis. The aim of the first project was to delineate the binding characteristics of kinase inhibitor affinity resins to advance kinase-selective analysis by mass spectrometry-based proteomics. The resin with the broadest identified kinase selectivity should be further exploited for a quantitative comparison of cellular kinase expression levels and a qualitative analysis of their phosphorylation status in three cancer cell lines.

The second project, which was in parts conducted in cooperation with Susanne Breitkopf (another PhD candidate of our group), had the goal to develop a strategy to identify direct cellular target proteins of the clinical Bcr-Abl inhibitor imatinib as well as small molecule-tractable signal transducers based on drug-induced alterations in their phosphorylation level.

A prerequisite for the third project of this thesis was to set up a stable workflow for the strong cation exchange chromatography-based phosphopeptide separation prior to phosphopeptide enrichment by means of immobilized metal affinity chromatography. This was then exploited in cooperation with the PhD candidate Kathrin Grundner-Culemann to develop an experimental strategy for the global analysis of cellular kinase-substrate relationships. Our intention was to

pursue a strategy that combines chemical genetics with quantitative phosphoproteomics analysis. For this purpose, we utilized genetically engineered cell lines expressing either wild-type Plk1 or an analog-sensitive kinase variant, which can be differentially inhibited by the small molecule inhibitor 3-MB-PP1.

III. Materials and Methods

3.1 Material sources

3.1.1 Laboratory chemicals and biochemicals

Acrylamide	Serva, Heidelberg
APS (Ammonium peroxydisulfate)	Bio-Rad, München
Bisacrylamide	Roth, Karlsruhe
BSA (Bovine serum albumin)	Sigma, Taufkirchen
HEPES (N-(2-Hydroxyethyl)piperazine-N'-(2-ethanesulfonic acid))	Serva, Heidelberg
IAA (Iodoacetic acid)	Sigma, Steinheim
L-Glutamine	(GibCo) Invitrogen, Eggenstein
PMSF (Phenylmethanesulfonyl fluoride)	Sigma, Taufkirchen
Ponceau S	Sigma, Taufkirchen
SDS (Sodium dodecyl sulfate)	Roth, Karlsruhe
Sodium azide	Serva, Heidelberg
Sodium fluoride	Sigma, Taufkirchen
Sodium orthovanadate	Sigma, Taufkirchen
TEMED (N,N,N',N'-Tetramethylethylenediamine)	Serva, Heidelberg
Triton X-100	Roth, Karlsruhe

All other chemicals were purchased in analytical grade from Merck (Darmstadt).

3.1.2 Chemicals for SILAC and MS-analysis

Acetonitrile for HPLC	Sigma, Taufkirchen
Ammoniumbicarbonate	Sigma, Taufkirchen
Ammonium hydroxide	Merck, Darmstadt
Antioxidance	Invitrogen, Eggenstein
2,5-Dihydroxybenzoic acid	Fluka, Taufkirchen
DTT	Sigma, Taufkirchen
Fetal bovine serum, dialyzed	Gibco, USA
Iodoacetamide	Sigma, Taufkirchen
L-Arginine	Gibco, USA
L-Arginine: HCl, U- ¹³ C ₆ ¹⁴ N ₄	Cambridge Isotope Laboratories, USA
L-Arginine: HCl, U- ¹³ C ₆ ¹⁵ N ₄	Cambridge Isotope Laboratories, USA

L-Glutamine	Gibco, USA
L-Lysine	Gibco, USA
L-Lysine: 2 HCl, 2H4	Cambridge Isotope Laboratories, USA
L-Lysine: 2 HCl, U-13C615N2	Cambridge Isotope Laboratories, USA
Lys-C	WAKO, Neuss
n-octosylglucoside	Roche, Mannheim
Penicillin/Streptomycin, 100x	PAA, Germany
SILAC DMEM	Gibco, USA; Thermo Fisher Scientific
SILAC DMEM:F12	Gibco, USA
SILAC RPMI	Gibco, USA; Thermo Fisher Scientific
Thio urea	Invitrogen, Eggenstein
Trypsin (seq. grade modified)	Promega, USA
Urea	Merck, Darmstadt

3.1.3 Other materials

Cell culture materials	Greiner, Solingen
	Nunclon, Dänemark
	Falcon, UK
Cellulose nitrate 0.45 µm	Schleicher & Schüll, Dassel
ECL Kit	PerkinElmer/NEN, Köln
Hyperfilm MP	Amersham Pharmacia, Freiburg
Micro BCA Protein Assay Kit	Pierce, Sankt Augustin
Parafilm	Dynatech, Denkendorf
Protein A-Sepharose	Amersham Pharmacia, Freiburg
Protein G-Sepharose	Amersham Pharmacia, Freiburg

3.2 Cell culture Media

Gibco™ media and additives were obtained from Invitrogen (Eggenstein). Media were supplemented to the requirements of each cell line. Freeze medium contained 95 % heatinactivated FCS and 5 % DMSO.

3.3 Stock solutions and commonly used buffers

Collecting gel buffer (4x)	0.5 M Tris/HCl pH6.8
	0.4 % SDS
Laemmli buffer (3x)	100 mM Tris/HCl pH 6.8
	3.0 % SDS
	45.0 % Glycerol

	0.01 % Bromphenol blue 7.5 % β -Mercaptoethanol
NET	50.0 mM Tris/HCl pH 7.4 5.0 mM EDTA 0.05 % Triton X-100 150.0 mM NaCl
PBS	137.0 mM NaCl 27.0 mM KCl 80.9 mM Na_2HPO_4 1.5 mM KH_2PO_4 pH 7.4
SD-Transblot	50.0 mM Tris/HCl pH 7.5 40.0 mM Glycine 20.0 % Methanol 0.004 % SDS
Separating gel buffer (4x)	0.5 M Tris/HCl pH 8.8 0.4 % SDS
“Strip” buffer	62.5 mM Tris/HCl pH 6.8 2.0 % SDS 100.0 mM β -Mercaptoethanol

3.4 Cells

Cell line	Description	Origin
HCT116	Colon, colorectal carcinoma	ATCC, USA
hTERT RPE Plk1 ^{as/wt}	Telomerase expressing human retinal pigment epithelial cells, expressing either wild-type (wt) or analog sensitive (as) variants of Plk1	123
K562	Chronic myelogenous leukemia cell line, Bcr-Abl positive	ATCC, USA
MDA-MB-435S	Melanoma derived cells*	ATCC, USA
MV4-11	Biphenotypic B myelomonocytic leukemia	ATCC, USA

ATCC, American Type Culture Collection, Manassas, USA

* 187

3.5 Antibodies

3.5.1 Primary antibodies

The following antibodies were used for immunoprecipitation or as primary antibodies in immunoblot analysis.

Antibody	Description	Origin/Reference
Axl	Goat, polyclonal	SC, USA
CDC2	Rabbit, polyclonal, recognizes	CST, USA
CK1 α	Goat, polyclonal	SC, USA
DDR1	Rabbit, polyclonal	SC, USA
FAK	Rabbit, polyclonal	SC, USA
Fer	Rabbit, polyclonal	188
Fes	Goat, polyclonal	SC, USA
HCK	Rabbit, polyclonal	SC, USA
JAK1	Rabbit, polyclonal	SC, USA
Met	Mouse, monoclonal	
Pak4	Rabbit, polyclonal	CST, USA
Plk1	Mouse, monoclonal	166
PYK2	Rabbit, polyclonal	Millipore, USA
Syk	Rabbit, polyclonal	SC, USA
pTyr (4G10)	Mouse, monoclonal, recognizes phosphorylated tyrosine residues	UBI, USA

CST, Cell Signaling Technology, Inc.; SC, Santa Cruz Biotechnology, Inc.

3.5.2 Secondary antibodies

For immunoblot analysis corresponding secondary antibodies conjugated with horseradish peroxidase (HRP) were utilized.

Antibody	Dilution	Origin/Reference
Goat anti-mouse-HRP	1 : 10,000	Sigma, Taufkirchen
Goat anti-rabbit-HRP	1 : 50,000	BioRad, München

3.6 Cell culture

Cell lines were grown in a humidified 93 % air, 7 % CO₂ incubator (Heraeus, B5060 EK/CO₂) at 37°C and routinely assayed for mycoplasma contamination using a bisbenzimidestaining kit (Sigma). Before seeding cells were counted with a Coulter Counter (Coulter Electronics). All of the cell lines (American Type Culture Collection, USA) were routinely grown according to the supplier's instructions.

3.7 Protein analytical methods

3.7.1 Determination of protein concentration in cell lysates

The "Micro BCA Protein Assay Kit" (Pierce, Sankt Augustin) and "BioRad protein assay" (BioRad, München) were used according to the manufacturer's instructions.

3.7.2 SDS-polyacrylamide-gel electrophoresis (SDS-PAGE)

SDS-PAGE was conducted as described previously¹⁸⁹. The following proteins were used as molecular weight standards:

Protein	MW (kDa)	Protein	MW (kDa)
Myosin	205.0	Ovalbumin	42.7
β-Galaktosidase	116.25	Carboanhydrase	29.0
Phosphorylase b	97.4	Trypsin -Inhibitor	21.5
BSA	66.2	Lysozym	14.4

3.7.3 Transfer of proteins onto nitrocellulose membranes

For immunoblot analysis proteins were transferred to nitrocellulose membranes¹⁹⁰ for 2 h at 0.8 mA/cm² using a "Semidry"-Blot device in the presence of Transblot-SD buffer. Following transfer, proteins were stained with Ponceau S (2 g/l in 2 % TCA) in order to visualize and mark standard protein bands. The membrane was destained in water.

3.7.4 Immunoblot detection

After electroblotting the transferred proteins are bound to the surface of the nitrocellulose membrane, providing access for reaction with immunodetection reagents. Remaining binding sites were blocked by immersing the membrane in 1x NET, 0.25 % gelatin for at least 1 h. The membrane was then probed with primary antibody (typically overnight).

Antibodies were diluted 1:500 to 1:2000 in NET, 0.25 % gelatin. The membrane was washed 3 times in 1x NET, 0.25 % gelatin, incubated for 1 h with secondary antibody and washed again 3x for 20 min. Antibody-antigen complexes were identified using horseradish peroxidase coupled to the secondary anti-IgG antibody. Luminescent substrates were used to visualize peroxidase activity. Signals were detected with X-ray films or a digital camera unit. Membranes were stripped of bound antibody by shaking in strip-buffer for 1 h at 50°C. Stripped membranes were blocked and re-probed with different primary antibody to confirm equal protein loading.

3.8 SILAC labeling, cell lysis and anti-pTyr immunoprecipitation

3.8.1 Cell culture in SILAC medium

For quantitative MS-based studies, all cells, except hTERT-RPE cells, were grown in media containing either 45 mg/l unlabeled L-arginine and 76 mg/l unlabeled L-lysine (Arg⁰, Lys⁰) or equimolar amounts of L-[U-¹³C₆, ¹⁴N₄]arginine and L-[²H₄]lysine (Arg⁶, Lys⁴), or L-[U-¹³C₆, ¹⁵N₄] and L-[U-¹³C₆, ¹⁵N₂]lysine (Arg¹⁰, Lys⁸) (Cambridge Isotope Laboratories or Sigma-Isotec) as well as dialyzed FBS (Gibco). All media were supplemented with penicillin and streptomycin (Invitrogen).

MV4-11 (ATCC, #CRL-9591) were grown in RPMI 1640 medium (Invitrogen) containing 20 % fetal bovine serum (Invitrogen), MDA-MB-435S (435S, ATCC #HTB-129) and HCT116 (ATCC #CCL-247) were grown in Dulbecco's modified Eagle's medium (Invitrogen) containing 10 % FBS. All cells were cultured for six cell doublings to achieve complete labeling of cellular proteins. The adherent HCT116 and 435S cells were lysed directly on cell culture plates, MV4-11 cells were harvested by centrifugation before cell lysis.

K562 cells (ATCC, # CCL-243) were cultured in suspension in RPMI1640 medium (Invitrogen) containing 10 % FBS. K562 cells were either grown in SILAC medium for six cell doublings on 15 cm dishes (chapter 4.2.1 and 4.2.3) or for five cell doublings on 15 cm dishes and then transferred to spinner flasks (BellCo Glass, USA) into 500 ml fresh SILAC medium at a cell density of 0.25 x 10⁶ cells/ml (chapter 4.2.2) and then grown for another two cell doublings before treatment with imatinib. As indicated in Table A. 1 K562 cells were either treated with 1 μM or 10 μM imatinib mesylate (ACC corporation, USA) or control-incubated with DMSO before harvesting by centrifugation.

hTERT-RPE Plk1^{as/wt} cells¹²³ were grown in (1:1) DMEM:F12 medium, supplemented with 10 % dialyzed FBS, sodium-pyruvate, L-glutamate and 1 % penicillin-streptomycin (Invitrogen). For each biological replicate experiment cells were labeled separately by

culturing in the presence of either 175 μM L-arginine and 250 μM L-lysine (Arg^0 , Lys^0) or L-[U- $^{13}\text{C}_6$, $^{14}\text{N}_4$]-arginine and L-[U- $^{13}\text{C}_6$, $^{15}\text{N}_2$]-lysine (Arg^{10} , Lys^8) (Cambridge Isotope Laboratories or Sigma). After six cell doublings and complete labeling of cellular proteins, cells were seeded at 1.6×10^6 cells per P15 dish (6 or 10 dishes, respectively, finally resulting in 2.5 or 4 mg per labeling condition; Table A. 3). After 18 h, 1 $\mu\text{g}/\text{ml}$ Aphidicolin (Sigma) was added for 12h for pre-synchronization. Cells were washed with 1xPBS and cultured for another 13 h in fresh medium containing the respective SILAC amino acids as well as 50 ng/ml nocodazole (Sigma) and 5 $\mu\text{g}/\text{ml}$ 3-MB-PP1 (Priaxon, Munich, Germany) to arrest the cells in M phase and selectively inhibit analogue sensitive Plk1. Cells were washed once with the respective wash-out medium (with FBS but without labeled amino acids) and respective wash-out media were added for 30 min. Wash-out media contained either 50 ng/ml nocodazole and 5 $\mu\text{g}/\text{ml}$ 3-MB-PP1 or only 50 ng/ml nocodazole in (Arg^0 , Lys^0)- or (Arg^{10} , Lys^8) in SILAC medium containing the respective isotope labeled amino acids. These allocations were switched for every other experiment (Table A. 3).

3.8.2 Cell lysis with Tritron X-100

HCT116, K562, MDA-MB-435S and MV4-11 cells were lysed in 50 mM Hepes-NaOH pH 7.5, 150 mM NaCl, 0.5 % Tritron X-100, 1 mM EDTA, 1 mM EGTA, 1 mM PMSF, 10 mM NaF, 2.5 mM Na_3VO_4 , 50 ng/ml calyculin A (Alexis Biochemicals, San Diego, USA), 10 $\mu\text{g}/\text{ml}$ aprotinin, 10 $\mu\text{g}/\text{ml}$ leupeptin and 1 % phosphatase inhibitor cocktail 1 and 2 (Sigma) for 1 h at 4°C. The cell debris was removed by centrifugation (20 min at 13.000 rpm) and by filtering through 0.22 μm mixed esters of cellulose membranes (Millipore). Protein concentration was measured using the BCA assay (Pierce).

3.8.3 Cell lysis with NP-40 and anti-pTyr immunoprecipitation

The enrichment of tyrosine phosphorylated proteins was conducted as described previously¹⁵⁸. Briefly, SILAC-encoded K562 cells (chapter 5.2.3, Table A. 1) (1×10^8 cells per SILAC-label resulting in 10 mg total protein per SILAC-label) were washed once with PBS and lysed for 20 min in lysis buffer (50 mM Tris, pH 7.5; 150 mM NaCl; 1 % NP40; 0.1 % sodium deoxycholate; 1 mM EDTA; 1 mM sodium orthovanadate; 1 mM PMSF; 0.1 $\mu\text{g}/\text{ml}$ aprotinin; 10 mM NaF). Cells were resuspended in lysis buffer while working on ice and then lysed at 4°C. In addition, all buffers were chilled at 4°C. Lysates were precleared by centrifugation at 13,000 rpm for 10 min. The BCA-assay (Pierce) was used to determine the absolute protein amount and thereupon mix the lysates in a 1:1 ratio. For anti-pTyr immunoprecipitation 200 μg 4G10 antibody was coupled to with 40 μl protein A-Sepharose (Amersham Biosciences) by pre-incubating for 2 h in NP40 lysis buffer. After washing once with lysis buffer, the anti-pTyr containing beads were added to the mixed cell lysates incubated for 4 h. Precipitates were subsequently washed 4x with lysis buffer and precipitated proteins were eluted twice with urea buffer (7 M; 2 M thiourea; 50 mM HEPES pH 7.5; 1 % n-octosyl glucoside) for 10 min at 37°C.

3.8.4 Cell lysis with 8M Urea

hTERT RPE Plk1^{as/wt} cells were lysed in 8 M Urea, 50 mM Tris pH 8.2, 75 mM NaCl, 1 mM EDTA, 1 mM EGTA, 1 mM PMSF, 10 mM NaF, 2.5 mM Na₃VO₄, 50 ng/ml calyculin A (Alexis Biochemicals, San Diego, USA), 10 µg/ml aprotinin, 10 µg/ml leupeptin and 1 % phosphatase inhibitor cocktail 1 and 2 (v/v) (Sigma) for 5 min on ice. Cell extracts were sonicated 3x for 1 minute on ice (Sonopulus GM70, Brandelin electronic, Berlin, Germany). The cell debris was removed by centrifugation (20 min at 13.000 rpm). Protein concentration was measured using the BioRad protein assay (BioRad) and cell populations were mixed 1:1.

3.9 Generation of kinase inhibitor resins and kinase-affinity enrichment

3.9.1 Study for the quantitative comparison of kinase inhibitor resins

The kinase inhibitor VI16832 was prepared as described¹⁶⁶. VI16741 and VI16743 were synthesized accordingly, except that 8-ethyl-2-methanesulfonyl-8*H*-pyrido[2,3-*d*]pyrimidin-7-one and 8-cyclopentyl-2-methanesulfonyl-8*H*-pyrido[2,3-*d*]pyrimidin-7-one were used as starting material instead of 8-bicyclo-[2.2.1]hept-2-yl-2-methanesulfonyl-8*H*-pyrido[2,3-*d*]pyrimidin-7-one in case of VI16832¹⁹¹. For preparation of the affinity resins used in the SILAC experiments, 2 volumes of a 3 mM inhibitor solution prepared in 50 % DMF, 50 % EtOH were mixed with 1 volume of drained ECH-Sepharose beads (GE Healthcare) and then subjected to carbodiimide-catalyzed immobilization according to described procedures¹⁸⁰. Coupling efficiencies were similar for all three inhibitors, resulting in a concentration of 1.5 mM immobilized ligand on Sepharose beads as determined by UV-Vis measurements (data not shown). Kinase enrichment in the phosphoproteomics experiments was performed with VI16832 covalently immobilized on epoxy-activated Sepharose (GE Healthcare) according to a reported coupling protocol¹⁷⁸. Here, 2 volumes of 1.5 mM VI16832 solution prepared in 50 % DMSO, 50 % 50 mM Na₂CO₃ pH 11 were subjected to 1 volume of drained epoxy-activated Sepharose to initiate the coupling reaction.

For comparative SILAC analysis of different inhibitor resins, 1.5 mg from each differentially labeled MV4-11 lysate was subjected to *in vitro* association with the respective kinase inhibitor resins. 30 µl of drained beads coupled with the respective kinase inhibitor were washed three times with lysis buffer and a further three times with lysis buffer containing 1 M NaCl. Washed beads were incubated for 2.5 hours at 4°C in the dark with the lysates that had been adjusted to 1 M NaCl in a final volume of 650 µl. In each experiment, aliquots of the three differentially labeled lysates were pooled to determine the initial SILAC ratios and resulting correction factors for the quantification after affinity enrichment. Beads were washed twice with lysis buffer containing 1 M NaCl and twice with lysis buffer containing 150 mM NaCl. For elution, resin-bound proteins were incubated for 10 minutes with 50 µl 0.5 % LDS buffer (Invitrogen) containing 50 mM DTT at 70°C.

Elution fractions were pooled and concentrated by a factor of three in a vacuum concentrator (Eppendorf). Moreover, aliquots of the different elution fractions were compared by immunoblotting with kinase-specific antibodies.

3.9. Study for the quantitative comparison of relative kinase expression levels

For SILAC-based comparison of protein kinases in MV4-11, HCT116 and 435S cells, total cell lysates were prepared as described above and all adjusted to 1.5 mg protein in a volume of 500 μ l. This amount of protein was obtained upon lysis of 17×10^6 MV4-11, 7.3×10^6 HCT116 and 5.3×10^6 435S cells, respectively. The three lysates were pooled prior to incubation with 90 μ l of drained VI16832 beads according to the same protocol as used for the inhibitor resin comparisons.

3.9.3 Study for the qualitative comparison of phospho-kinomes

Protein kinase enrichment for phosphorylation site mapping was performed using an ÄKTA explorer system and Tricorn 5/20 chromatography columns (GE Healthcare) packed with 500 μ l of VI16832 resin. Cells were lysed in a volume of 35 to 40 ml per experiment. The protein amounts of the starting extracts used in the first and second experiments were: 435S, 85 and 120 mg; HCT116, 240 and 175 mg; MV4-11, 180 and 120 mg. Lysates were adjusted to 1M NaCl prior to loading onto the VI16832 column at a flow rate of 0.07 ml/min. Subsequent washing and elution steps were performed as described previously¹⁸⁰. Protein-containing elution fractions were lyophilized, re-suspended in one tenth of the initial volume, and then desalted by protein precipitation¹⁹² prior to 1D gel electrophoresis.

3.9.4 Study for the identification of cellular imatinib targets and imatinib-sensitive phosphorylation sites

Kinase inhibitor resins containing the immobilized compounds VI16832, purvalanol B, bisindolylmaleimide X, AX14596 and SU6668 were essentially prepared as described previously^{166, 179-180} with the only differences that 2 volumes of 1.5 mM (instead of previously 0.75 mM)¹⁶⁶ VI16832 solution and 2 volumes of 5 mM (instead of 10 mM)¹⁸⁰ bisindolylmaleimide X were coupled to 1 volume of aspirated epoxy-activated Sepharose 6B for immobilization.

For the initially performed multicolumn affinity chromatography (chapter 4.2.1), we, in addition to the 5 above described inhibitor resins, also prepared a VI16741 inhibitor resin. Therefore 2 volumes of 5 mM VI16741 were coupled to 1 volume of aspirated epoxy-activated Sepharose 6B for immobilization. 0,5 ml of the respective resins were packed in

either individual Tricorn 5/20 chromatography columns (GE Healthcare) (VI16832, purvalanol B and bisindolylmaleimide X resins) or 0.33 ml of each resin were packed successively in a Tricorn 5/50 chromatography column (GE Healthcare) (VI16741, AX14596 and SU6668 resins). The columns were connected as indicated in Figure 26C. Cell lysates of 4×10^8 cells per SILAC-label, resulting in a about 35 mg total protein per SILAC-label were pooled (1:1:1) and were adjusted to 1M NaCl prior to loading onto the columns at a flow rate of 0.07 ml/min. Subsequent washing and elution steps were performed as described previously¹⁸⁰. Protein-containing elution fractions were lyophilized, re-suspended with ddH₂O in one tenth of the initial volume, and then desalted by protein precipitation according to Wessel & Flügge¹⁹² prior to one-dimensional gel electrophoresis and tryptic in-gel digest or in-solution digest with trypsin and subsequent strong cation exchange chromatography.

For parallel, batch-wise, kinase-affinity enrichment in each of the two replicate experiments (chapter 4.2.2), we prepared a mixed kinase inhibitor resin containing 0,5 ml of the VI16832 and purvalanol B resins and 0,33 ml of the bisindolylmaleimide X, AX14596 and SU6668 resins. Frozen cell pellets from differentially encoded and treated K562 cell populations were solubilized with 9 ml of lysis buffer containing 50 mM Hepes-NaOH, pH 7.5, 150 mM NaCl, 0.5 % Triton X-100, 1 mM EDTA, 1 mM EGTA, 1mM PMSF, 10 mM NaF, 2.5 mM Na₃VO₄, 50 ng/ml calyculin A (Alexis Biochemicals, San Diego, CA), 10 µg/ml aprotinin, 10 µg/ml leupeptin, and 1 % phosphatase inhibitor mixtures 1 and 2 (Sigma) for 1 h at 4°C. Cell debris was removed by centrifugation (20 min at 13,000 rpm) and by further filtering through 0.22-µm mixed esters of cellulose membranes (Millipore). Protein concentration was measured using the BCA assay (Pierce). 55 mg of each of the three differentially labeled K562 lysates were adjusted to a final concentration of 1 M NaCl and a final volume of 10 ml. SILAC-encoded samples were then subjected to parallel *in vitro* associations with 0.7 ml mixed kinase inhibitor resin for 2 h at 4°C in the dark. Beads were then washed three times with 10 ml lysis buffer adjusted to 1 M NaCl and twice with lysis buffer containing 150 mM NaCl. For elution of bound proteins, mixed kinase inhibitor beads were repeatedly incubated for 10 min with 1.4 ml elution buffer (20 mM Tris-HCl pH 7.5, 5mM DTT, 0.5 % SDS) at 50°C. Aliquots of the resulting elution fractions were analyzed by SDS-PAGE and silver-staining. Protein-containing elution fractions were pooled and lyophilized, and then resuspended with ddH₂O in one tenths of the initial volume prior to protein precipitation according to the protocol by Wessel & Flügge¹⁹².

3.10 Mass spectrometry sample preparation

3.10.1 In-solution protein digest

For subsequent strong cation exchange chromatography with the ResourceS column (Amersham) Precipitated PK-enriched samples were dissolved in 7 M urea; 2 M thiourea; 50 mM HEPES pH 7.5; 1 % n-octosyl glucoside. Protein samples, that were previously purified by anti-pTyr immunoprecipitation were directly eluted in the above described urea buffer. Thiol groups on proteins were reduced by adding 2 mM DTT (final conc.) for 45

min at 25°C and cysteines were then carboxymethylated with 5.5 mM IAA for 30 min at RT. The endoproteinase Lys-C (Wako) was added in an enzyme/substrate ratio of 1/100 (wt/wt) and the proteins were digested for 4 h at RT. Thereafter, the resulting peptide mixtures were diluted with ddH₂O to achieve a final urea concentration below 2 M. Then, modified trypsin (sequencing grade, Promega) was added in an enzyme/substrate ratio of 1/100 (wt/wt) and the digest was incubated at RT over night. In the end, trypsin activity was quenched by adding 1 % trifluoroacetic acid (TFA).

3.10.2 In-gel protein digest

Kinase enriched samples were separated by SDS-PAGE, using NuPAGE Novex Bis-Tris gels (Invitrogen) according to the manufacturer's instructions. The colloidal Blue Staining Kit (Invitrogen) was used to stain the gel with Coomassie blue. The protein-containing lane(s) were cut into 3, 6 or 16 slices as indicated in the different chapters. In-gel digestion which was performed as described¹⁹³. Gel slices were cut into small pieces and washed with 50 mM ammonium bicarbonate (ABC) / 50 % ethanol until cubes were fully destained. Gel pieces were dehydrated with ethanol and rehydrated with 50 mM ABC containing 10 mM DTT. Thiol groups on proteins were reduced for 1 h at 56°C. The reduced thiol groups were then alkylated by adding 55 mM IAA in 50 mM ABC for 1 h at 25° C in the dark. Gel pieces were again washed twice with a 50 mM ABC / 50 % ethanol solution, dehydrated with 100 % ethanol and dried in a concentrator 5301 (Eppendorf). Each gel fraction was rehydrated in 50 mM ABC solution containing trypsin (1:100 wt/wt) and samples were digested at 37° C over night. Supernatants were collected and residual peptides were extracted by incubating twice with 30 % acetonitrile (MeCN) in 3 % TFA followed by two incubations with 100 % MeCN. All extracts of a respective fraction were combined and the samples were concentrated in a concentrator 5301 (Eppendorf) to remove all MeCN. Then, samples were desalted and enriched using in-house made C₁₈ STAGE Tip columns¹⁹³⁻¹⁹⁴. Eluted peptides were concentrated in a concentrator 5301 (Eppendorf) to a final volume of 3-4 µl. For MS-analysis samples were then mixed 1:1 with 1 % TFA and 5 % MeCN.

3.10.3 Titanium dioxide microsphere-based enrichment of phosphopeptides

Subsequently to the trypsin digest, phosphopeptides were enriched using Titanium dioxide (TiO₂) microspheres as described^{150, 163-164}. Peptide samples were diluted 1:6 with 30 g/L 2,5-dihydroxybenzoic acid (DHB) in 80 % MeCN/ 0.1 % TFA. 5 µg TiO₂ microspheres (GL Sciences Inc.) were washed once with elution buffer (NH₃ water in 20 % MeCN, pH 10.5) and equilibrated with washing buffer (50 % MeCN, 0.1 % TFA). The TiO₂ resin was preloaded with DHB by washing with loading buffer (6 g/L DHB in 15 % MeCN). Peptide samples were then loaded onto the TiO₂ resin for 30-60 min at RT on a spinning wheel. The resin was then washed 3 times with washing buffer and bound phosphopeptides were eluted twice for 10 min at RT with elution buffer while constantly rocking. The eluted peptides were filtered through in-house made C₈ StageTips in 200 µl pipette-tips. This was followed by a subsequent rinse of the C₈ StageTips with 30 µl of 80 % MeCN / 0.5 % acetic, which

was combined with the filtered sample. Then the pH value of the sample was adjusted to approximately pH 7 by adding TFA and the eluates were concentrated in a concentrator 5301 (Eppendorf) to a final volume of 3-4 μ l. For MS-analysis samples were then mixed 1:1 with 4% MeCN and 0.2 % TFA.

3.10.4 Immobilized metal affinity chromatography for phosphopeptide enrichment

Lyophilized peptides of each sample were resuspended in 200 μ l 40 % MeCN (vol/vol), 25 mM formic acid and incubated with 5 μ l PHOS-Select Iron Affinity Gel (Sigma) for 1 h at 25 °C shaking at 1.400 rpm in a Thermomixer comfort (Eppendorf). C₁₈ StageTips were prepared as described by Rappsilber et al.¹⁹⁴. Equilibration of the StageTips, loading, wash- and elution steps were done as described by Villen & Gygi in the protocol for the 'combined IMAC enrichment and phosphopeptide desalting'¹⁹⁵. Eluted peptides were concentrated to a volume of 4 μ l and mixed 1:1 with 4 % MeCN (vol/vol), 0.2 % trifluoroacetic acid (vol/vol) prior to LC-MS/MS analysis.

3.10.5 Strong cation exchange chromatography for phosphopeptide separation (ResourceS column)

Strong cation exchange chromatography was performed based on two previously described protocols^{144, 196}. Briefly, kinase-enriched proteins from SILAC-encoded K562 cells were employed for in-solution digest with trypsin. Peptide mixture was diluted with ddH₂O to result in a conductivity < 4 mS/cm and filled onto a 50 ml Superloop™ (Amersham Biosciences) and loaded at a flow rate of 1 ml/min on a 1ml Resource S column (Amersham Biosciences) operated with an Äkta Explorer system (GE Healthcare) equipped with a fraction collector. Phosphopeptides were separated by applying a linear gradient from 100 % buffer A (30 % MeCN, 5mM KH₂PO₄, pH 2.7) to 60 % buffer B (30 % MeCN, 5mM KH₂PO₄, 350mM KCl, pH 2.7) at a flow rate of 1 ml/min over 30 column volumes. Fractions were pooled to obtain a total of 7 samples, which were concentrated in a concentrator 5301 (Eppendorf) and subsequently employed for TiO₂ microsphere phosphopeptide enrichment.

3.10.5 Strong cation exchange chromatography for phosphopeptide separation (polySULFOETHYL A column)

Different amounts of lyophilized peptides (Table A. 3) were dissolved in 600 μ l 30 % MeCN (vol/vol), 7 mM KH₂PO₄, pH 2.65 and loaded on a polySULFOETHYL A column 250x9.4 mm, 200 Å pore size and 5 mm particle size (PolyLC) operated with an Äkta

Explorer system (GE Healthcare) at 3 ml/min. The flow through was collected and bound peptides were separated by applying a gradient from 0 to 105 mM KCl over 33 minutes followed by 350 mM KCl, H₂O and 500 mM NaCl each for 10 minutes. During the whole gradient fractions of 3 ml are collected and later pooled based on the measured absorbance at 215 nm to obtain a set of twelve distinct samples. After removing the MeCN in a concentrator 5301 (Eppendorf) samples are desalted in 100mg reverse-phase tC18 SepPak solid-phase extraction cartridges (Waters) as described above. Two aliquots per sample were snap-frozen in liquid N₂, lyophilized and stored at -20°C until phosphopeptide enrichment by means of IMAC.

3.10.6 Sample processing for the comparison of inhibitor-resins, kinase expression levels and the phospho-kinome analysis

Kinase-enriched protein samples were separated by gel electrophoresis. In all SILAC experiments, gels were cut into three slices followed by in-gel digestion with trypsin and peptide purification with StageTips as described¹⁹³⁻¹⁹⁴. For phosphopeptide identification experiments gels-lanes were cut in either three (experiment 1) or 6 (experiment 2) distinct molecular weight regions, prior to in-gel proteolysis with trypsin. Phosphopeptides were thereupon specifically enriched using TiO₂ microspheres.

3.10.7 Sample processing for the identification of imatinib targets and imatinib-sensitive phosphorylation events

Either 50 % or 25 % of the total kinase-enriched protein amount, from SILAC-encoded K562 cells, were employed for in-solution digest with trypsin for subsequent SCX (ResourceS column) (Table A. 1). The remaining 50 % or 75 %, respectively, were dissolved in 1.5x LDS-Buffer and employed to in-gel digest. 20 % of the resulting peptide mixture was mixed with an equal volume of 1 % TFA, 5 % MeCN and then desalted on C₁₈ StageTips. The larger part of 80 % of each fraction from the tryptic in-gel digests were subjected to phosphopeptide enrichment using titanium dioxide (TiO₂) microspheres.

3.10.8 Sample processing for the cellular substrate identification for Polo-like-kinase 1

Pooled lysates (8-10 mg total protein, Table A. 3) were adjusted to 6 M Urea and 1.5 M Thiourea for Tryptic in-solution digest. Samples are reduced in the presence of 1mM DTT (Sigma) in 20 mM ammonium bicarbonate for 45 min at 25°C, and then alkylated with 5.5 mM IAA (Sigma) in 20 mM ammonium bicarbonate for 30 minutes at 25°C. Proteins were

first digested for 4 h by adding Lys-C (Wako) at an enzyme /substrate ratio of 1/100 (wt/wt) then samples were diluted 1:4 with H₂O and sequencing grade trypsin (Promega) was added at an enzyme /substrate ratio of 1/150 (wt/wt) for overnight digest. Temperature was adjusted and samples constantly rocked at 450 rpm in a Thermomixer comfort (Eppendorf). Digest was stopped by acidification with trifluoroacetic acid (Fluka).

Tryptic peptides were then filtered through a 0.22 µm polyvinylidene fluorid membrane (Millipore) and desalted using 500 mg reverse-phase tC₁₈ SepPak solid-phase extraction cartridges (Waters). Equilibration of the cartridges, sample loading, washing and elution of desalted peptides was done as described previously¹⁹⁵. Desalted peptides were frozen with liquid N₂ and lyophilized using a Lyovac GT2 (Leybold-Heraeus) equipped with a Chemie-HYBRID-Pumpe RC 6 (VACUUBRAND, Wertheim, Germany). Lyophilized peptides were stored at -20°C.

3.11 MS analysis and data processing

3.11.1 MS analysis on the LTQ-Orbitrap

MS analyses were done as described previously^{150, 166}. Briefly, peptide separations were done on 15 cm analytical columns (75 µm inner diameter) in-house packed with 3 µm C₁₈ beads (Reprosil-AQ Pur, Dr. Maisch) using a nanoflow HPLC system (Agilent Technologies 1100), which was coupled online to a LTQ-Orbitrap mass spectrometer (Thermo Fisher Scientific) via a nanoelectrospray ion source (Proxeon Biosystems). The LTQ-Orbitrap was operated in the data-dependent mode to automatically switch between full scan MS in the orbitrap analyzer (with resolution R=60,000 at m/z 400) and the fragmentation of the five most intense peptide ions (for all experiments in chapter 4.1 and 4.2) by either MS/MS or multi-stage activation in the LTQ part of the instrument, the latter being triggered on neutral loss species at 97.97, 48.99, or 32.66 m/z below the precursor ion for 30 ms¹⁹⁷. Notably, in all experiments for the cellular substrate identification of Plk1 (chapter 5.3), the ten most intense peptide ions were subjected to fragmentation and MS² acquisition. For all measurements with the orbitrap detector, a lock-mass strategy was used for internal calibration as described¹⁹⁸.

3.11.2 Peptide identification, quantification and data analysis (MSQuant)

All experiments presented in chapter 5.1 were performed with MSQuant. Raw MS files acquired from individual experiments were merged using the Raw2msm software¹⁹⁸ and the resulting msm files were searched against concatenated forward and reversed versions of the human IPI protein database version 3.13 (SILAC-based inhibitor comparison),

version 3.19 (phosphorylation site mapping) or version 3.24 (SILAC-based kinome profiling) containing 57,032, 60,397 and 66,921 protein entries, using the Mascot search engine (Matrix Science). All databases contained frequently occurring contaminants including human keratins, porcine trypsin and endopeptidase Lys-C. Search parameters were set to up to three missed cleavages, mass tolerances of 25 ppm for MS and 0.5 Da for MS/MS scans. Carbamidomethylation of cysteine was set as fixed modification; variable modifications included oxidized methionine, phosphorylation of serine, threonine and tyrosine, N-acetyl protein, N-pyroglutamine and, in the SILAC experiments, the isotopic variants Lys⁴, Lys⁸, Arg⁶ and Arg¹⁰.

The html output files generated by Mascot together with the raw data files were then further processed using the MSQuant software (<http://msquant.sourceforge.net>, versions 1.4.0 used for SILAC-based inhibitor comparison and version 1.4.3 for SILAC-based kinome profiling and phosphorylation site identification). Prior to peptide quantification or computation of post-translational modification (PTM) scores, peptide datasets were filtered for a false-discovery rate (FDR) of less than 1 % ($p < 0.01$) according to a target/decoy database searching strategy. To achieve a FDR of less than 1 %, filtering criteria such as a peptide length ≥ 6 and a mass error < 5 ppm were applied together with a minimal Mascot score that ranged from 21 to 29 depending on the experiment. MSQuant determines the average ratio over the peptide elution profile and all precursor ion assignments used for quantitation were manually validated^{150, 199}. Upon normalization for the initial SILAC pooling error, protein ratios were calculated as the mean of all ratios from uniquely assigned peptides.

To identify highly significant differences in relative protein abundance, the relative ratios of the protein quantifications from the two biological replicate experiments were analyzed for their normal distribution to account for the combined biological and technical variation in the quantitative MS analyses. Protein abundance was considered as significantly different ($p < 0.01$) in case ratios differed from the mean by 2.58σ as determined from the 'ratio of ratios' distributions of the biological replicate analyses.

The assignment of phosphorylation sites in identified phosphopeptides was done with the PTM scoring algorithm implemented in MSQuant as described previously¹⁵⁰. In this study, phosphorylation sites were rated as class I in case of a localization probability of at least 0.95. The localization p-values for all identified phosphopeptides as well as the corresponding annotated MS/MS spectra can be accessed online at <http://www.phosida.org>

3.11.3 Peptide identification and quantification (MaxQuant)

All experiments presented in chapter 5.2 and 5.3 were performed with MaxQuant (<http://www.maxquant.org/>).

All MS raw files from the respective experiment were collectively processed with the MaxQuant software suite version 1.0.13.12 (chapter 4.1 and 4.2) or version 1.0.12.5 (chapter 4.3). MaxQuant performs peak list generation, SILAC-based quantitation, estimation of false discovery rates, peptide to protein group assembly, and data filtration and presentation as described²⁰¹. Data were searched against a concatenated forward and reversed version of the human International Protein Index (IPI) database version 3.37 containing 69141 protein entries and 175 frequently detected contaminants (such as porcine trypsin, human keratins and Lys-C) using the Mascot search engine (Matrix Science; version 2.2.04). Cysteine carbamidomethylation was set as a fixed modification and methionine oxidation, protein *N*-acetylation, loss of ammonia from N-terminal glutamine as well as phosphorylation of serine, threonine and tyrosine residues were allowed as variable modifications. Spectra resulting from isotopically labeled peptides, as revealed by presearch MaxQuant analysis of SILAC partners, were searched with the fixed modifications Arg⁶ and Lys⁴ or Arg¹⁰ and Lys⁸, respectively, whereas spectra for which a SILAC state could not be assigned before database searching were searched with Arg⁶, Arg¹⁰, Lys⁴ and Lys⁸ as variable modifications. The accepted mass tolerance was set to 5 p.p.m for precursor ions and to 0.5 Da for fragment ions. The minimum required peptide length was 6 amino acids and up to three missed cleavage sites and three isotopically labeled amino acids were permitted. The accepted FDR was 1 % for both protein and peptide identifications, and the cut-off for the posterior error probability (PEP) of peptides set to 10 %. Phosphorylation site assignments were performed by a modified version of the PTM scoring algorithm¹⁵⁰ implemented in MaxQuant. Phosphorylation site assignments were classified as class I sites in case of a localization probability of at least 0.75 and a score difference of at least 5 to the second most likely assignment.

3.11.4 Determine Ratio similarity coefficient curves (RSC)

We defined the ratio of similarity coefficient (RSC) by the absolute value of the difference between a minimum of two ratios divided by the sum of the ratios, which were required to be quantified in at least two biological replicate experiments. For each phosphopeptide, the ratios of two or all biological experiments with opposite label assignment were averaged for PLK1^{as} and PLK1^{wt} cells respectively and the corresponding RSC was calculated. Sites were arbitrarily considered as regulated when the logarithmized average value was greater than 1 or less than -1. Accordingly, sites were assigned to one of the following categories: (A) as and wt not regulated, (B) as regulated, wt not regulated, (C) as not regulated wt regulated and (D) as and wt regulated. The resulting numbers, when all experiments were considered, were plotted against an increasing RSC cut-off.

3.11.5 Gene ontology analysis

For enrichment analysis of gene ontology (GO) categories, Cytoscape²⁰² together with the BinGO plugin²⁰²⁻²⁰³ was used to identify statistically over-represented GO biological process, cellular component and molecular function terms compared to a reference dataset consisting of all IPI entries and their respective GO identifiers essentially as described²⁰⁴. Selected GO terms being significantly enriched in the set of cellular Plk1 substrates over all identified phosphoproteins ($p < 0.01$), in the analysis on non-PK binders to the VI16832 kinase-affinity resin ($p < 0.001$) were displayed.

3.11.6 Phosphorylation site overlap between technical and biological replicates.

For visualizing the overlap of quantified class I phosphosites of each individual experiment (18 technical and 9 biological) versus all other we calculated the overlap of two datasets as percent overlap to the smaller one (A) and similarity in form of the Jaccard coefficient (B) as described by Choudhary *et al.*²⁰⁵ defined by the following equations:

$$(A) \frac{n[\text{Data1, Data2}]}{\min[\text{Data1, Data2}]} \times 100 \quad (B) \frac{n[\text{Data1, Data2}]}{u[\text{Data1, Data2}]} \times 100$$

IV. Results

Protein kinases are key regulators of most eukaryotic signal transduction pathways that can modify the function of substrate proteins through reversible phosphorylation of serine, threonine and tyrosine residues. Thus, protein kinases are crucially involved in the regulation of nearly all biological processes. Moreover, overexpression or aberrant activity of multiple kinases has been correlated to the emergence and progression of human cancers. Protein kinases are therefore regarded as important drug targets for therapeutic intervention.

In the first part of this study, a generic strategy for the MS-based quantitative assessment of immobilized small molecule kinase inhibitors will be presented. Subsequently we employed kinase pre-fractionation for a quantitative comparison of kinase expression levels across different cancer cell lines and for comprehensive kinase-centric phosphoproteomics analysis.

In the second part we report a strategy for the identification of target proteins for small molecule kinase inhibitors based on competitive protein capturing by kinase-affinity resins. We confirmed previously reported targets of imatinib and in addition present novel proteins that function as mediators in the cellular signaling cascades that are initiated by the target proteins of imatinib.

For conducting the third part of this thesis we combined strong cation exchange chromatography and immobilized metal affinity chromatography for phosphopeptide enrichment and demonstrate its effectiveness. Integrating this phosphoproteomics workflow with chemical genetics we report an experimental approach for the systematic *in vivo* analysis of kinase-substrate relationships and applied it to identify cellular substrates of Plk1.

4.1 Large-scale Proteomics Analysis of the Human Kinome

Signal transduction through reversible phosphorylation is a ubiquitous and the most intensely studied type of eukaryotic PTMs. The targeted analysis of PKs through antibody-based enrichment has been limited by the availability of efficient antibodies and is of only low throughput. Initially, immobilized small molecule kinase inhibitors were used as affinity capture reagents to identify the respective interacting PKs and other proteins^{175, 206-207}. Recently, strategies for the efficient pre-fractionation of PKs, by utilizing several non-selective immobilized compounds, significantly expanded the toolbox for kinase-centric proteomics^{57, 166, 180}. Ideally, the set of small molecules should result in the enrichment of all human PKs and thus enable truly global kinase-centric proteomics analysis. However, as even the largest reported study to date covers only an estimated 70 % of the expressed human kinase complement¹⁶⁶ there is the continued need to further improve kinase-selective proteomics analysis.

4.1.1 Comparative profiling for kinase-selective pre-fractionation reagents

The pyrido[2,3-*d*]pyrimidine-based small molecule compound PP58 has been previously reported to interact with more than 30 PKs¹⁷⁷. A common characteristic of many of these kinases is the presence of a small amino acid at the ‘gate-keeper’ position, which allows positioning of the spacious dichlorophenyl moiety of PP58 in a hydrophobic pocket near the ATP binding site²⁰⁸. We therefore reasoned that a PP58 derivate lacking the dichlorophenyl moiety should also effectively target PKs possessing larger amino acid residues at the crucial ‘gate-keeper’ position, which account for the majority of protein kinases encoded by the human genome. However, initial experiments with such a truncated version of PP58 indicated rather weak kinase affinity. Therefore, and to analyze the effect of different N8 substituents, we designed a set of pyrido[2,3-*d*]pyrimidine-based derivatives with N8 substituents of varying size which were synthesized in the lab of György Kéri. The chemical structures of three compounds with either comparatively large cyclopentyl or norbornyl moieties, termed VI16743 and VI16832, or a smaller ethyl moiety, termed VI16741, are shown in Figure 9A.

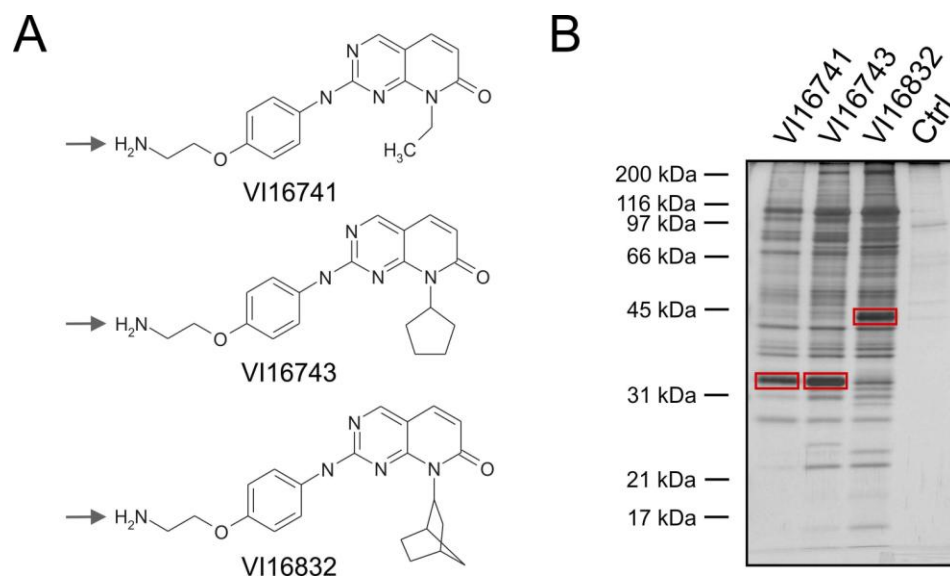


Figure 9: Pyrido[2,3-*d*]pyrimidine-based kinase inhibitor resins and silver-stained elution fractions. (A) Chemical structures of pyrido[2,3-*d*]pyrimidine-based inhibitors used as affinity capture reagents for protein kinase enrichment. The amino groups (marked by arrows) were used for immobilization on a Sepharose matrix. Aliquots of the elution fractions from either kinase inhibitor resins or control resin devoid of an immobilized ligand were analyzed by SDS-PAGE and silver-staining. (B) Individual protein bands indicated by a red box were analyzed in a separate LS-MS/MS experiment and identified as delta(3,5),delta(2,4)-dienoyl-CoA isomerase in case of the VI16741 and VI16743 resins and as the multifunctional protein ADE2 in the eluate of the VI16832 resin, respectively.

To utilize the compounds for later affinity enrichment we initially generated the respective affinity resins by immobilizing the compounds through their primary amino groups (Figure 9A). To enable quantitative MS analysis¹⁴⁹ we performed SILAC with the acute myelogenous leukemia (AML) cell line MV4-11. Cells were lysed after complete labeling of the cells with either normal arginine and lysine (Arg0/Lys0) or the ‘medium’ (Arg6/Lys4) and ‘heavy’ (Arg10/Lys8) isotopic variants. Thereupon, the differentially SILAC-encoded MV4-11 lysates were incubated with a respective resin. In a second biological replicate, a so-called ‘label-switch’ experiment, the affinity resins were incubated with differently SILAC-encoded cell lysates (Figure 10). After *in vitro* association and elution of the captured proteins an aliquot of each elution fraction was analyzed by gel electrophoresis and silver-staining (Figure 9B).

Overall, the three elution fractions derived from the affinity capture resins show a similar protein band pattern, although compared to the VI16741 fraction most proteins appeared to

be slightly more abundant in the VI16743 and VI16832 eluates. Interestingly, some protein bands seemed to show resin-specific binding. We therefore analyzed these bands in separate LC-MS/MS experiments. The prominent 35 kDa protein band in the VI16741 and VI16743 elution fraction was identified as delta(3,5),delta(2,4)-dienoyl-CoA isomerase, and the VI16832 resin-specific 50 kDa protein as the multifunctional protein ADE2. This apparently resin-specific capturing of purine-binding non-PK proteins indicates different binding properties of the pyrido[2,3-*d*]pyrimidine-based derivatives conferred by the distinct hydrophobic moieties in the N8 position.

The major part of the elution fractions was then combined and proteins were separated by gel electrophoresis. Sample complexity was reduced by cutting the gel-lane into three slices comprising proteins of different molecular weight ranges prior to tryptic protein digestion. Tryptic peptides of each fraction were enriched and desalted by C₁₈ StageTips¹⁹⁴ and subjected to LC-MS/MS analysis on a LTQ-Orbitrap hybrid mass spectrometer.

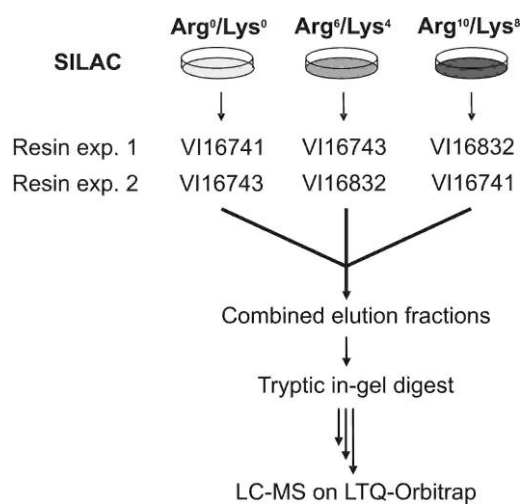


Figure 10: Quantitative chemical proteomics to evaluate kinase inhibitor resins. Schematic workflow used for comparative quantitative MS analysis of cellular proteins enriched by the different inhibitor resins from SILAC-encoded MV4-11 total cell extracts.

The generated MS raw files were combined, converted into peak lists, and searches against a concatenated database containing both forward and reversed sequences²⁰⁹, were done using the Mascot search engine. This target/decoy search strategy allowed defining cut-off thresholds regarding the Mascot scores and mass errors of all identified peptides. These were specified in each individual experiment to filter for an estimated false-positive rate of less

than one percent ($p < 0.01$) on the peptide level according to the peptide-spectrum matches involving reversed sequences. The resulting peptide lists were then employed for SILAC-based quantification using the MSQuant software and all peptides were manually checked¹⁹⁹. The abundance ratios determined for all unique peptides were used to calculate the corresponding relative protein levels in the different resin eluates. Taken both experiments together, quantitative data for more than 130 PKs derived from the MV4-11 affinity capture resin eluates was obtained.

These calculated protein ratios reflect the amount of a particular PK or other non-PK protein captured by the respective affinity resin. For pair-wise comparisons of the affinity resins we averaged the protein ratios of two independent experiments and plotted them on a logarithmic scale (\log_2). A considerable subset of protein kinases interacted more strongly with the VI16743 and V16832 resins compared to the VI16741-containing beads, indicating that the space-filling cyclopentyl and norbonyl moieties in the N8 position resulted in an overall increase in potency with respect to kinase binding (Figure 11A). However, in a few cases the comparatively bulky N8-substituents of the VI16743 and VI16832 resins abolished protein kinase binding. Notably, various NIMA-related expressed kinase (NEK) family members (NEK3, 6 and 7) were found in higher abundance in the VI16741 resin eluates. In contrast, the differences between the VI16743 and V16832 resins were less pronounced, with only small subsets of PKs preferentially bound by either affinity matrix (Figure 11A). Similar comparisons were also made for the more than 250 non-protein kinase proteins quantified from the affinity resin eluates (Figure 11B). Similar to the outcome of the pair-wise PK comparisons non-PK proteins were also more efficiently retained by the VI16743 and V16832 resins compared to the VI16741-containing beads. However, the VI16832 resin showed an overall stronger affinity towards non-PK proteins compared to the VI16743 resin.

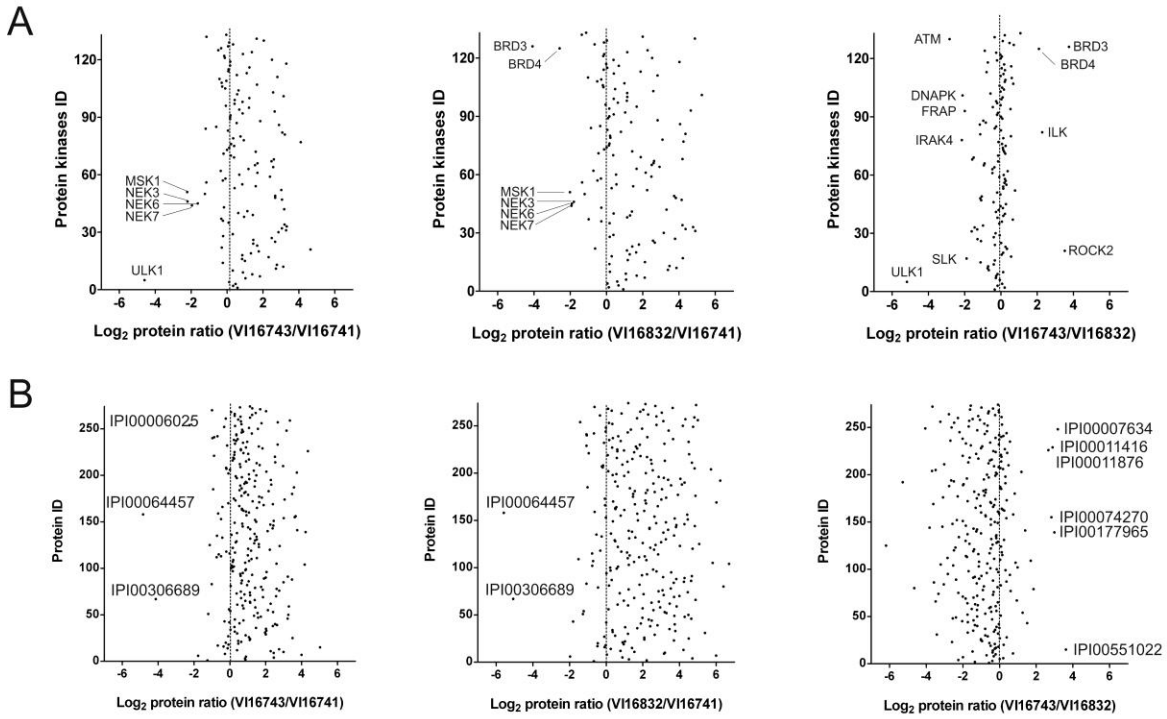


Figure 11: Comparison of the analyzed pyrido[2,3-d]pyrimidine-based affinity resins. Relative protein binding to the affinity resins was determined by SILAC-based quantitative MS of unique peptides. For the pair-wise resin comparisons, the averaged ratios of two independent experiments were plotted on a logarithmic scale (log₂) for all protein kinases (A) and all other quantified non-protein kinase proteins (B).

To verify the quantitative MS approach by a different method, immunoblot analyses were performed with a selection of kinase-specific antibodies. The outcome of this analysis was in full concordance with the MS results (Figure 12A, B).

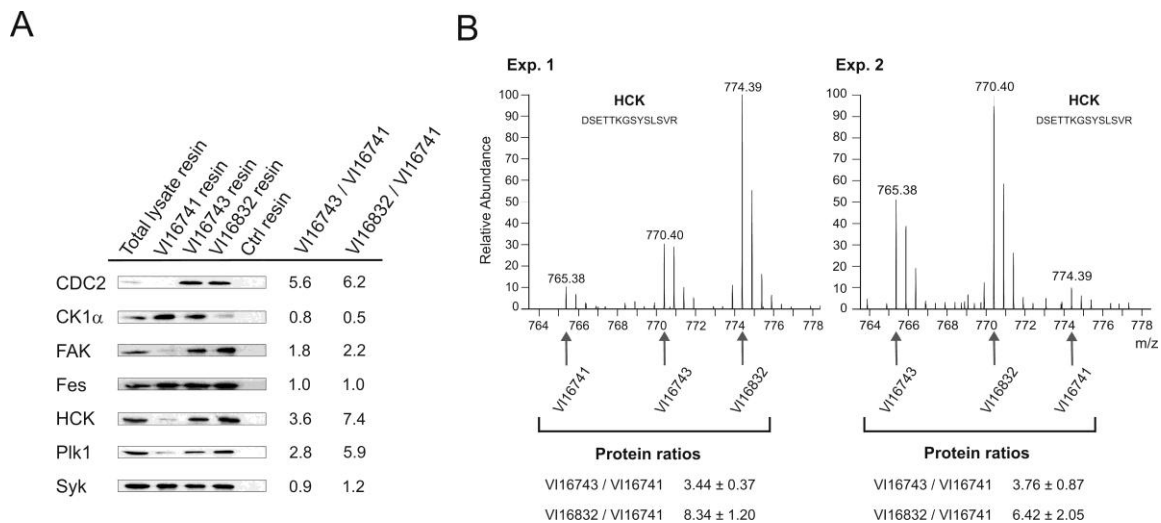


Figure 12: Analysis of protein kinases enriched with three different pyrido[2,3-*d*]pyrimidine-based affinity resins. (A) Aliquots of MV4-11 cell lysate and eluted protein from incubations with the indicated inhibitor resins or control (Ctrl) beads were separated by SDS-PAGE and immunoblotted with antibodies recognizing the kinases CDC2, CK1 α , FAK, Fes, HCK, Plk1 and Syk. For comparison, ratios of relative kinase binding according to the quantitative MS analysis are shown. (B) MS spectra of a HCK peptide detected as a triplet due to SILAC encoding. Upon swapped SILAC labeling relative ion intensities changed accordingly in replicate experiments. Peptide species derived from the different affinity purifications are marked by arrows and the resulting ratios are shown for both experiments.

As we used the averaged ratios from both individual SILAC-based quantitative MS experiments for the comparisons of the resins we further scrutinized the reproducibility of our SILAC-based quantification strategy. Therefore, protein kinase ratios obtained in biological replicate analyses were visualized in scatter plot (Figure 13A). Notably, independent experimental ratios for VI16743 *versus* VI16741 as well as for VI16832 *versus* VI16741 resin binding were highly similar, demonstrating high accuracy and reliability of the quantitative MS approach. Comparable results were obtained for the identified non-protein kinases (Figure 13B).

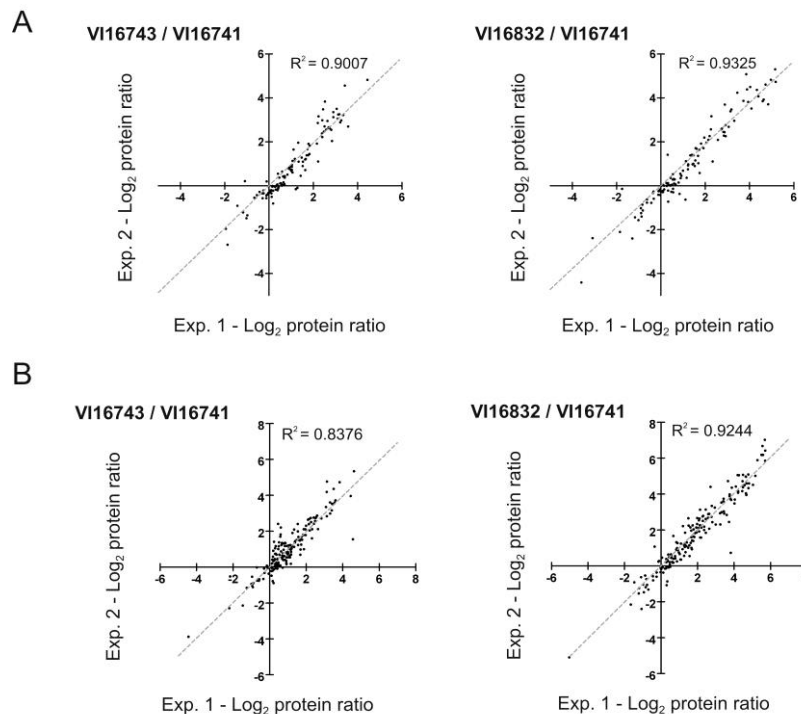


Figure 13: Comparison of protein kinases enriched with three different pyrido[2,3-*d*]pyrimidine ligands. Log₂ transformed ratios of proteins binding to the different resins are shown in scatter plot comparisons of two independent experiments for all protein kinases (A) and all other quantified non-

protein kinase proteins (B). Pearson correlation coefficients (R^2) close to one indicated an overall high concordance of measured protein ratios in biological replicates.

We next plotted the ‘ratio of ratio’ distribution from the biological replicate analyses (Figure 14) and determined the corresponding values for protein ratios that indicate preferential binding to one or the other resin with high confidence ($p < 0.01$). According to this assessment ratios of less than 0.38 or higher than 2.65 indicated resin-specific protein binding.

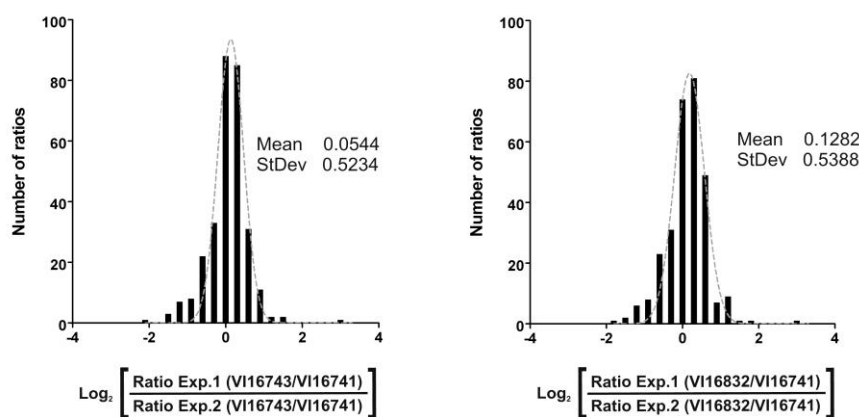


Figure 14: Reproducibility of protein binding in biological replicate analysis. Proteins were binned according their \log_2 values of the VI16743/V16741 or the VI16832/V16741 resin binding ratios. Gaussian regression analysis was applied to calculate the mean and standard deviation for the \log_2 transformed ratios-of-ratios.

For a more thorough analysis of the set of affinity resin enriched proteins we initially performed Gene ontology (GO) analysis of all quantified proteins. This analysis revealed highly significant overrepresentation ($p < 0.001$) of various GO molecular function terms directly linked to PKs like ATP binding, phosphotransferase activity and magnesium ion binding (Figure 15A). This information adds further proof for the effectiveness of the exploited kinase pre-fractionation resins. In addition, albeit PKs accounted for only about one third of all quantified proteins, they were on average quantified with three times more peptides compared to non-PK proteins pointing towards even higher enrichment efficiency as evident from the GO analysis.

To gain additional information on the non-PK proteins that were selectively enriched by the tested pyrido[2,3-*d*]pyrimidine-based affinity ligands, we next performed a GO analysis with

solely this subset of proteins (Figure 15B). This analysis revealed significant overrepresentation ($p < 0.001$) for multiple GO molecular function terms related to general nucleotide-utilizing enzymes such as oxidoreductases, dehydrogenases, and lipid kinase. Remarkably, these enriched enzymes comprised additional important signaling factors like phosphatidylinositol 3-kinase and phosphatidylinositol-4,5-bisphosphate 3- kinase, besides others. Moreover, the GO analysis of the non-PK proteins detected over-representation of the molecular function term “protein kinase binding” which resulted from specific co-purification of PK interactors such as various cyclins as well as other regulatory kinase subunits.

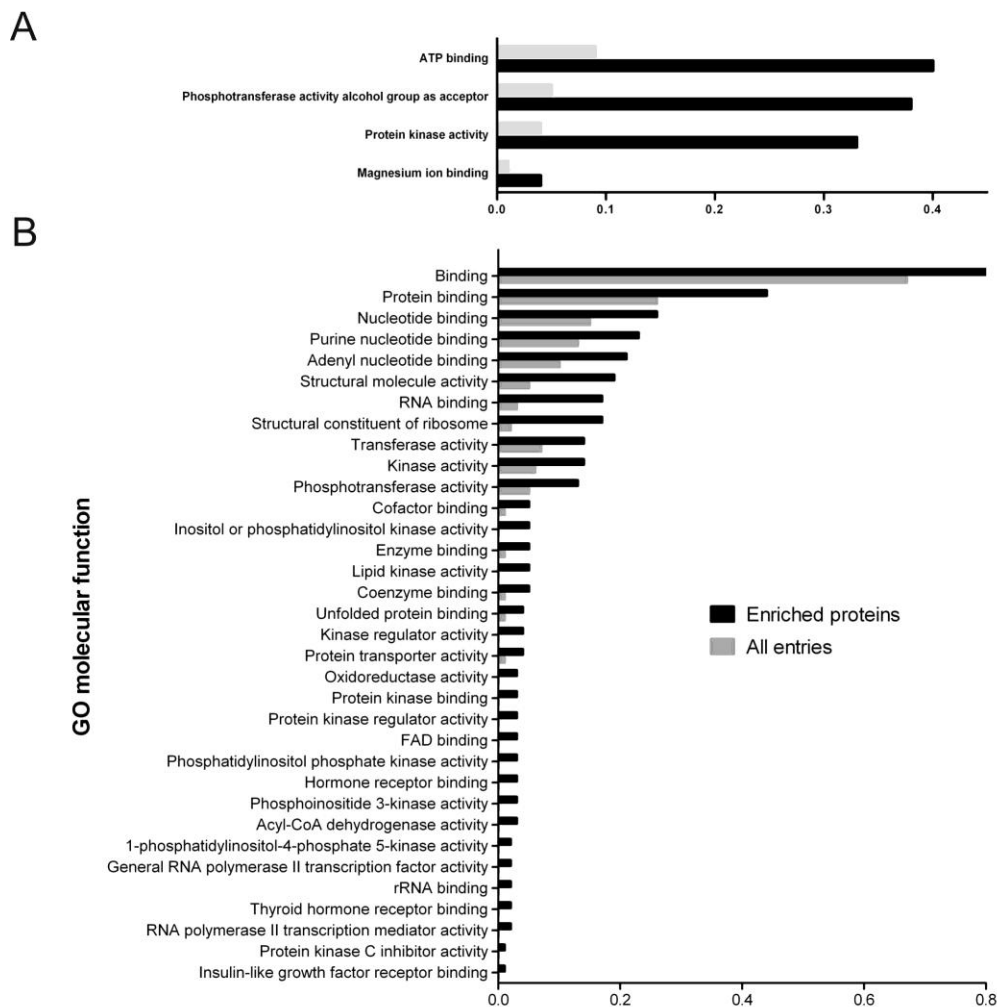


Figure 15: Gene ontology analysis of proteins enriched with immobilized kinase inhibitors. (A) All proteins, or (B) all non-protein kinases that were identified with at least one unique peptide upon

pre-fractionation by pyrido[2,3-*d*]pyrimidine affinity resins from MV4-11 cell extracts were compared to the entire list of IPI entries (IPI Human version 3.13). Selected, significantly over-represented GO molecular function terms ($p < 0.001$) are shown. Ratios represent the numbers of either inhibitor-enriched proteins or all IPI entries annotated to the listed GO molecular function term divided by the respective numbers of all proteins with annotated GO molecular function terms.

4.1.2 Comparative Kinase Expression Analysis in Different Cancer Cell Lines

As delineated above, the quantitative comparison of pyrido[2,3-*d*]pyrimidine affinity resins revealed efficient kinome pre-fractionation by the VI16743 and VI16832 resins. We choose to further employ the VI16832 affinity resin to monitor cell type-specific differences of relative kinase expression levels. Application of such an approach for a comparative analysis of tumor cells is particularly relevant, given that constitutive activation or overexpression of various members of the protein kinase superfamily has been described as important events in tumorigenesis. To test this strategy, a set of rather diverse cancer cell lines (MV4-11 leukemia, HCT-116 colon carcinoma and 435S melanoma-derived cells) were differentially SILAC-encoded prior to cell lysis. Total cell extracts were subsequently combined and subjected to VI16832 affinity resin chromatography, followed by sample processing and quantitative MS as described above for the quantitative affinity resin comparison (Figure 16).

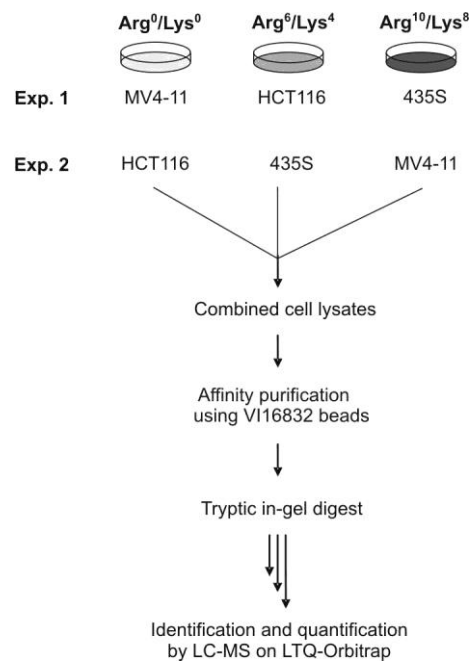


Figure 16: Schematic workflow for the comparison of protein kinase expression profiles. Three cancer cell lines (MV4-11 leukemia, HCT-116 colon carcinoma and 435S melanoma-derived cells) were differentially SILAC-encoded for quantitative MS-based comparison of VI16832-interacting sub-proteomes.

In total, more than 170 protein kinases and almost 40 other nucleotide-utilizing enzymes were identified and their relative expression levels in the three cancer cell lines were quantitatively assessed. We performed two replicate biological experiments and calculated the average protein ratios to evaluate the reproducibility of our experimental procedure. Therefore, protein ratios of biological replicate experiments were visualized in scatter plots (Figure 17). The overall high accuracy and trustworthiness of the approach were again indicated by high Pearson correlation coefficients (R^2).

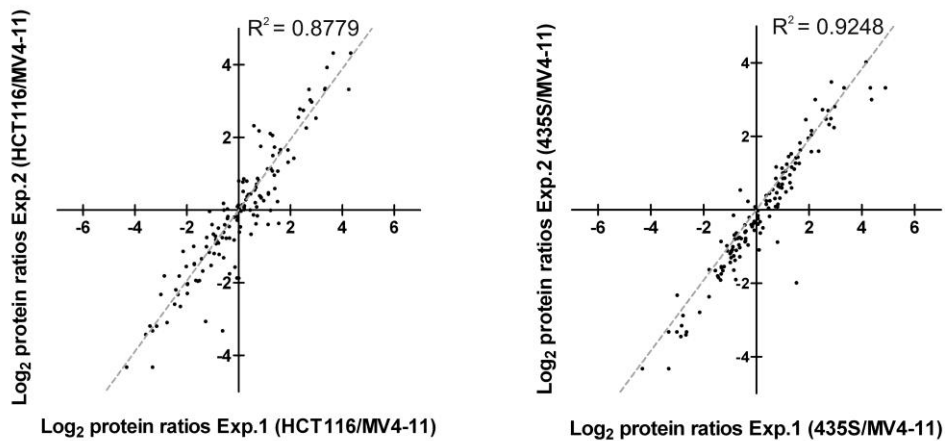


Figure 17: Concordance of expression analysis across different cancer cell lines in biological replicate experiments. Log_2 transformed protein ratios of cell line *versus* cell line expression are shown in scatter plot comparisons of two independent experiments. High Pearson correlation coefficients (R^2) indicated an overall high reproducibility of measured protein ratios in biological replicates.

To compare relative expression profiles for the set of quantified proteins we arbitrarily set the relative expression value in the cell line with the highest protein abundance to 100 %. Based on this the quantified ratios were then used to determine percentage values reflecting the relative expression in the other two cell lines. In cases where no peptide ion signals were recorded in one or two of the analyzed cell lines, expression values were set to 0 %. Next, we generated a heat map to analyze and categorize quantified PKs and other nucleotide-binding

enzymes according to their relative expression patterns across the three cancer cell lines (Figure 18).

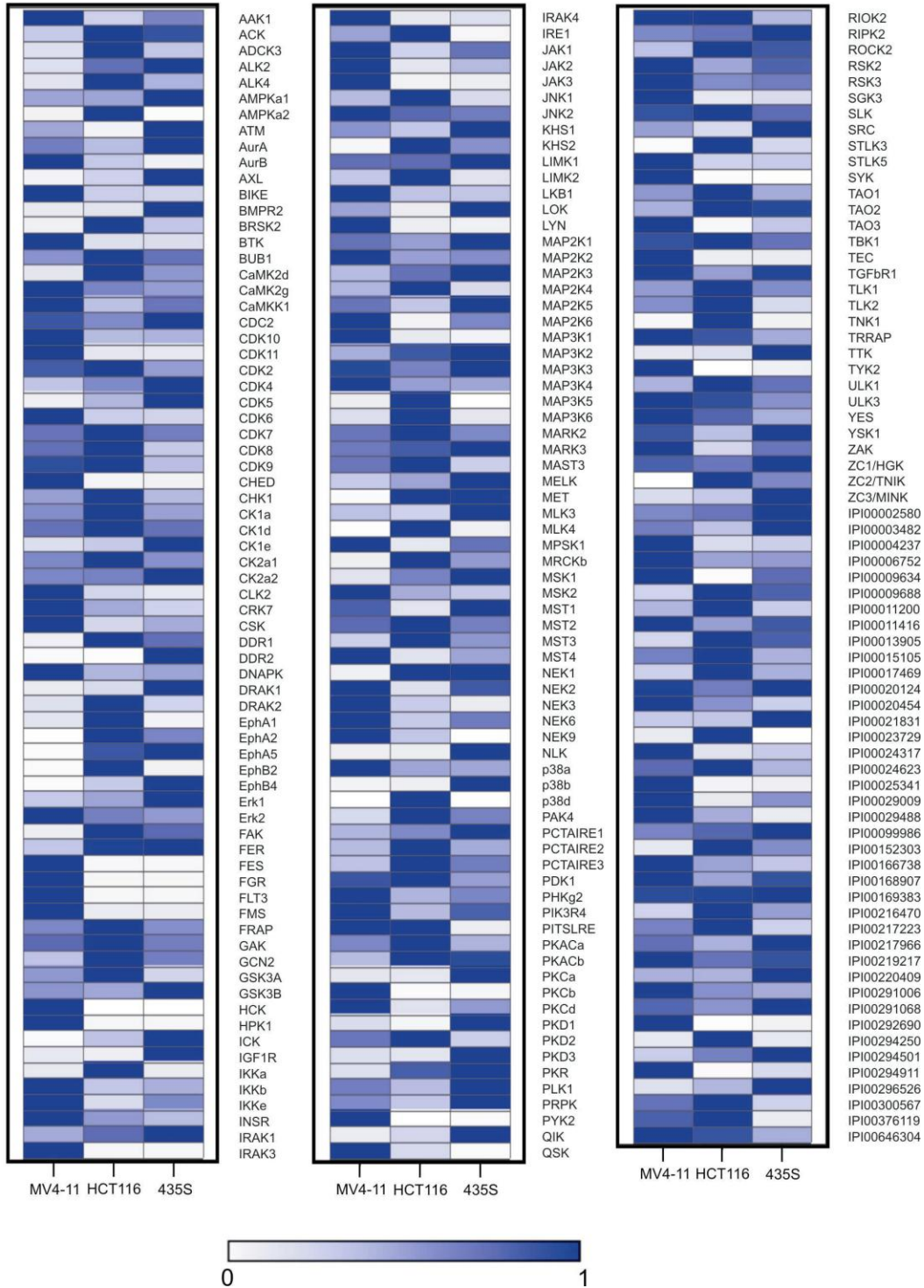


Figure 18: Comparative kinase expression analysis across different cancer cell lines. Quantified ratios for protein kinases and other nucleotide-binding proteins were transformed into relative expression levels with the highest expression in any of the three cell lines set to 1. Based on these values, a heat map was generated to visualize relative expression levels across the analyzed cancer cell lines.

Cells of the acute myelogenous leukemia (AML) cell line MV4-11 harbor an internal tandem duplication in the juxtamembrane domain of the FMS-like tyrosine kinase 3 (FLT3). This mutation is also present in a subset of AML patients and results in constitutive up-regulation of growth-promoting FLT3 tyrosine kinase activity²¹⁰. Strikingly, detection of FLT3 expression was exclusive to MV4-11 cells (Figure 18), demonstrating that our comparative analysis revealed this key oncogenic kinase in AML pathogenesis.

To verify that differential resin binding measured by quantitative MS reflects the actual cell type-specific kinase expression we furthermore performed immunoblot analysis with whole cell extracts by applying denaturing lysis conditions. Moreover, we thereby aimed to investigate whether the detected differences might be due to possible cell-type specific localization to certain cellular compartments, which might be more or less soluble under non-denaturing lysis conditions. These conditions are necessary to enable subsequent affinity purification of native PKs. In addition, these validation experiments were conducted with cells cultured in normal growth medium, to verify that the chosen SILAC approach does not provoke cell-type specific effects that might have caused some of the detected protein expression differences. As shown in Figure 19A for a set of selected PKs found to be differentially expressed in the analyzed cell lines, the immunoblot analyses were in good agreement with the measured SILAC ratios. This indicated that other potential sources of variation that could affect the affinity purification approach apparently had no major influence on the SILAC-based quantitative cell line comparisons.

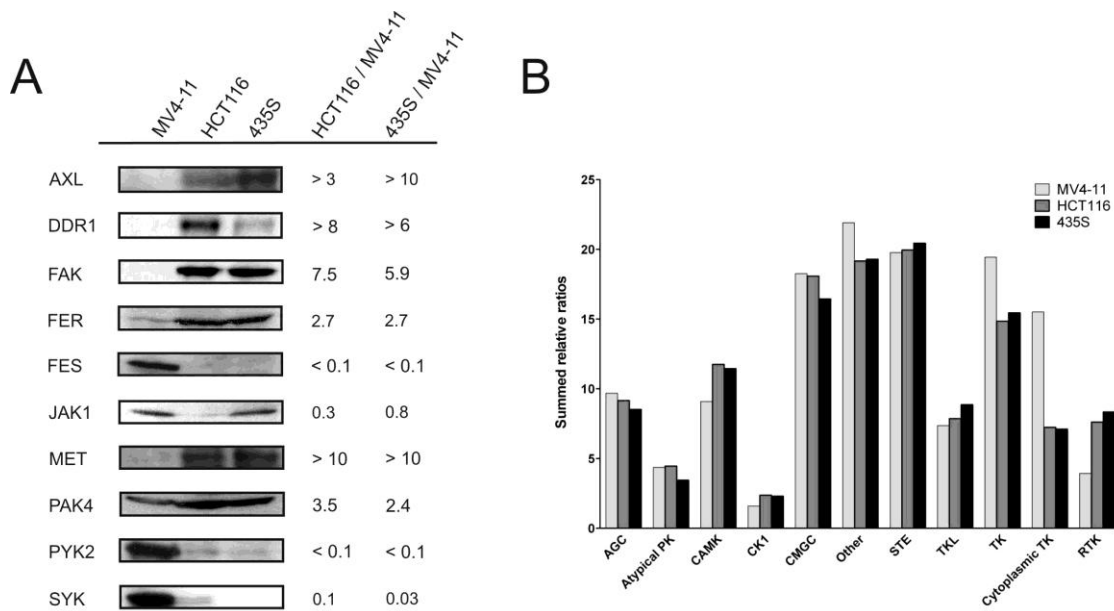


Figure 19: Immunoblot verification of MS-based kinase expression analysis across different cancer cell lines and comparison of kinase relative expression values according in the major groups of the kinome. (A) Total cell lysates of MV4-11, HCT116, and 435S cells were immunoblotted with antibodies recognizing the kinases Axl, DDR1, FAK, Fer, Fes, JAK1, Met, PAK4, PYK2, and Syk. For comparison, binding ratios according to the SILAC-based quantification of VI16832 resin-bound protein kinases are shown. (B) Summed relative expression values for the seven major kinase groups as well as the atypical and other kinases according to Manning et al. were compared for MV4-11, HCT116 and 435S cells. Members of the tyrosine kinase (TK) group were further subdivided into cytoplasmic and receptor tyrosine kinases.

For a more general comparative analysis of PK expression differences across the investigated cancer cell lines the relative expression values for all PKs of the seven major groups of the kinome as well as for the other and atypical kinases were summed (Figure 19B). In the majority of the groups this comparison revealed highly similar overall expression levels. Remarkably, when we divided the tyrosine kinase group into its cytoplasmic and receptor-type members, we found the summed relative expression level of cytoplasmic PTKs to be higher in the MV4-11 suspension cells compared to the adherent HCT116 and 435S cell lines. Notably, some PKs, namely several members of the Src family (Lyn, Fgr and HCK), Syk and the Tec family kinases (Btk and Tec), were expressed solely or at distinctly higher levels in MV4-11 cells. Interestingly, we also detected cases of an inverse expression of the closely related cytoplasmic PTKs. Fes and PYK2 were far more prominent in MV4-11 cells, whereas Fer and FAK were found in much higher levels in HCT116 and 435S cells. In

contrast to cytoplasmic PTKs, our analysis revealed an overall higher expression status of RTKs in the adherent cell lines HCT116 and 435S (Figure 19B).

4.1.3 Benchmark analysis of the PTM scoring algorithm

The analysis of site-specific phosphorylation events on PKs and other proteins is of particular relevance, as these PTMs can be indicative of their cellular catalytic activities^{166, 211}. Thus, the accurate localization of phosphorylation sites in phosphopeptides is of central importance in phosphoproteomics analyses. The algorithm implemented in the data analysis and quantitation software MSQuant and MaxQuant was originally described by Olsen *et al.*^{150, 212}. These software suites were utilized for automated, probability-based localization of phosphorylation sites in this study. The principles of this algorithm have been described in detail also by Daub *et al.*¹⁶⁶.

To validate the applied algorithm we analyzed a set of known synthetic and casein-derived phosphopeptides. The phosphorylation sites of casein derived phosphopeptides have been frequently analyzed and recently revisited²¹³. Thus, this set of phosphopeptides was selected to serve as a reference and each phosphopeptide was required to contain at least one non-phosphorylated residue. α - and β -casein were digested with trypsin and thereupon we enriched phosphopeptides utilizing TiO₂ microspheres¹⁶³⁻¹⁶⁴. About 500 fmol of each peptide were combined and analyzed by LC-MS/MS on the LTQ-Orbitrap. Next, we exploited Mascot for peptide identification and MSQuant was used to calculate the PTM scores for all phosphopeptide spectra and to determine phosphorylation site probabilities (Table 1).

Table 1: Analysis of synthetic- and casein-derived phosphopeptides for benchmarking of the PTM scoring algorithm.

Peptide (known sequence)	Origin	Sequence (identified)	Charge	Score	PTM score	pSTY	pSTY probabilities (PTM scoring)
ASpSPLNIGAYKK	synthetic	ASSPLNGAYKK	2	27	41.82	1	AS(0.5)S(0.5)PLNGAYKK
DpSEGRGpSGDGPgK	synthetic	DSEGRGSGDGPgK	2	26	48.23	1	DSEGRGS(1)GDGPgK
FSIAPSTIDQpSLR	synthetic	FSIAPSTIDQSLR	2	41	84.26	1	FSIAPSTIDQs(1)LR
GESSRSGpSDGTPGPGK	synthetic	GESSRSGSDGTPGPGK	2	16	17.53	1	GES(0.25)S(0.25)RS(0.25)GS(0.25)DGTGPGGK
KIGEGpTYGVVYK	synthetic	KIGEGTYGVVYK	2	51	101.78	1	KIGEGT(1)YGVVYK
KpTLCGTPNYIAPEVLgK	synthetic	KTLCGTPNYIAPEVLgK	2	74	28.02	1	KT(1)LCGTPNYIAPEVLgK
PpYLKTK	synthetic	PYLKTK	2	11	63.74	1	PYLKT(1)K
VNqIGTLpSEpSIK	synthetic	VNqIGTLSESik	2	30	64.21	2	VNqIGTLs(1)ES(1)IK
VNqIGpTLSESik	synthetic	VNqIGTLSESik	2	42	79.77	1	VNqIGT(1)LESik
VYgKpTSHLR	synthetic	VYgKTSHLR	2	51	126.36	1	VYgKT(1)SHLR
WVDYpSDK	synthetic	WVDYSDK	2	21	56.74	1	WVDY(0.5)S(0.5)DK
DIGpSEpSTEDQAMEDIK	casein alpha S1	DIGSESTEDQAMEDIK	2	51	35.73	2	DIGS(1)ES(1)TEDQAMEDIK
EQLpSTpSEENSK	casein alpha S2	EQLSTSEENSK	2	30	48.23	2	EQLS(1)TS(1)EENSK
FQpSEECQQTEDELQDK	casein beta	FQSEECQQTEDELQDK	2	89	138.22	1	FQS(1)EECQQTEDELQDK
NANEEEEYSIGpSpSpSEEpSAEVATEEVK	casein alpha S2	NANEEEEYSIGSSSEESA EVATEEVK	3	37	61.24	4	NANEEEEYS(0.75)IGS(0.75)S(0.75)S(0.75)EES(1)AEVATEEVK
KNTMEHVpSpSpSEESIlpSQETyK	casein alpha S2	NTMEHVSSSEESIlSQETyK	2	32	34.23	4	NTMEHVS(1)S(1)S(1)EES(1)ISQETyK
QMEAESIpSpSpSEEEIVPNSVEQK	casein alpha S1	QMEAESISSSEEEIVPNSVEQK	2	19	26.54	4	QMEAES(0.75)S(0.75)S(0.75)S(0.75)EEIVPNS(1)VEQK
RELEELNVPGEIVepSLpSpSpSEESITR	casein beta	RELEELNVPGEIVESLSSSEESITR	2	69	60.49	4	RELEELNVPGEIVES(1)LS(1)S(1)S(1)EESITR
TVDMepSTEVFTK	casein alpha S2	TVDMESTEVFTK	2	88	141.55	1	TVDMES(0.5)TD(0.5)EVFTK
TVDMepSTEVFTKk	casein alpha S2	TVDMESTEVFTKk	2	59	84.26	1	TVDMES(1)TEVFTKk
VPQLEIVPNSAEER	casein alpha S1	VPQLEIVPNSAEERLSMK	3	26	37.78	1	VPQLEIVPNS(1)AEERLSMK
YKVPQLEIVPNSAEER	casein alpha S1	YKVPQLEIVPNSAEER	2	75	126.01	1	YKVPQLEIVPNS(1)AEER

This dataset was then used to calculate the corresponding PTM precision and sensitivity in respect to the p-values of the phosphorylation site probability (Figure 20). Together, 27 out of the 37 phosphorylated residues were identified and assigned correctly with a p-value of 1. Notably, for all sites identified with a p-value of 1 there was no false assignment. For class I phosphorylation sites localized with a p-value of 0.75 or higher, the precision was still 94 % thus validating the PTM scoring algorithm as a reliable tool for the confident assignment of phosphorylated residues within identified phosphopeptides.

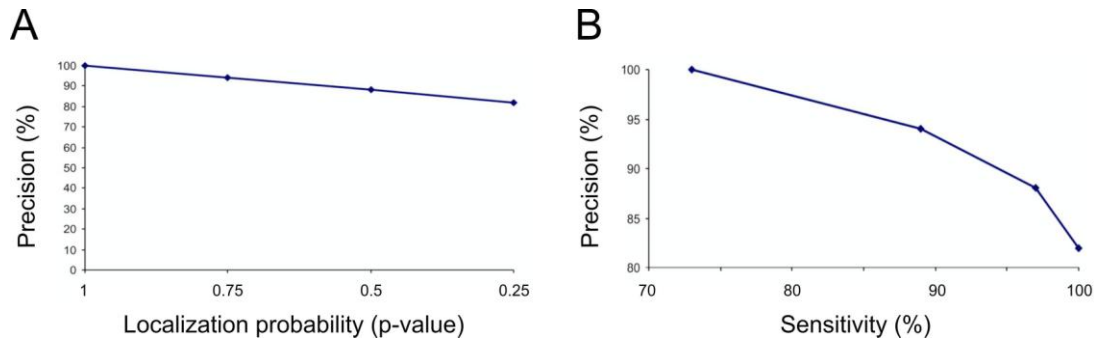


Figure 20: Benchmarking of the PTM Scoring Algorithm. The PTM scoring algorithm implemented in MSQuant and MaxQuant was benchmarked against a set of synthetic and casein-derived phosphopeptides. MSQuant was used to calculate the PTM scores for all phosphopeptide spectra and to determine phosphorylation site probabilities (see Table 1). The precision of the algorithm in relation to the p-values of the phosphorylation site probabilities (A) and its sensitivity of phosphorylation site identification (B) was analyzed. For all class I phosphorylation sites (p-value > 0.75) the precision was still 94 %.

4.1.4 Kinase-centric phosphoproteomics analysis of cancer cell lines

The coordinated regulation of kinase function occurs on multiple levels. Besides regulation on the respective expression level, catalytic activity can be modified by site-specific phosphorylations. Moreover, protein kinases can not only modulate each other's functions and activities through site-specific phosphorylations, but often also undergo specific autophosphorylation once they get activated¹². As many PKs represent key regulators in cellular signal transduction pathways, the comprehensive analysis of the PK phosphorylation state can provide valuable information about the activation state of phosphorylation-controlled signaling.

For the global analysis of site-specific phosphorylations on PKs pre-fractionation strategies have proven to be particularly useful^{166, 180}. In this study we demonstrated the effectiveness of the VI16832 affinity resin for the thorough comparison of PK expression pattern among different cancer cell lines. Furthermore, we aimed to exploit its potential for PK phosphoproteomics analysis. Therefore, we employed the VI16832 resin for PK enrichments from MV4-11, HCT116 and 435S cell lysates. In contrast to the above described inhibitor resin and PK expression level comparisons, which were conducted by batch-wise purification from cell extracts, we choose a column chromatography set-up to allow for the processing of larger amounts of cell-derived material^{166, 180}. Aliquots of each elution fraction of the PK pre-fractionation were analyzed by gel electrophoresis and silver-staining before protein-containing elution fractions were pooled and precipitated. To further reduce the sample complexity prior to subsequent phosphopeptide enrichment by means of TiO₂ microspheres¹⁶³⁻¹⁶⁴ the enriched protein samples were fractionated by 1D gel electrophoresis prior to trypsin digestion and phosphopeptide enrichment. All raw data files from the LC-MS/MS analyses derived from each cell line were merged and processed together. Identified phosphopeptides were further filtered for identifications with a false-discovery rate of less than 1 % for each individual experiment as described above. Site-specific identification of phosphosites was achieved by applying the computational PTM scoring algorithm implemented in the MSQuant software¹⁵⁰. The high accuracy of the PTM scoring algorithm has been demonstrated previously see chapter 5.1.3¹⁶⁶.

Taken together, the phosphoproteomics analysis of VI16832-enriched fractions from MV4-11, HCT116 and 435S cells resulted in more than 8,500 phosphopeptide identifications.

These translated into almost 1,700 distinct phosphopeptide species derived from 212 different members of the PK superfamily. In addition, we could identify more than 1,300 distinct phosphopeptides on 563 non-PK proteins. Together, these comprised more than 1,200 phosphorylation sites on PKs and about 900 phosphorylation sites on other non-PK proteins that were pinpointed with very high confidence ($p > 0.95$) (Table 2). The annotated MS/MS spectra of identified phosphopeptides are deposited and accessible through the Phosida database (<http://www.phosida.com>)²⁰⁰.

Table 2: Overview of the results from the phospho-kinome analysis. Numbers of identified phosphoproteins, phosphopeptide sequences, phosphopeptides and confidently assigned phosphorylation sites ($p > 0.95$) are shown either for protein kinases or for all other proteins analyzed upon VI16832 affinity chromatography.

	Protein kinase	Non protein kinase
Phosphoproteins	212	563
Phosphopeptide sequences	1431	1224
Phosphopeptides	1695	1329
Phosphosites (class I)	1201	904

To evaluate the distribution of phosphorylated PKs upon enrichment with the VI16832 resin across the human kinome we marked all PKs that were identified with at least one unique phosphopeptide and indicated their cell line origin in the dendrogram of the human kinome (Figure 21). Apparently, the VI16832 resin did not select for specific groups or families of the kinome as the more than 200 identified PKs are rather evenly distributed. Thus, this non-selective enrichment of PKs derived from all branches of the human kinome further highlights the utility of the VI16832 affinity resin as powerful enrichment tool for PKs, in particular if combined with subsequent phosphopeptide enrichment.

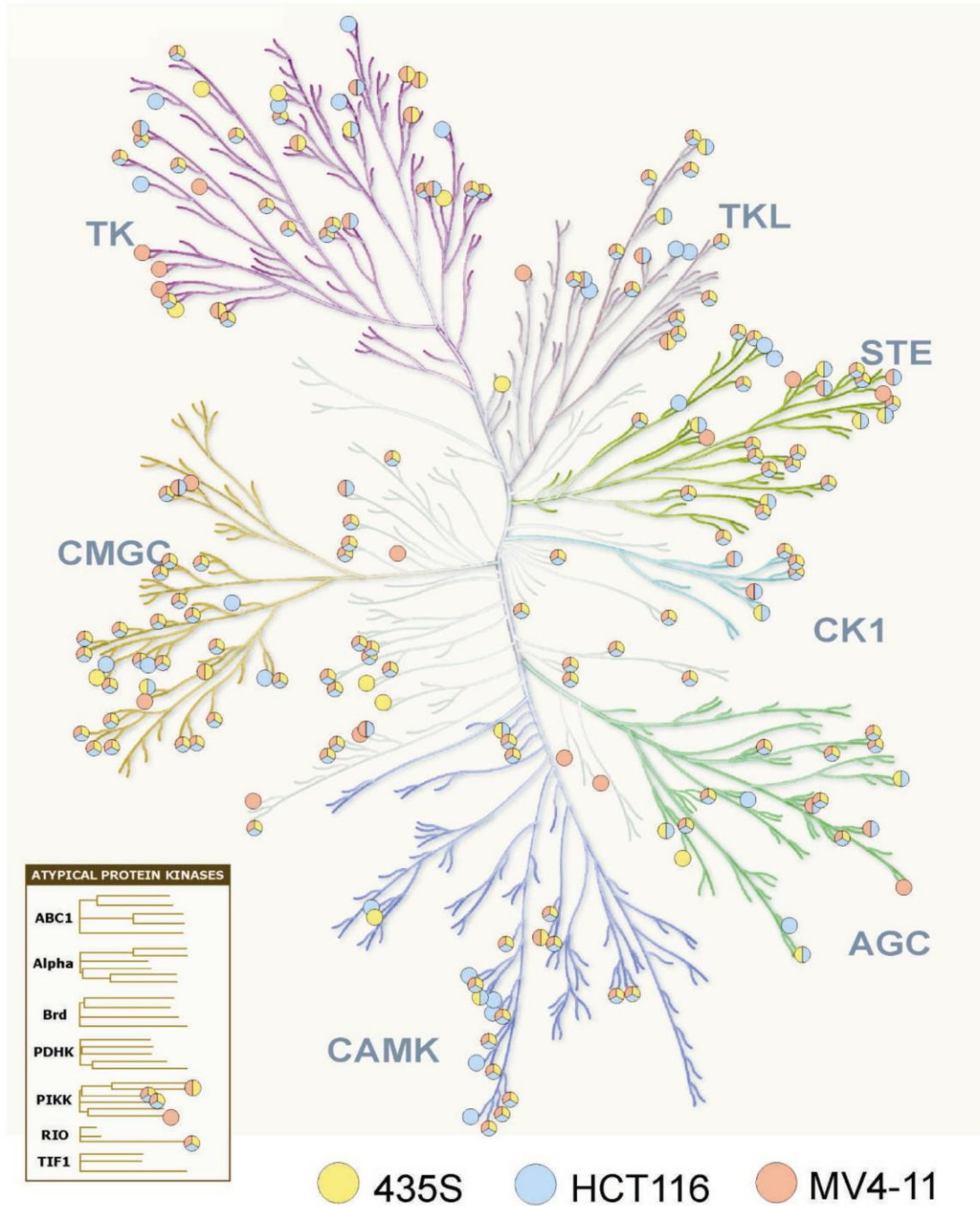


Figure 21: Phosphorylation site mapping across the human kinome. Protein kinase-derived phosphopeptides identified upon enrichment by VI16832 affinity chromatography are marked in the dendrogram of the human kinome⁸. Colors indicate in which of the analyzed cell lines phosphopeptides were identified. The kinome tree illustration was adapted with permission from Cell Signaling Technology, Inc. (<http://www.cellsignal.com/>).

About 50 % of the protein kinases were identified with phosphopeptides in all three cell lines (Figure 21). However, different phosphorylation sites were often identified on commonly expressed protein kinases, suggesting a considerable degree of cell type-specific phospho-

regulation of kinase functions. Therefore, we analyzed the cell line specific distribution of the identified phosphorylation sites on PKs as illustrated in the Venn diagrams shown in Figure 22. Importantly, the analysis of VI16832-retained proteins from the three distinct cancer cell lines considerably increased the overall number of identified phosphorylation sites on protein kinases.

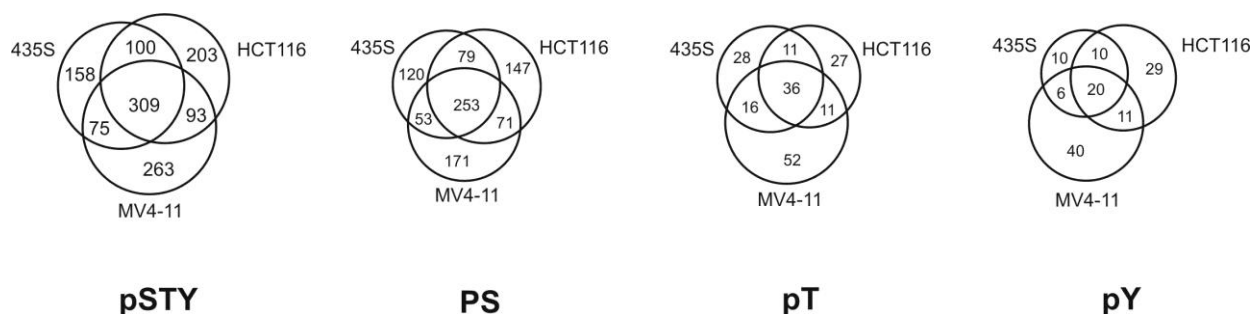


Figure 22: Comparison of identified phosphorylation sites in the analyzed cell lines. Cell line comparisons of the identified phosphorylation sites on protein kinases, which were confidently localized to specific serines, threonines or tyrosines (class I sites, $p > 0.95$). Numbers are shown for all phosphorylation sites combined (pSTY) and separately for phosphoserine, -threonine and -tyrosine (pS, pT and pY).

In addition to PKs, phosphorylation sites were also identified on various nucleotide-binding enzymes as well as other proteins including regulatory subunits of protein kinases (Table 2, Figure 23A). Notably, even if about two thirds of all proteins enriched through the VI16832 affinity resin accounted for non-PKs, PKs were on average identified with considerably more peptides per protein. Moreover, we summed the phosphopeptide signal intensities for all identified PKs and non-PKs and found more than 80 % to be derived from PKs captured by the VI16832 affinity resin (Figure 23A). The summed phosphopeptide intensities per protein kinase resemble a normal distribution (Figure 23B), which further underscores the remarkable dynamic range of the phosphoproteomics workflow applied in this study (Figure A. 1).

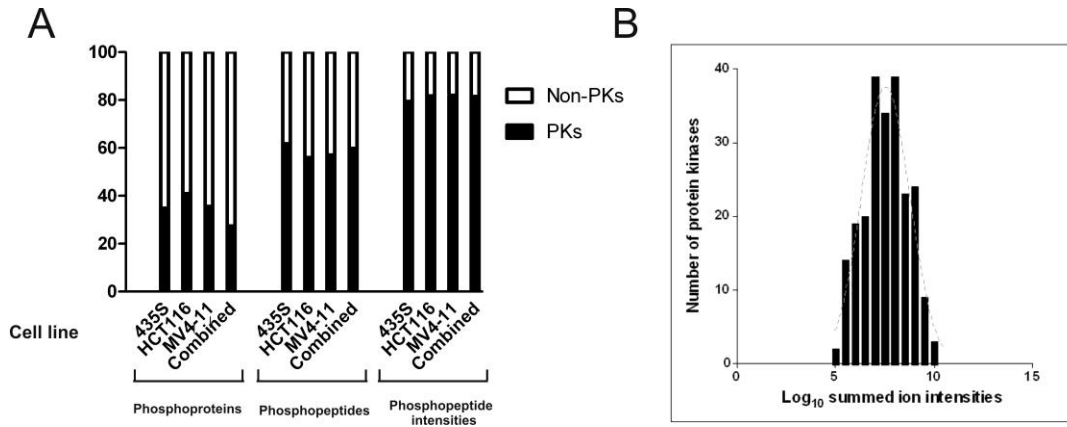


Figure 23: Efficiency of protein kinase pre-fractionation. To evaluate the efficiency of the VI16832 affinity resin for protein kinase pre-fractionation the relative distributions of protein kinases (PK) and all other phosphoproteins (non-PKs) are shown in respect to the numbers of identified proteins and phosphopeptides, and in respect to the sum of all phosphopeptide intensities.

The seminal analysis of cellular phosphoamino acid distribution by Hunter and Sefton revealed 0.05 % pTyr, 10 % pThr and 90 % pSer, 90%⁴. Recently, global phosphoproteomics analyses by Olsen *et al.* found phosphotyrosine to be more prominent as these results comprised about 2 % pTyr, 12 % pThr and 86 % pSer¹⁵⁰. Interestingly, when we analyzed the distribution of phosphoserine, -threonine and -tyrosine sites in our dataset we found tyrosine phosphorylation to be considerably more prominent on PKs than on non-PK proteins (Table 3). When we restricted our analysis to the activation segment of PKs tyrosine phosphorylation was even identified as the most abundant type of modification (Table 3, Figure 24).

Table 3: Distribution of Ser(P), Thr(P) and Tyr(P). Distributions of phosphorylation sites by amino acid are shown for affinity purified fractions from 435S, HCT116 and MV4-11 cells. Percentages are shown for protein kinases, for the activation loop regions of protein kinases and for all other phosphoproteins.

	% Ser(P)	% Thr(P)	% Tyr(P)
Protein kinases			
435S	78.5	14.1	7.4
HCT116	77.2	12.1	10.2
MV4-11	73.9	15.5	10.6
PK activation loop			
435S	32.2	28.8	39.0
HCT116	28.6	27.0	44.4
MV4-11	34.4	28.1	37.5
Other phosphoproteins			
435S	88.8	9.9	1.3
HCT116	90.1	9.5	1.4
MV4-11	86.3	9.2	4.5

PK catalytic activity is often induced once PKs adopt a dedicated conformational state upon phosphorylations in their activation segments. Thus, these specific modifications are crucial for activity control and information about the actual phosphorylation state of a PK activation segment can therefore indicate the respective kinase's cellular activity¹². Our study underpins the high importance of tyrosine phosphorylation for the activity control of kinase-mediated signal transduction. Altogether, PK-affinity enrichment by the VI16832 resin allowed the detection of these key regulatory modifications on more than 50 PKs as shown in Figure 24.

				435S	HCT116	MV4-11
ABL (ARG)	-----LVKVA DFGLSR IMTGD-----	-----TYTAHAGAKF-----	-----PIKWTAP ESL AYNK-----	X	X	X
ACK	-----LVKIG DFGLMR ALPQND-----	-----DHYV MQEHR KV-----	-----PFAWC AP ESLKRTR-----	X		
BARK1 (BARK2)	-----VRIS DLGLAC DFSS--KKK-----	-----PHA AVGT HGYMAPEVLQ--KGVA-----	-----	X		
BTK	-----VVKV SD FGLSR YV LDD-----	-----EY TSSV SGSKF-----	-----PVRW S PEV LM YSK-----			X
CDC2	-----DKGTIKLAD FGLAR -AFGIP--IR-----	-----VY THEV VT WLWYR PEVLLGS-----	-----	X	X	X
CDK4	-----SGGT VKLAD FGLAR- IYSY --QM-----	-----AL T PVV VT WLWYR PEV LLQS-----	-----		X	
CDK7	-----EN GV LKLAD FGLAK -SFGSP--NR-----	-----AY THQV VT WRWYR PEVLLFGA-----	-----	X	X	X
CDK9	-----RD GV LKLAD FGLAR -AFSLAK NSQPN -----	-----RY TNR V VT WLWYR PEV LLGE-----	-----	X	X	X
CDK10	-----DK GC VKTAD FGLAR - AYGV P--VK-----	-----IM TPK V VT WLWYR PEV LLGT-----	-----	X		X
CDKL5	-----HND V LK CD F GFAR -- NLSEGNNA -----	-----NY TEYV AT RYR PEVLLG-----	-----	X	X	
CHED	-----NR GQ IKLAD FGLAR - LYS -SEESRP-----	-----Y TNK V IT WLWYR PEV LLGE-----	-----	X	X	X
CK2a1 (CK2a2)	-----DHE HR KLRLID WGLAE --FYHP Q Q EYN -----	-----V RVAS RY FK PEVLLV DY -----	-----	X	X	X
CRK7	-----NS GQ IKLAD FGLAR - LYN -SEESRP-----	-----Y TNK V IT WLWYR PEV LLGE-----	-----	X	X	X
DYRK1A	-----IKIV DF GS SC -- QLQR -----	-----I YQY IQ S RFYR PEV LLG-----	-----	X	X	X
EphA1	-----CCK VSD FGL TR IL DD ED-----	-----G TYE TQ--GGK I -----	-----PIR WT AP EA IA HR I-----		X	
EphA2	-----VCK VSD FGL SR VLEDDP-----	-----E A Y T S--GGK I -----	-----PIR WT AP EA IS YR K-----	X	X	X
EphA3 (EphA4, A5)	-----VCK VSD F GMSR VLEDDP-----	-----E A A Y T R --GGK I -----	-----PIR WT AP EA IA YR K-----	X		
EphB2	-----VCK VSD FGL SR FLEDDT S -----	-----D P TY T SALGGK I -----	-----PIR WT AP EA IQ YR K-----		X	
EphB2	-----VCK VSD FGL SR FLEDDT S -----	-----D P TY T SALGGK I -----	-----PIR WT AP EA IQ YR K-----	X	X	
EphB3	-----VCK VSD FGL SR FLEDDP S -----	-----D P TY T S L GGK I -----	-----PIR WT AP EA IA YR K-----		X	
EphB4	-----VCK VSD FGL SR FLEEN S -----	-----D P TY T S L GGK I -----	-----PIR WT AP EA IA FR K-----	X		
EphB4	-----VCK VSD FGL SR FLEEN S -----	-----D P TY T S L GGK I -----	-----PIR WT AP EA IA FR K-----		X	
EphB4	-----VCK VSD FGL SR FLEEN S -----	-----D P TY T S L GGK I -----	-----PIR WT AP EA IA FR K-----	X	X	X
EphB4	-----VCK VSD FGL SR FLEEN S -----	-----D P TY T S L GGK I -----	-----PIR WT AP EA IA FR K-----		X	
Erk1	-----TTC DLK IC DF GLAR- I -AD PE HDHTG-----	-----FL TEYV AT RYR PEV IM LN S -----	-----	X	X	X
Erk2	-----TTC DLK IC DF GLAR- V -AD DP HDHTG-----	-----FL TEYV AT RYR PEV IM LN S -----	-----	X	X	X
Erk3	-----EDL V LKIG DF GLAR--IM DP HY S H K G-----	-----HL SE GL V TR KWYR PEV LL SP-----	-----	X	X	X
Erk5	-----EN C ELKIG DF GM ARG L- CTS PA EHQY -----	-----EM TEYV AT RYR PEV LM LS-----	-----		X	X
Erk7	-----AN C TVK CD FGLAR SL GD L PE GP EDQ-----	-----AV TEYV AT RYR PEV LL SS-----	-----		X	X
FAK	-----CVK L GD F GL SR Y M ED ST -----	-----Y YK AS K G K L-----	-----PIK WM AP ES IN F RR-----	X	X	X
FAK	-----CVK L GD F GL SR Y M ED ST -----	-----Y YK AS K G K L-----	-----PIK WM AP ES IN F RR-----	X		
FAK	-----CVK L GD F GL SR Y M ED ST -----	-----Y YK AS K G K L-----	-----PIK WM AP ES IN F RR-----	X	X	
FER	-----VLK IS DF GMSR Q ED GG-----	-----V Y SS S G--L RQ I-----	-----PIK WT AP EA LN YR G-----	X	X	X
FGR	-----ACK I AD F GLAR L L KDD -----	-----E YN PC Q SK F -----	-----PIK WT AP EA AL F GR-----		X	
FLT3	-----VVK I CD F GLAR D IM S D S -----	-----N Y V R GNAR L -----	-----P V K WM AP ES LF E GI-----	X	X	X
GSK3B (GSK3A)	-----DT AV LK CD F GS AK-- QLV R-- GE -----	-----I NV S Y IC S RYR AP EL I FGA-----	-----	X	X	X
HCK (Lyn)	-----VCK I AD F GLAR V IED N -----	-----E Y T A RE G AK F -----	-----PIK WT AP EA IN F GS-----	X	X	X
HIPK1 (HIPK2)	-----V K VID F GSAS-- HV SK A -----	-----V C ST YL Q S RYR AP EL I LG-----	-----	X	X	X
HIPK3	-----V K VID F GSAS-- HV SK T -----	-----V C ST YL Q S RYR AP EL I LG-----	-----		X	
ICK	-----PEL V K--I A D F GLAR-- E IR S K P -----	-----P Y T D Y V ST RYR AP EL LL S -----	-----	X	X	X
INSR (IGF1R)	-----T V KIG DF GM TR D I Y E T D -----	-----Y Y --R K GG G LL-----	-----P V R WM AP ES L K D GV -----		X	
IRE1	-----K I K A M S DF L CK L AV GR H S F S -----	-----R R SG V PT E GW I AP EL ML S ED C KE-----	-----		X	
JNK1 (JNK3)	-----SD CT LK IL DFGLAR-- T AG T S F -----	-----M M T P Y V VT RYR AP EL VL G -----	-----		X	
JNK2	-----SD CT LK IL DFGLAR-- T ACT N F-----	-----M M T P Y V VT RYR AP EL VL G -----	-----	X	X	X
LOK	-----D F GV S AK N L K T-----	-----L Q R D S F I G T P Y WM AP EV VM C ET M K-----	-----	X	X	X
LOK	-----D F GV S AK N L K T-----	-----L Q R D S F I G T P Y WM AP EV VM C ET M K-----	-----	X	X	
MAP3K2	-----D F GA S K R I Q T IC L S G T G-----	-----M K S V T G T P Y WM AP EV IS G -----	-----	X	X	X
MAP3K5	-----D F G T S K R L AG IN P-----	-----C T E T F T G T L Q Y M AP E I D K G P-----	-----		X	
MET	-----T V K V AD F GLAR D Y D KE-----	-----Y Y S V H N K T G A K L -----	-----P V K WM AP ES L S L Q T O K-----		X	
MST3 (YSK1)	-----D F GV A G Q L T D T -----	-----Q I K R N T F V G T P E W M AP E V I K-----	-----	X		X
NEK1	-----L G D F GIAR V LN-----	-----S T VE L AR T CI G T P Y L EL IC EN-----	-----	X	X	
NEK6	-----L G D L GL R FF S -----	-----S E T T AA H S L VG T P Y Y M SP E R I HE-----	-----		X	
NEK7	-----L G D L GL R FF S -----	-----S K T T AA H S L VG T P Y Y M SP E R I HE-----	-----		X	
NLK	-----S N CVL K IC DF GLAR-- V E L DE S R-----	-----H M T Q EV T Q Y YR AP EL M GS-----	-----	X	X	X
p38a	-----E D CELK IL DFGLAR-- H T D D-----	-----E M T G Y V AT RYR AP EL ML N W-----	-----	X	X	X
p38b	-----E D CEL R IL D FGLAR-- Q A D E-----	-----E M T G Y V AT RYR AP EL ML N W-----	-----	X		
PDK1	-----I Q IT D F G T A K V L S P E S K Q A -----	-----R A N S F V G T A Q Y S PE L L T --E K S-----	-----	X	X	X
PKAcA (PKAcB, PKAcG)	-----I Q VT D F G FA K R V K G -----	-----R T W T LC G T P EY L A P E I L-- S K G -----	-----	X	X	X
PKD1 (PDK3)	-----V K L CD F G FA R I I GE K S-----	-----F R R S V G T P AY L AP EL VL LN K-----	-----	X	X	X
PKD1 (PDK2, PDK3)	-----V K L CD F G FA R I I GE K S-----	-----F R R S V G T P AY L AP EL VL LN K-----	-----	X	X	X
PKG1	-----A K L V DF G FA K K I G F G-----	-----R T W T FC G T P EY V A P E I L-- N K G -----	-----		X	
PLK1	-----V K IG DF GLAT K VEY D GE-----	-----R K K T LC G T P NY I A P E V LS K -----	-----		X	
PLK1	-----V K IG DF GLAT K VEY D GE-----	-----R K K T LC G T P NY I A P E V LS K -----	-----	X		
PRPK	-----I V LID F GL S FISAL P ED-----	-----K G V D L V Y L E K AF L S-----	-----		X	
PYK2	-----C V K L GD F GL S RY I E D ED-----	-----Y Y K A S V TR L -----	-----PIK WM AP ES IN F RR-----	X		X
PYK2	-----C V K L GD F GL S RY I E D ED-----	-----Y Y K A S V TR L -----	-----PIK WM AP ES IN F RR-----		X	X
RIPK2	-----F H V K IAD F GL S K WR -----	-----M M S L S Q S R S S K S A-----	-----P E G G T I I Y M P EN Y E P G Q K S -----	X	X	
RIPK2	-----F H V K IAD F GL S K WR -----	-----M M S L S Q S R S S K S A-----	-----P E G G T I I Y M P EN Y E P G Q K S -----	X		
RIPK2	-----F H V K IAD F GL S K WR -----	-----M M S L S Q S R S S K S A-----	-----P E G G T I I Y M P EN Y E P G Q K S -----			X
RSK2 (RSK3, RSK4)	-----I K L T DF L S K E S I D HE-----	-----K K A S F C G T V E Y M AP EV V N --R R G-----	-----	X	X	X
RSK3	-----I K L T DF L S K E A I D HE-----	-----K K A S F C G T V E Y M AP EV V N --R R G-----	-----	X	X	X
RSK2_2 (RSK3_2)	-----L R IC D F G FA K Q L R A E-----	-----N G L I M T EC Y T A N F V A P E V L K R Q G -----	-----	X	X	X
SLK	-----D F GV S AK N T R T-----	-----I Q R D S F I G T P Y WM AP EV VM C ET S K-----	-----	X		X
SLK	-----D F GV S AK N T R T-----	-----I Q R D S F I G T P Y WM AP EV VM C ET S K-----	-----	X	X	X
TBK1	-----I G ED G S V Y K L T D F GA R E L ED D -----	-----E Q F S LY G T E E Y L H P D MY R AV L R K -----	-----		X	X
YES (FYN, LCK, SRC)	-----V C K I AD F GLAR L IED N -----	-----E Y T A R Q AK F -----	-----PIK WT AP EA LY R -----	X	X	X
ZAK	-----D G V L IC D F G A S R-----	-----F H N-- H T T H M S L V-----	-----G T FP WM AP EV IQ S L P -----	X		

Figure 24: Identified phosphorylation sites in the kinase activation loop region of protein kinases. Phosphopeptides with at least one confidently assigned phosphorylation site (class I, in bold red) in at least one cell line (marked by X) are shown and highlighted in yellow. Additional class III phosphorylation sites are shown in light red. Cell lines in which the same sequence and number of phosphorylations was found in the absence of site-determining information are indicated by X. In case activation segment phosphopeptides are shared among different members of the expressed kinome, alternative protein kinases are indicated in parentheses.

To compare the qualitative phosphoproteomics dataset generated in this study with other large-scale studies focusing on phosphorylation events on PKs we utilized the data available

from three previous quantitative phosphoproteomics studies on human proteins. In their global analysis of EGF-mediated signaling Olsen *et al.* identified almost 6,000 site-specific phosphorylation events¹⁵⁰. Our generated dataset comprises about four times more phosphorylation sites assigned to PKs compared to the 270 of that study. In addition, our data identified about twice as much phosphorylation sites on PKs as found by Dephoure *et al.* in their analysis of mitotic phosphorylation¹⁶⁷. Moreover, when compared to a previous quantitative analysis of our group that detected 1,007 confidently localized phosphorylation events on PKs of which many were regulated in a cell cycle-dependent manner¹⁶⁶, the 1,201 PK-assigned phosphorylation sites of this study even exceed the number identified in this previous study. In addition, even if there is a high overlap between these two studies, PK phosphorylation analysis upon VI16832 affinity resin enrichment identified more than 600 additional sites (Figure 25). Thus, at the time of its publication, this study represented the most comprehensive phosphoproteomics analysis on PKs.

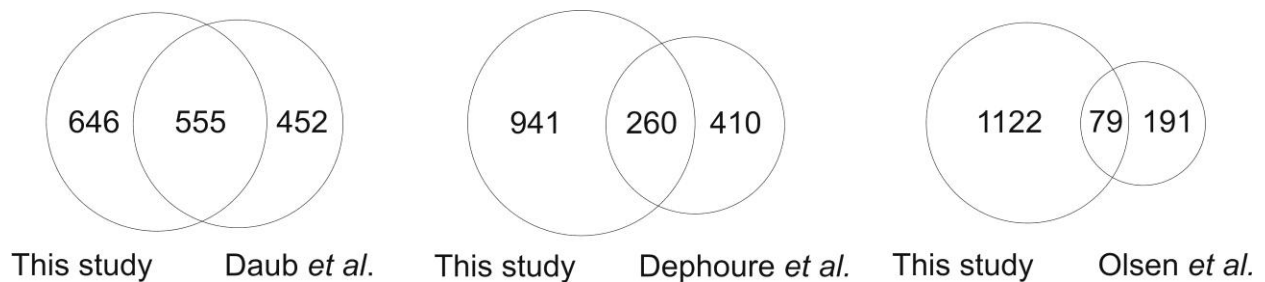


Figure 26: Comparison of kinase-derived phosphorylation sites in large-scale phosphoproteomics datasets. Overlap of the identified class I phosphorylation sites derived from protein kinases in this study ($p > 0,95$) with the sites reported in previous study by Olsen *et al.* (class I, $p > 0,75$), Dephoure *et al.* (Ascore >13 , $p > 0,95$) and Daub *et al.* (class I, $p > 0,75$)^{150, 166-167}.

4.2 Identification of cellular imatinib targets and imatinib-sensitive phosphorylation sites

The targeted inhibition of deregulated protein kinase activity has evolved as major therapeutic concept in treating human cancer²¹⁴. In case of chronic myelogenous leukemia (CML) there is a direct link between the expression of the fusion protein Bcr-Abl and the emergence of this multiproliferative disease of hematopoietic stem cells²². Therefore, inhibition of the Bcr-Abl kinase activity by the small molecule kinase inhibitor imatinib has proven highly efficient for treating patients in the chronic phase of the disease⁶⁸⁻⁶⁹. However, during continued treatment, especially during more advanced disease stages, resistances often occur^{71, 73}. Thus, in addition to a detailed knowledge of the cellular targets of imatinib, a comprehensive understanding of the downstream mediators of Bcr-Abl signaling is of crucial importance for the identification of potential candidate proteins for novel therapeutic intervention strategies.

4.2.1 Multicolumn-based protein kinase affinity chromatography

We aimed to develop a strategy that integrates the identification of potential direct cellular targets of a small molecule inhibitor as well as mediators of associated downstream signaling cascades in a single experiment. Therefore, we choose the well characterized inhibitor of the Bcr-Abl fusion protein, imatinib, to test our experimental strategy.

Initially, we analyzed the effect of different imatinib concentrations and treatment times in the human myeloid leukemia cell line K562²¹⁵ by immunoblot analysis of total cell lysates using a phosphotyrosine-specific antibody. After 24 h we detected a marked reduction in global tyrosine phosphorylation with an imatinib concentration of 10 μ M (Figure 26B). Thus, to compare early and late effects of cellular imatinib-responsiveness, we choose to culture K562 cells in 10 μ M imatinib for either 90 min or 16 compared to DMSO-treated cells that served as control. We reasoned that binding of imatinib to either the ATP-binding pocket of a PK or other nucleotide-utilizing protein should result in reduced retention of these proteins by the PK-selective affinity resins. Thus, according to this rationale, proteins detected in

reduced amounts compared to the control cells should either represent direct targets of imatinib, like Bcr-Abl, or interacting proteins of such direct targets

Efficient pre-fractionation strategies that utilize multiple kinase-selective molecules with rather broad selectivity have been developed and shown to enable global MS-based analysis of PKs^{57, 166, 180}. To further improve this technique we included an additional compound, termed VII6741, to a previous five-resin multicolumn approach developed by our group¹⁶⁶. The molecular structures of all six compounds employed for the modified multicolumn PK enrichment approach are depicted in Figure 26A. To allow successive protein-binding to the distinct kinase-selective affinity resins the four columns were connected in series (Figure 26C). The experimental workflow of the entire experiment is depicted in Figure 26D. For quantitative MS analysis three populations of K562 cells were cultured for six cell doublings in different SILAC medium containing either ‘light’ (Arg0/Lys0), ‘medium’ (Arg6/Lys4) or ‘heavy’ (Arg10/Lys8) isotopic variants. Cells were then supplemented with 10 μ M imatinib (‘medium’ and ‘heavy’) or DMSO (‘light’) as control and cultured for another 16 hours (‘light’ and ‘heavy’) or 90 minutes (‘medium’) prior to cell lysis (Table A. 1). Cleared cell lysates were mixed in a 1:1:1 ratio and loaded onto the affinity resins at 4°C in the dark to avoid possible light-induced decay of the affinity resin inhibitors. In case of the purvalanol B affinity resin an initial specific elution with an excess of free inhibitor was performed. Thereupon, all columns were reconnected and submitted to an unspecific elution with SDS-containing buffer. Elution fractions were collected and aliquots were analyzed by SDS-PAGE and silver-staining (data not shown). The protein-containing fractions were pooled followed by lyophilization, and then precipitated in aliquots according to the protocol of Wessel & Flügge. To enhance the overall analytical depth we combined two MS sample separation-strategies. One half of the proteins were separated according to their respective molecular weight by 1D gel electrophoresis prior to tryptic protein digestion of six distinct molecular weight regions. The other part was subjected to tryptic digestion in-solution and resulting peptide mixture was separated by SCX into seven consecutive fractions^{150, 166}. A fifth of the gel-extracted peptides was used for subsequent total peptide enrichment and desalting by C₁₈ StageTip purification¹⁹⁴. The larger remainders and the complete SCX-derived peptide fractions were subjected to phosphopeptide enrichment by means for TiO₂ microspheres¹⁶³⁻¹⁶⁴. All samples were analyzed in LC-MS/MS analyses with the LTQ-

Orbitrap. Initially, raw file processing and quantification was done with MSQuant as described above. For a recent re-analysis the results of which are shown here MaxQuant was utilized²¹⁶.

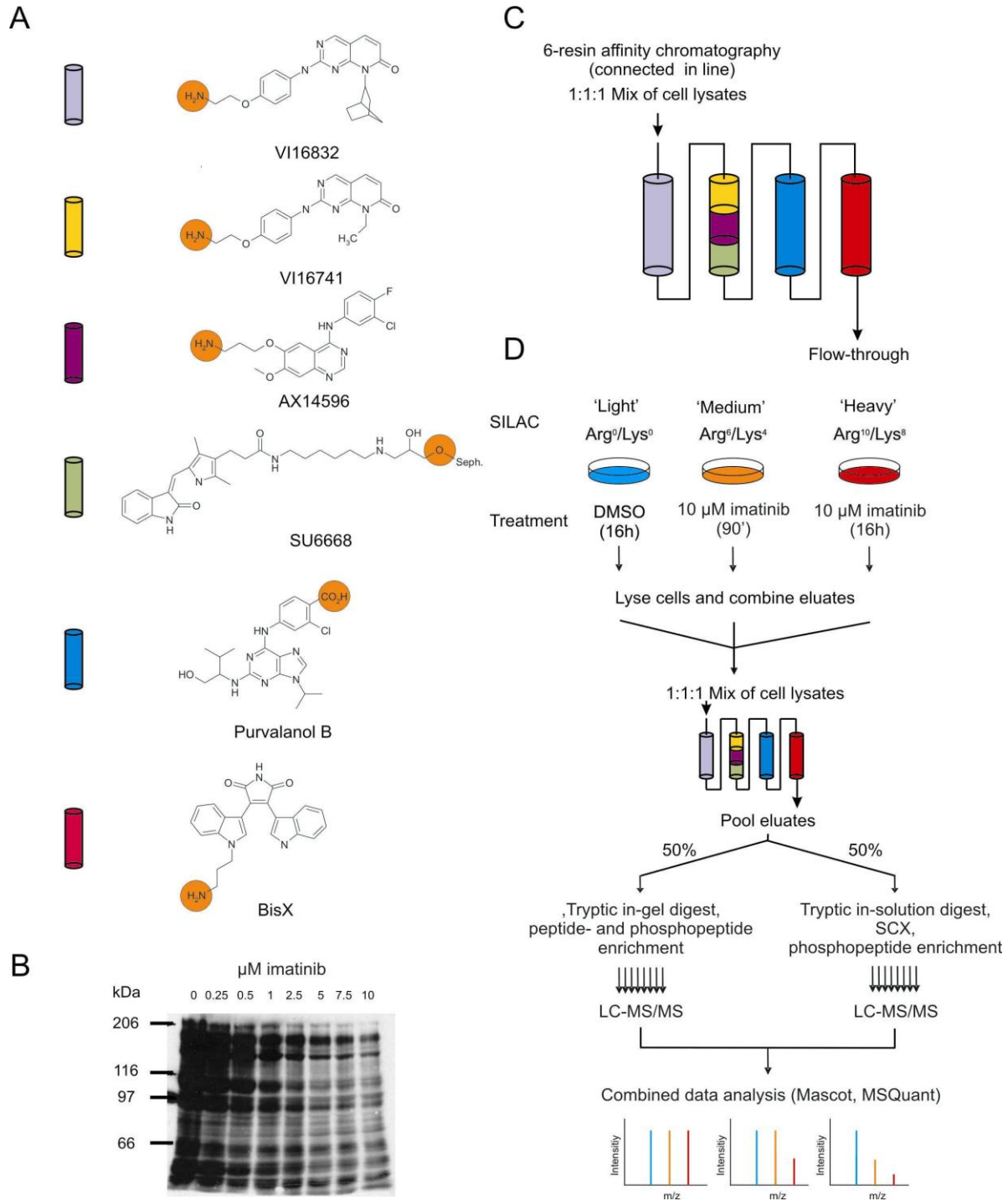


Figure 26: Column-based, 6-resin affinity chromatography for protein kinase pre-fractionation. (A) Molecular structures of the compounds utilized for generating the affinity resins. The reactive group used for immobilization of the respective compound on a Sepharose matrix is indicated by an orange circle. (B) K562 cells were treated with different imatinib concentrations for 24h before cell lysis and immunoblot analysis with a pTyr-specific antibody. (C) PK pre-fractionation was conducted by a combination of six distinct PK-selective affinity resins employed in a multicolumn affinity chromatography approach. Mixed cell lysates derived from differently treated, SILAC-encoded, K562 cell populations were loaded onto four serially connected columns containing the respective affinity resin (indicated by the color-code) and bound proteins were subsequently eluted. (D) K562 cells, grown in cell culture dishes, were differentially SILAC-encoded before treatment with 10 μ M imatinib or DMSO for 90 minutes and 16 hours, respectively. The combined elution fractions were split in two parts. One part was separated by 1D gel electrophoresis prior to tryptic protein digest. The major part of the extracted peptides was used for phosphopeptide enrichment by means of titanium dioxide before LC-MS/MS analysis. The remainders of each fraction was enriched and desalted via C₁₈ StageTips and directly analyzed. The other part of the pooled elution fractions was subjected to a tryptic in-solution digest. Peptides were then fractionated by strong cation exchange (SCX) chromatography and collected peptide fractions were used for phosphopeptide enrichment.

The determined ratios of selected proteins like Abl1, Abl2, BCR and Grb2 are shown in Table 4. Notably, in case of the main target of imatinib Bcr-Abl no protein-ratios were determined as we detected only phosphorylated peptides that cannot be utilized for protein quantification. In addition, for the reported Bcr-Abl interactor Grb2^{50, 217} no significant reduction in protein binding upon imatinib treatment was observed. Moreover, as shown for SYK and NQO2, two other reported targets of imatinib^{57, 218}, we detected only a slight reduction in protein binding according to quantified protein species from imatinib-treated samples. Thus, these results indicated that the employed multicolumn affinity approach did not allow the identification of potential direct cellular targets of imatinib. This was likely due to imatinib exchange reactions among proteins derived from differentially labeled and treated cells that occurred post-lysis prior to chromatographic separation.

Table 4: Selected identified- and quantified proteins upon 6-resin affinity chromatography. Ratio M/L reflects the protein derived from K562 cells treated for 90 minutes with 10 μ M imatinib compared to the DMSO-incubated control cells. Ratio H/L reflects the protein derived from K562 cells treated for 16 hours with 10 μ M imatinib compared to DMSO-treated control cells. n.a., protein ratio was not determined.

Accession no.	Protein Names	Gene Names	Ratio M/L	Ratio H/L
IPI00221171	Proto-oncogene tyrosine-protein kinase ABL1	ABL1	n.a.	n.a.
IPI00329488	Tyrosine-protein kinase ABL2	ABL2	n.a.	n.a.
IPI00004497	Breakpoint cluster region protein	BCR	n.a.	n.a.
IPI00021327	Growth factor receptor-bound protein 2	GRB2	0.74	0.86
IPI00021326	Src homology 2 domain-containing-transforming protein C1	SHC1	n.a.	n.a.
IPI00018597	Spleen tyrosine kinase	SYK	0.65	0.75
IPI00219129	NAD(P)H dehydrogenase, quinone 2	NQO2	0.84	0.85

Nevertheless, we could quantify more than 1,100 class I phosphosites ($p > 0.75$) and this set comprised unique phosphopeptides of about 130 distinct PKs. Among others, we detected phosphopeptides for Abl1, Abl2 and SHC1, some of which showed more than twofold down-regulation upon imatinib-treatment (data not shown).

4.2.2 Parallel, batch-wise processing for protein kinase enrichment

Above we described that kinase enrichment by a multicolumn approach did not allow to identify potential direct targets of imatinib. Therefore, we decided to develop a different strategy for this project - the simultaneous processing of multiple cell lysates in parallel, batch-wise affinity enrichments. Furthermore, as we demonstrated in the PK-selective affinity resin comparisons that the VI16832 resin captures a higher number and larger amount of PKs compared to the VI16741 resin, the latter material was not included anymore and we used a mix of kinase inhibitor resins containing the immobilized compounds VI16832, purvalanol B, bisindolylmaleimide X, AX14596 and SU6668.

In addition, we modified our previously applied experimental workflow as depicted in Figure 27. K562 cells were grown in SILAC medium for five cell doublings on 15 cm dishes and then transferred into spinner flasks. After two further rounds of cell division, K562 cells were treated with either 1 μ M or 10 μ M imatinib or were control-incubated with DMSO for 90 min (Table A. 1). Cell pellets were aliquoted, snap-frozen and stored at -80°C until cell lysis.

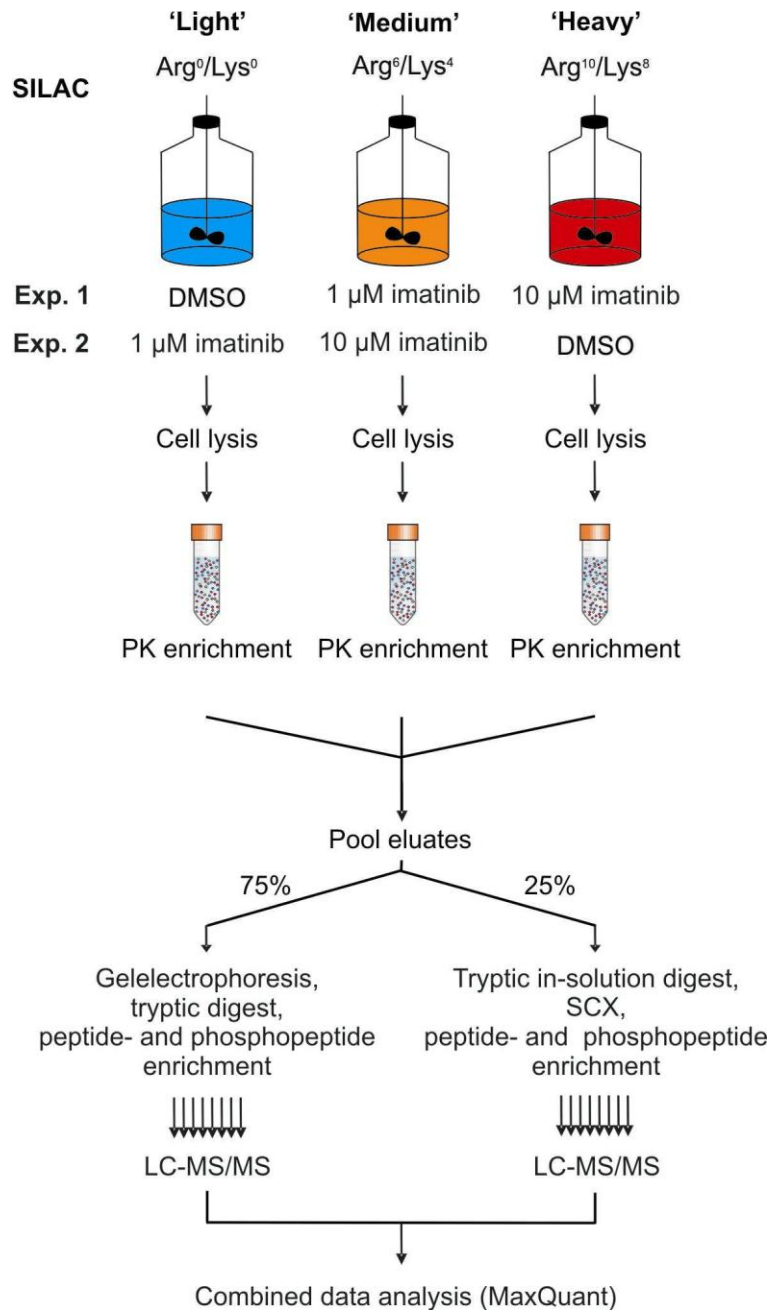


Figure 27: Schematic workflow for the MS-based identification of potential imatinib targets in combination with phosphoproteomics analysis in K562 cells by batch-wise, parallel kinase enrichment. SILAC-encoded K562 cells were grown in spinner flasks before treatment with the indicated concentrations of imatinib or DMSO as control for 90 minutes. Upon cell lysis, protein kinases (PK) were enriched separately for each SILAC state by batch-wise incubations with a combination of five different PK-selective affinity resins. Enriched proteins were eluted and combined. The bulk of the combined elution fractions (75 %) were separated by 1D gel electrophoresis prior to tryptic protein digest. The major part of the extracted peptides was used for phosphopeptide enrichment utilizing titanium dioxide before LC-MS/MS analysis. The remainders were filtered via C₁₈ StageTips and directly analyzed. The smaller part of the pooled elution fractions (25 %) was subjected to tryptic in-solution digests and peptides were thereupon fractionated by strong cation exchange (SCX) chromatography. The major part

of these collected fractions was used for phosphopeptide enrichment. Peptides in the remainders were extracted with C₁₈ StageTips and directly analyzed. Peptide identification and quantification was conducted with MaxQuant.

Equal amounts of the respective cell lysates were individually incubated for PK pre-fractionation. An aliquot of each elution fraction was analyzed by SDS-PAGE and silver-staining. Protein-containing elution fractions were pooled, lyophilized and then precipitated. A quarter of this material was in-solution digested and afterwards separated in seven fractions by means of SCX as described above. The larger remainder was separated by 1D gel electrophoresis, but, in contrast to the previous experiment, the gel was cut into 16 distinct molecular weight regions. In both replicate analyses, 20 % of every fraction of the gel-extracted peptides or from each SCX fraction were directly desalted with C₁₈ StageTips¹⁹⁴. The remaining peptides were subjected to TiO₂-based phosphopeptide enrichment¹⁶³⁻¹⁶⁴. Two consecutive fractions of the gel-extracted peptides were combined resulting in 8 phosphopeptide enrichments from gel-derived material. Upon LC-MS/MS all generated raw files were collectively processed with the MaxQuant software suite²¹⁶. In total, the analysis of two biological replicate experiments resulted in the quantification of more than 1,200 proteins with a false-discovery rate of below 1 % (Table 5). More than half of them were detected in both biological replicate experiments. In case of the 183 quantified PKs about two thirds were repeatedly detected.

Table 5: Overview of quantified phosphosites and proteins after batch-wise 5-resin protein kinase pre-fractionation. Numbers of quantified and confidently assigned phosphorylation sites ($p > 0.75$), protein kinases and non-protein kinase proteins are shown for the two biological replicate experiments individually as well as the resulting experimental overlap and total numbers of the whole study.

	Experiment I	Experiment II	Overlap	Total
All proteins	1170	788	683	1275
Protein kinases	170	150	137	183
pSTY ratios (all proteins)	1472	1268	898	1842
pSTY ratios (PK)	705	667	504	868

Altogether, more than 1,800 confidently assigned phosphorylation sites (class I, $p > 0.75$) were quantified (Table 5). About half of these were derived from PKs. Again, the

phosphosites derived from PKs revealed a slightly higher overlap between the two biological replicate experiments compared to all quantified phosphosites. The distribution analysis of site-specific phosphorylations revealed that about 81 % of all quantified events were on serine residues whereas 13 % and 6 % were located on threonine and tyrosine residues, respectively (Table 6). Compared to our previous analysis (see chapter 4.1.4), this indicates a slight increase in the overall level of tyrosine phosphorylation which might reflect the constantly active tyrosine kinase activity of the Bcr-Abl fusion protein in the untreated K562 control population.

Table 6: Distribution of Ser(P), Thr(P) and Tyr(P). Distributions of phosphorylation sites by amino acid are shown for 5-resin pre-fractionated proteins from K562 cells. Percentages reflect all quantified class I phosphosites ($p > 0.75$) derived from the two biological replicate experiments.

% Ser(P)	% Thr(P)	% Tyr(P)
81.1	13.2	5.7

Next, we analyzed whether our experimental concept of parallel, batch-wise PK pre-fractionations upon prior imatinib treatment enabled us to reach our major goal – the identification of direct targets for a small molecule inhibitor. Therefore, we applied rather restrictive cut-off criteria and required all proteins to be quantified in both biological replicate experiments. In addition, candidate imatinib targets had to exhibit reduced binding to the PK-selective affinity resins by at least a factor two in case of SILAC-encoded cell population treated with 10 μ M imatinib. Obviously, proteins that fulfill these criteria will not only comprise direct cellular imatinib targets but in addition also their interaction partners.

The quantified protein ratios were \log_2 transformed and plotted for the two replicate experiments. Notably, this analysis revealed the known imatinib target Bcr-Abl and its associated signal transducers Grb2 and SHIP2^{50, 217} to be markedly reduced already upon exposure to 1 μ M imatinib (Figure 28A). In accordance with the reported high affinity of imatinib for Bcr-Abl, the binding of Bcr-Abl to the multi-inhibitor resin was almost completely suppressed upon treatment of K562 cells with 1 μ M imatinib. In addition, we detected a comparatively pronounced reduction in protein retention for discoidin domain receptor 1 (DDR1). This receptor tyrosine kinase has recently been identified as a high-affinity target of imatinib by Bantscheff and colleagues⁵⁷. Furthermore, our analysis revealed

imatinib-dependent competition for quinone reductase 2 (NQO2) and the tyrosine kinase Syk. Again, these two enzymes have been reported as additional imatinib targets^{57, 207, 218}.

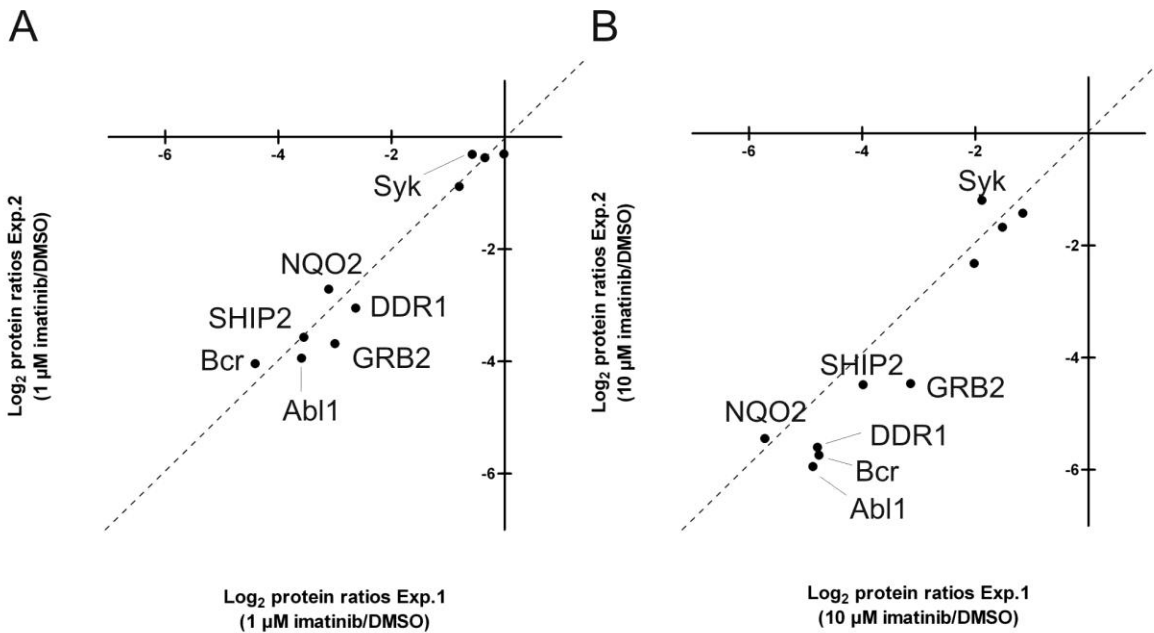


Figure 28: Identified direct and indirect cellular imatinib targets. Log₂ transformed protein ratios are shown in scatter plot comparisons of the two biological replicate experiments (A) after 1 μM imatinib treatment, (B) after 10 μM imatinib treatment.

In addition to establishing an experimental strategy for the identification of direct targets of small molecule kinase inhibitors, the second goal of this study was to conduct an integrated phosphoproteomics analysis to identify protein kinases in downstream signaling cascades of direct imatinib targets. Therefore, we set stringent cut-off criteria and only considered sites that were either more than twofold regulated in both experiments or showed an average regulation of greater than twofold with both ratios differing by a factor of less than two. Notably, solely on the Bcr-Abl protein we quantified 15 tyrosine phosphorylated peptides which showed strongly reduced phosphopeptide ratios. In cases in which regulated phosphopeptides derived from a direct or indirect imatinib target are detected, special precaution is warranted, as these quantified ratios likely reflect a combination of reduced protein retention and cellular dephosphorylation. Very low SILAC ratios, caused by strong reduction of the amount of retained protein upon imatinib treatment, are difficult to measure with high accuracy due to the limited dynamic range of SILAC-based quantification. Thus,

we did not consider regulated phosphorylation events on Bcr-Abl and its interacting proteins in our subsequent analysis.

In contrast to direct cellular imatinib targets, imatinib treatment would not affect inhibitor resin binding of downstream kinases but instead result in the repression of site-specific phosphorylations. Therefore, we calculated \log_2 transformed phosphopeptide ratios of the biological replicate analyses and visualized these in scatter plots (Figure 29). As indicated by the dense cloud around \log_2 values of zero the majority of the quantified phosphorylation events remained unchanged upon imatinib treatment. However, we observed consistent down- or up-regulation on about 70 distinct phosphorylation sites upon treatment of K562 cells with the higher imatinib concentration.

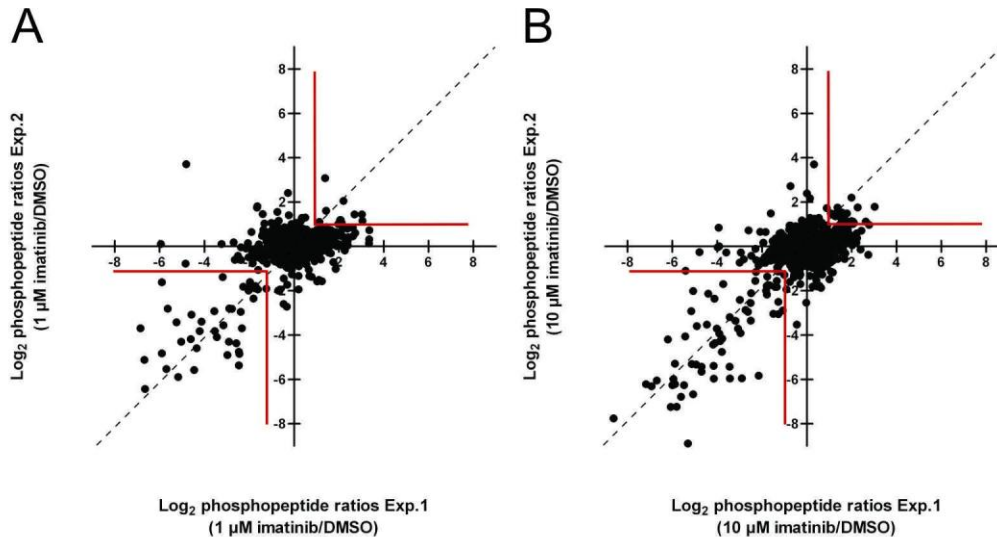


Figure 29: Concordance of quantified phosphopeptide ratios upon previous imatinib treatment. \log_2 transformed protein ratios are shown in scatter plot comparisons of the two biological replicate experiments (A) after 1 μM imatinib treatment, (B) after 10 μM imatinib treatment. The red lines indicate phosphopeptides that are more than twofold regulated in both experiments.

Notably, for a considerable number of identified phosphoproteins our experimental approach provided additional information on the retained relative protein amount. Therefore, for almost two thirds of all quantified phosphosites we could normalize the reported ratio according to measure protein abundance levels. A selected list of proteins, which were found to comprise imatinib-sensitive phosphorylation sites normalize for protein abundance, such as FAK, Syk and Plk1, is shown in Table A. 2. Among others, we observed a dose-dependent

down-regulation on pTyr-551 of the cytoplasmic tyrosine kinase BTK, with an almost 70 % reduction measured for the 10 μ M imatinib concentration (Figure 30A). Importantly, quantification of non-phosphorylated peptides from BTK revealed that comparable protein amounts were retained by the inhibitor resin from imatinib-treated cells. In addition, we detected a similar regulation on pTyr-774 of the receptor tyrosine kinase EphB4 (Figure 30B).

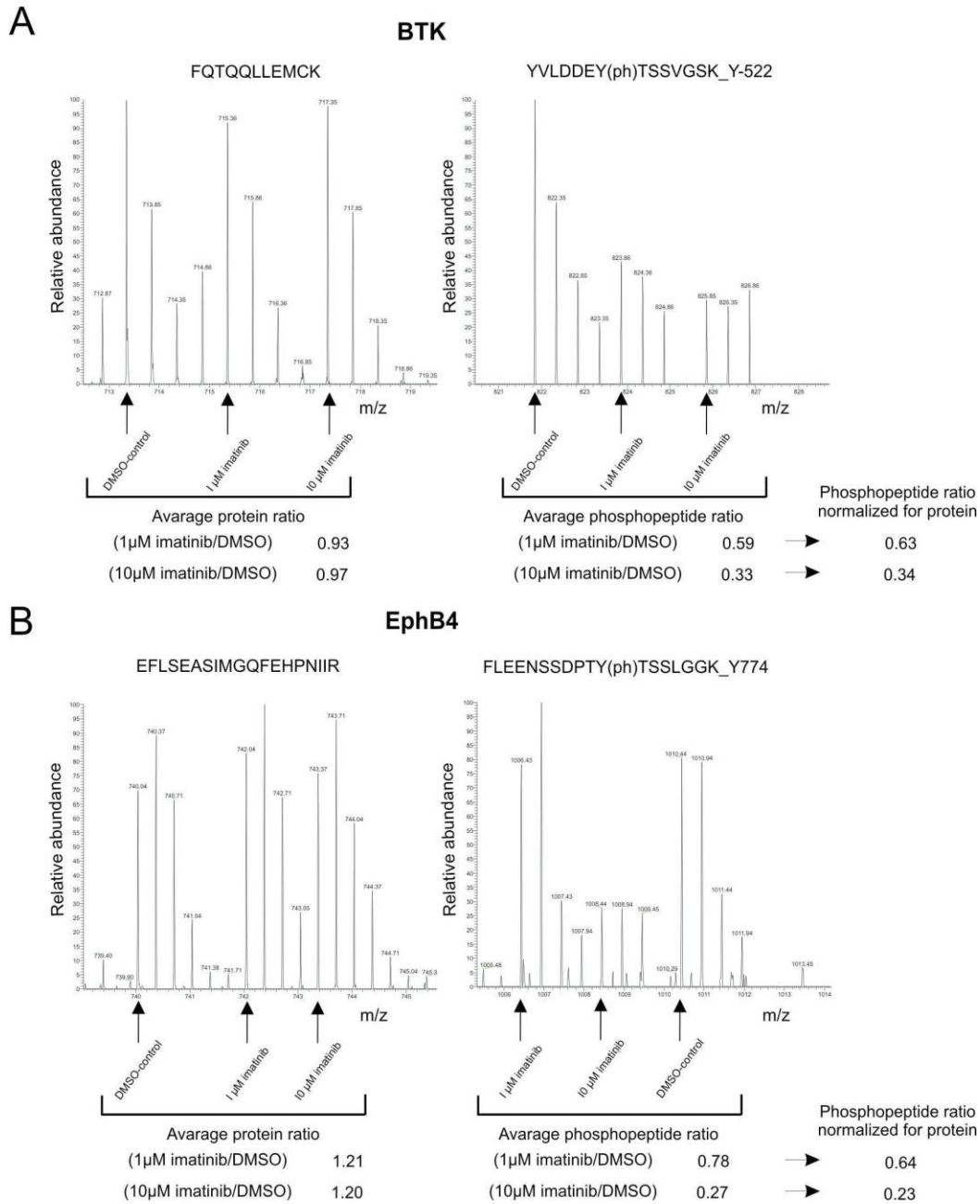


Figure 30: Imatinib-sensitive phosphorylation sites. MS scan of a typical unmodified peptide representing the amount of protein (left side) and a specific class I phosphopeptide ($p > 0.75$) that was found to be sensitive to imatinib treatment (right side). These proteins are therefore classified as mediators in the signaling cascade downstream of direct imatinib targets. The respective treatment of the SILA-encoded K562 cell population, as well as the resulting quantified peptide ratios and the protein-normalized phosphopeptide ratios are indicated below. The peptides shown are derived from the tyrosine kinase BTK (A) and the receptor tyrosine kinase EphB4 (B).

Notably, we not only identified down-regulated phosphorylation events but also detected a total of 24 proteins that harbor phosphorylation sites that were reproducibly up-regulated upon treatment with 10 μ M imatinib (Figure 24). Besides others, these included Polo-like-kinase 1, TTK, Wee1 and Myt (Table A. 2).

4.2.3 Analysis of the phosphotyrosine-containing sub-proteome upon imatinib treatment

Among cellular phosphorylation events the phosphorylation of tyrosine residues is the least abundant. In addition to recent global phosphoproteomics analyses, e.g. by Olsen *et al.* (ref.), this was also evident from experiments reported in this thesis. As a consequence, global phosphopeptide enrichment strategies such as TiO_2 - or IMAC-based methods often reveal rather few pTyr sites although these modifications often have important regulatory functions. However, in contrast to phosphorylated serine and threonine residues, antibodies with high affinity and specificity for phosphotyrosine-containing proteins or peptides have been generated. To monitor imatinib-induced changes on the cellular phosphotyrosine level with maximum sensitivity we cultured SILAC-encoded cell populations for 90 minutes either in the presence of 10 μ M imatinib or DMSO as control in two biological replicate experiments (Figure 31A; Table A. 1). Upon cell lysis tyrosine phosphorylated proteins were immunoprecipitated by anti-phosphotyrosine antibodies captured on protein-A Sepharose beads. Subsequently, phosphopeptide enrichment and MS analysis were performed as described above and MaxQuant was used for quantification.

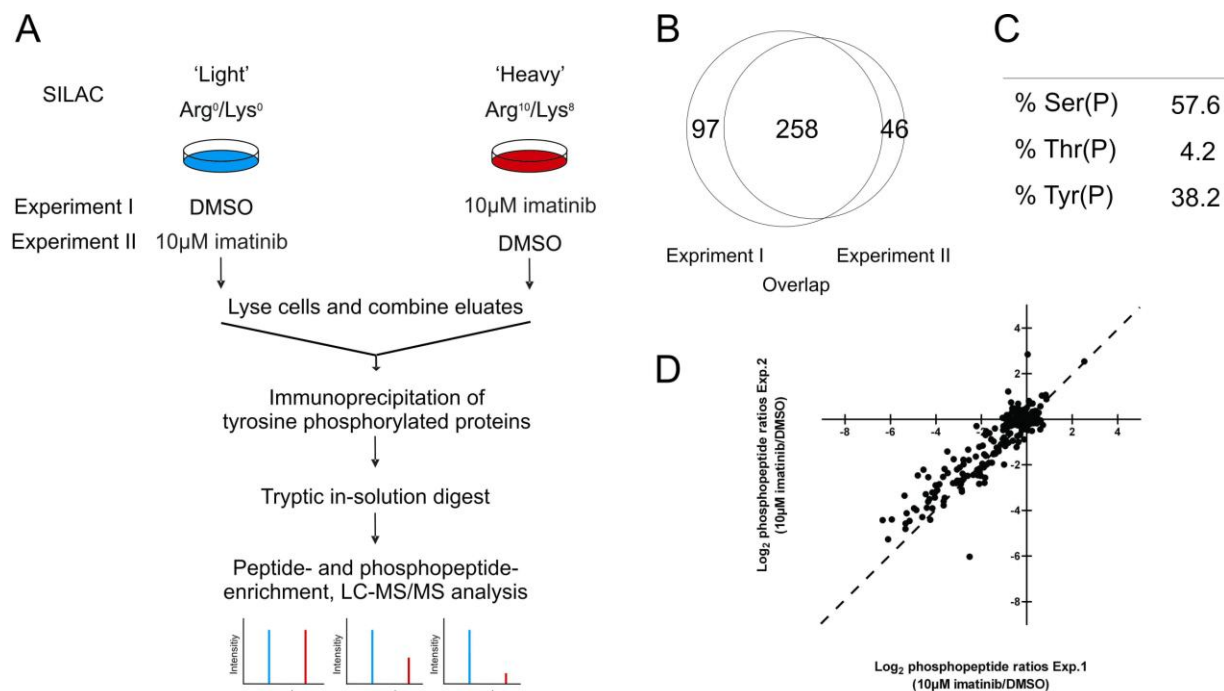


Figure 11: Experimental scheme and overview of quantified phosphosites upon imatinib treatment and immunoprecipitation of tyrosine phosphorylated proteins. (A) SILAC encoded cells were incubated with either 10 μ M imatinib or DMSO as control before α -pTyr immunoprecipitation of tyrosine phosphorylated proteins. (B) Venn diagram showing the number of quantified phosphopeptides in the two replicate experiments and their overlap. (C) Distribution of phosphorylation sites by amino acid. Percentages reflect class I phosphosites ($p > 0.75$) quantified in both replicate experiments. (D) Log₂ transformed phosphopeptide ratios are shown in scatter plot comparison of the independent experiments.

Altogether, this straightforward experimental setup, which required less than 10 h of LTQ-Orbitrap measuring time, allowed for the confident identification of 401 class I phosphosites ($p > 0.75$) comprising 153 phosphotyrosine residues (Figure 31B). We next analyzed the distribution of phosphorylation sites by amino acids for all class I phosphosites that were quantified in one or both biological replicate experiments. Notably, almost 40 % of these sites were phosphotyrosine sites and about 55 % and 5 % were sites on serine- and threonine, respectively (Figure 31C). In addition, to address the question of experimental reproducibility the phosphosite ratios of two separate experiments were log₂ transformed and plotted in scatter plot comparison (Figure 31D). As evident from this analysis most of the phosphosites are not regulated upon imatinib treatment, as indicated by the dense ‘cloud’ around log₂ values of about zero. However, as expected upon inhibition of the catalytic activity of Bcr-Abl by imatinib, a certain amount of phosphosites was identified to be down-

regulated. Notably, as evident from the overall close proximity to the diagonal line indicating 100 % experimental reproducibility, in most cases such down-regulation events were consistently observed in two independent analyses.

We choose a conservative cut-off threshold to identify imatinib-responsive sites and required a minimum twofold regulation in both replicate experiments. Based on these criteria, our set of reproducibly down-regulated phosphosites comprised a multitude of sites that have been previously reported to be sensitive to imatinib, such as various Bcr-Abl sites in addition to pTyr on interacting proteins like Abi-1, Gab1 and Shc as well as on downstream mediators of Bcr-Abl signaling such as Erk2, SHIP2 and STAT5A (Table 7) ⁵⁶. Notably, we also identified many unreported imatinib-sensitive phosphorylation sites on proteins previously implicated as imatinib-sensitive such as Abi-1, Erk2, SHIP-2 and ZO2. Furthermore, our study identified several new proteins as sensitive to imatinib treatment such as Casc3, Gab2, Ptp2c, Tpx2, SgK269, ZO1 and others (Table 7).

Table 7: Selected imatinib-sensitive phosphopeptides. The phosphopeptide ratios reflect (10 μ M imatinib/DMSO) for experiment 1 (Exp. I) and experiment 2 (Exp. II).

Gene Names	Protein	Position	Modified Sequence	Exp. I	Exp. II
ABI1	IPI00480028	S-226	LGSQHS(ph)PGR	0.02	0.10
ABI1	IPI00480028	Y-214	TLEPVKPPTVPNDY(ph)M(ox)TSPAR	0.02	0.04
ABL1	IPI00221171	Y-272	LGGGQY(ph)GEVYEGVWK	0.24	0.19
ABL1	IPI00221171	Y-412	LM(ox)TGDTY(ph)TAHAGAK	0.27	0.23
ABL1	IPI00221171	Y-134	NGQGWWPSNY(ph)ITPVNSLEK	0.01	0.03
ABL1	IPI00221171	Y-245	NKPTY(ph)GVSPNYDK	0.14	0.12
BCR	IPI00004497	Y-360	VSPS(ph)PTTY(ph)R	0.06	0.11
BCR	IPI00004497	Y-554	VPELY(ph)EIHK	0.04	0.22
BCR	IPI00004497	Y-246	SSESSCGVDGDY(ph)EDAELNPR	0.27	0.34
CASC3	IPI00289491	S-363	RLEQTSVRDPS(ph)PEADAPVLGSPEK	0.29	0.25
CASS4/HEFL	IPI00160340	Y-195	QQLY(ph)DIPASPK	0.40	0.42
CASS4/HEFL	IPI00160340	Y-350	VEQQNTKPNY(ph)DIPK	0.42	0.38
CBL	IPI00027269	S-483	VERPPS(ph)PFSM(ox)APQASLPPVPPR	0.07	0.14
CBL	IPI00027269	S-675	IKPSSSANAIYS(ph)LAARPLPVPK	0.08	0.08
CBLB	IPI00292856	S-480	QNSPVTS(ph)PGSSPLAQR	0.04	0.05
CD2AP	IPI00872533	S-555	FNGGHS(ph)PTHS(ph)PEK	0.32	0.27
CD2AP	IPI00872533	S-551	FNGGHS(ph)PTHSPEK	0.26	0.26
CRKL	IPI00004839	S-184	LVRSPHSPHGK	0.05	0.05
CRKL	IPI00004839	Y-251	RVPCAY(ph)DK	0.03	0.05
DOK1	IPI00015287	Y-296	LSPSPGQELLDSPPALY(ph)AEPLDSLRL	0.14	0.29
DOK2	IPI00022602	Y-299	GQEGEY(ph)AVPFDAVAR	0.05	0.09
GAB1	IPI00410383	Y-242	HGMNGFFQQMIY(ph)DSPPSR	0.23	0.14
GAB1	IPI00410383	Y-406	DASSQDCY(ph)DIPR	0.11	0.14
GAB1	IPI00410383	Y-259	APSASVDSSLY(ph)NLPR	0.05	0.07
GAB2	IPI00749276	S-292	GSLTGS(ph)ETDNEDVYTFK	0.25	0.18
GAB2	IPI00749276	S-638	KPS(ph)TSSVTSDEK	0.24	0.20
GAB2	IPI00749276	S-550	NNTVIDELPFKS(ph)PITK	0.05	0.10
GAB2	IPI00749276	S-147	S(ph)SPAELSSSQHLLR	0.13	0.15
ITSN2	IPI00414027	Y-968	REEPEALY(ph)AAVNK	0.34	0.27
MAPK1/ERK2	IPI00003479	Y-187	VADPDHDHTGFLTEY(ph)VATR	0.27	0.14
MAPK1/ERK2	IPI00003479	T-185	VADPDHDHTGFLT(ph)EYVATR	0.28	0.17
MAPK3/ERK1	IPI00018195	Y-204	IADPEHDHTGFLTEY(ph)VATR	0.20	0.18
PDLIM5	IPI00007935	Y-251	YTEFY(ph)HVPTHS DASK	0.05	0.08
PTP2C	IPI00658023	Y-584	VY(ph)ENVGLM(ox)QQQK	0.29	0.33
SGK269	IPI00737545	S-281	ANTLS(ph)PVR	0.49	0.49
SH2D2A	IPI00220388	Y-226	SQDPNPQY(ph)SPIIK	0.24	0.22
SH2D2A	IPI00220388	Y-315	GSPGEAPSNIY(ph)VEVEDEGLPATLGHPVLR	0.14	0.25
SH2D2A	IPI00220388	Y-300	PSNPIYNEPDEPIAFY(ph)AMGR	0.07	0.12
SHC1	IPI00021326	Y-428	ELFDDPSY(ph)VNVQNLDK	0.02	0.04
SHIP2	IPI00016932	Y-671	DTY(ph)AWHK	0.03	0.06
SHIP2	IPI00016932	Y-886	LY(ph)EWISIDK	0.06	0.11
STAT5B	IPI00103415	Y-699	AVDGY(ph)VKPQIK	0.17	0.02
TJP1/ZO1	IPI00216219	S-329	HS(ph)PQQPSNGSLR	0.17	0.29
TJP1/ZO1	IPI00216219	S-617	S(ph)REDLSAQPVQTK	0.22	0.22
TJP2/ZO2	IPI00003843	S-1159	GSYGS(ph)DAEEEEYRQQLSEHSK	0.12	0.22
TJP2/ZO2	IPI00003843	S-266	AYS(ph)PEYR	0.12	0.15
TJP2/ZO2	IPI00003843	S-441	ERPSS(ph)REDTPSR	0.16	0.18
TPX2	IPI00102661	Y-555	AQPVPHY(ph)GVFPKQIPEAR	0.02	0.05

4.3 Identification of Plk1 cellular substrates

Polo-like kinase 1 is known to be a key regulator that orchestrates progression through mitosis and the mechanisms involved in its spatio-temporal regulation have been intensely studied^{87, 97}. Generally, detailed knowledge of cellular kinase-substrate relationships is essential to chart the information flow within signal transduction networks. In case of Plk1 several cellular substrates have been reported and a linear consensus motif for Plk1-mediated substrate phosphorylation has been determined^{97, 102, 219-220}. Previously, progress in the identification of *in vivo* kinase substrates has been rather slow, as these efforts were mostly hypothesis-driven and involved tedious validation work. Here, we present an experimental concept that integrates chemical genetics, quantitative mass spectrometry and large-scale data processing including statistical testing to allow for efficient and trustworthy cellular substrate identification (CSI).

4.3.1 Implementation of an efficient phosphopeptide enrichment strategy

About one third of all cellular proteins are thought to be modified by phosphorylation⁹. Protein phosphorylations are often sub-stoichiometric events¹⁵⁶. In addition, many regulatory phosphoproteins are of low cellular abundance. Thus, to overcome the resulting challenges for the comprehensive large-scale phosphoproteomics analysis efficient phosphoprotein and/or phosphopeptide enrichment methods are needed. To implement a stable work-flow for gel-free phosphopeptide enrichment we modified a recently published protocol that combines SCX and IMAC techniques¹⁹⁵.

To enable quantitative MS analysis human retinal pigment epithelial (RPE) cells, in which both copies of the *PLK1* loci had been disrupted and which were reconstituted with either wild-type *PLK1* (*PLK1*^{wt}) or an analog-sensitive *PLK1* mutant (*PLK1*^{as})¹²³, were grown under light- and heavy SILAC conditions¹⁴⁹. Mitotic extracts of the cells were combined, proteins were digested with trypsin, and proteolytically generated peptides were then desalted and lyophilized. Tryptic peptides were separated by SCX by applying a salt gradient directly after sample loading (Figure 32A). A total of twelve pooled SCX fractions were then again desalted, aliquoted in two fractions, and lyophilized. Lyophilized peptides were subjected to

IMAC-based phosphopeptide enrichment prior to subsequent MS analysis. To analyze the separation power of our SCX we visualized the solution charge separation of identified phosphopeptides in the SCX fractions (Figure 32C). Phosphopeptides with a negative charge or an overall charge of zero are most prominent in SCX flow-through fractions one and two. With increasing salt concentrations phosphopeptides carrying one, two or more positive net charges are successively eluted. The analysis of the percentage of identified phosphopeptides over the percentage of non-phosphorylated peptides derived from every SCX fraction revealed efficient enrichment of >70 % in most fractions (Figure 32B). Notably, the phosphopeptide overlap between two consecutive SCX fractions is fairly low, as demonstrated by the comparatively low numbers of phosphopeptides from SCX fractions that were already identified already in the previous SCX fraction (Figure 32D).

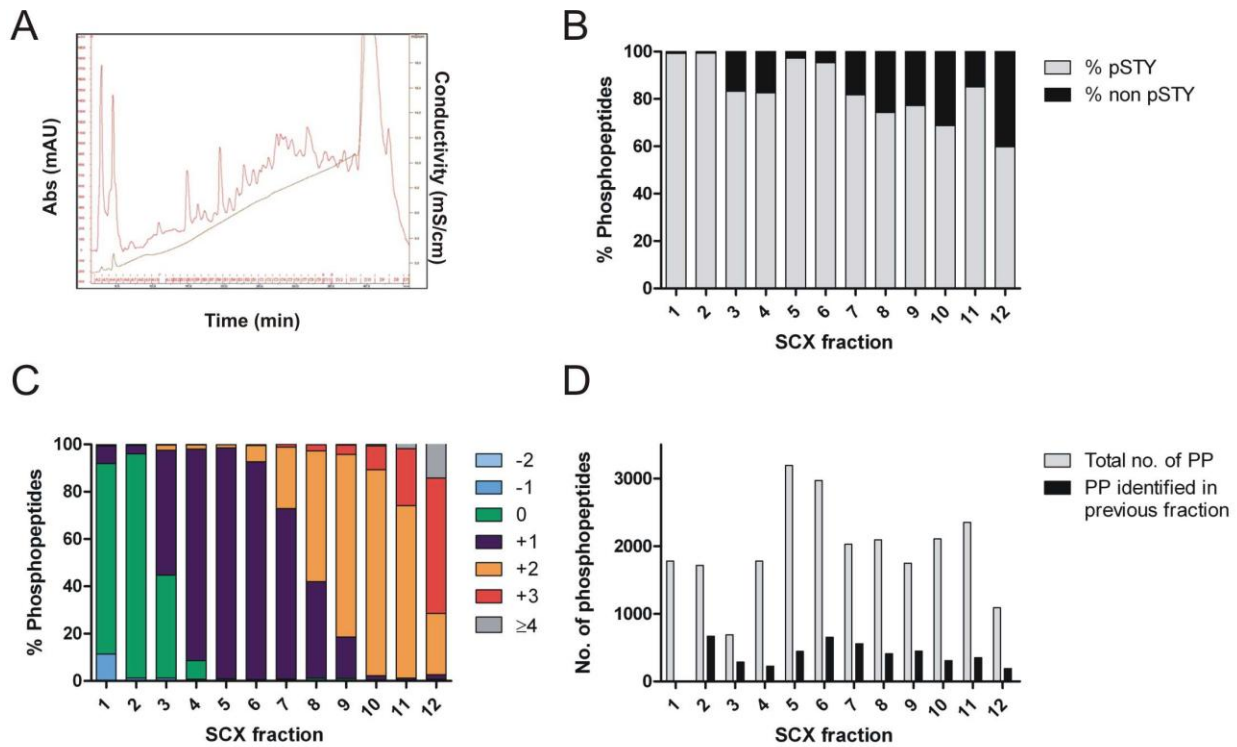


Figure 32: Combination of strong cation exchange chromatography (SCX) and immobilized metal affinity chromatography (IMAC) for advanced phosphopeptide separation and enrichment. (A) Chromatogram of the SCX-based separation of tryptic peptides. Conductivity is shown in brown and the absorbance at 215 nm is indicated in red. (B) Solution-charge distribution of all quantified peptides in the twelve SCX fractions. (C) Ratio of identified phosphopeptides to non-phosphorylated peptides after phosphopeptide-enrichment by IMAC. (D) Phosphopeptide distribution, shown as the overlap between consecutive SCX fractions (black) and the total number of identified phosphopeptides (grey). Data

derived from a single technical replicate analysis. PP, phosphopeptide; pSTY, phosphorylation site on serine, threonine or tyrosine

Taken together, this demonstrates the high separation power of the SCX combined with highly efficient phosphopeptide enrichment by IMAC. In addition, this approach resulted in the quantification of almost 10,000 phosphorylation sites from a single experiment involving MS analysis of 12 sample fractions.

4.3.2 New strategy for the identification of cellular substrates of Plk1

For the identification of cellular substrates for Plk1 we employed allele-sensitive mutants of *PLK1*, generated and previously validated in cellular assays¹²³, in combination with a highly optimized and automated phosphoproteomics workflow as described above and depicted in Figure 33A. *PLK1*^{wt} or *PLK1*^{as} cells, the latter expressing a Plk1 variant that can be specifically inhibited by the small molecule 3-MB-PP1, were encoded by SILAC. During a mitotic arrest in the presence of 3-MB-PP1, the enzymatic activity of Plk1 is repressed in the *PLK1*^{as}- but not the *PLK1*^{wt} cells. We then washed the cells to remove 3-MB-PP1 and subsequently incubated them for another 30 min in nocodazole-containing medium with or without 3-MB-PP1. This enabled us to compare *PLK1*^{as} cells with repressed Plk1 activity to mitotically arrested cells in which Plk1 activity had been re-activated. In parallel, *PLK1*^{wt} cells were treated in essentially the same way to control for potential off-target effects of 3-MB-PP1 (Figure 33A). As we could demonstrate in immunoblot analysis for the reported Plk1 substrate BubR1²²¹, the above described inhibitor wash-out strategy proved to be quite effective (data not shown).

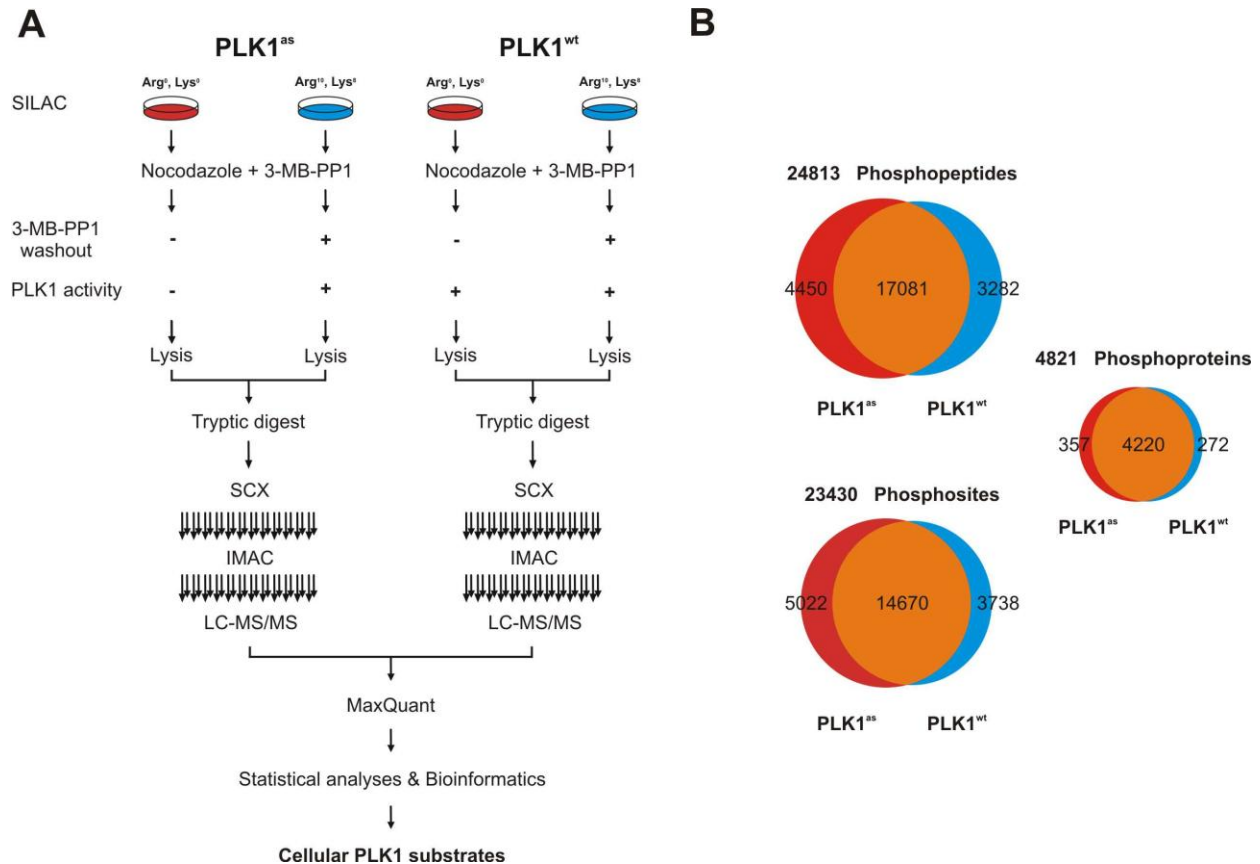


Figure 33: Experimental strategy and resulting phosphopeptide-, site- and protein identifications in the Plk1 cellular substrate identification. (A) Workflow in the Plk1 cellular substrate identification experiments. Mitotic arrest of SILAC-labeled $PLK1^{as/wt}$ cells is done in nocodazole and 3-MB-PP1. Thereupon, wash-out is performed in either 3-MB-PP1-containing or 3-MB-PP1-free media for 30 minutes prior to cell lysis and protein digestion. Desalted peptides are separated by SCX, desalted again and phosphopeptides are enriched by means of IMAC prior to LC-MS/MS analysis. Peptide identification and quantification is conducted with MaxQuant before bioinformatics data processing for high confidence identification of cellular substrates. (B) Venn diagrams of all phosphopeptides, class I phosphosites and phosphoproteins detected in $PLK1^{as-}$ or $PLK1^{wt}$ experiments.

Total cell lysates of differentially treated $PLK1^{as}$ or $PLK1^{wt}$ cells were pooled and phosphopeptides enriched according to the aforementioned workflow. The MaxQuant software suite was used for peptide identification and quantification²¹⁶. To attain high coverage of the cellular phosphoproteome we performed a total of nine biological replicate experiments with altered SILAC labeling regimes and further analyzed technical replicates in each of these biological replicate experiments (Table A. 3). The generated raw files were combined and processed together. In total, this resulted in the hitherto most comprehensive

phosphoproteomics dataset comprising more than 23,000 class I phosphosites on about 4,500 phosphoproteins (Figure 33B, Table 8).

Table 8: Overview of the results in the Plk1 cellular substrate identification. All quantified phosphosites, phosphopeptides and phosphoproteins of the cellular substrate identification study for Plk1 and the comprised regulated species, revealed by ratio of similarity coefficient analysis, derived from either $PLK1^{as}$ or $PLK1^{wt}$ cells or combined are shown.

	$PLK1^{as}$	$PLK1^{wt}$	Total
Phosphosites	19692	18408	23430
Phosphopeptides	21531	20363	24813
Phosphoproteins	4577	4492	4849
Regulated Phosphopeptides	404	1	-
Regulated Phosphoproteins	284	1	-

Individual comparison of all technical replicates and biological experiments revealed a high overlap and similarity proving good reproducibility of our workflow (Figure 34A, B; Figure A.2 and A.3). Notably, in both cell systems, we could gradually increase the total number of quantified phosphopeptides by incrementing the number of biological experiments (Figure 35C). This was also the case when we analyzed the number of phosphopeptides that were identified in at least two biological replicate experiments (Figure 34D). This enabled us to filter for reproducible ratios across biological replicate analyses.

Intriguingly, the experimental set-up employed in this study not only provided a dataset of altered phosphorylation events upon catalytic reactivation of Plk1 after inhibitor wash-out in the $PLK1^{as}$ cells but, in addition, also enabled the monitoring of Plk1-unrelated 3-MB-PP1 off-target effects due to the concomitant analysis of $PLK1^{wt}$ cells after inhibitor wash-out.

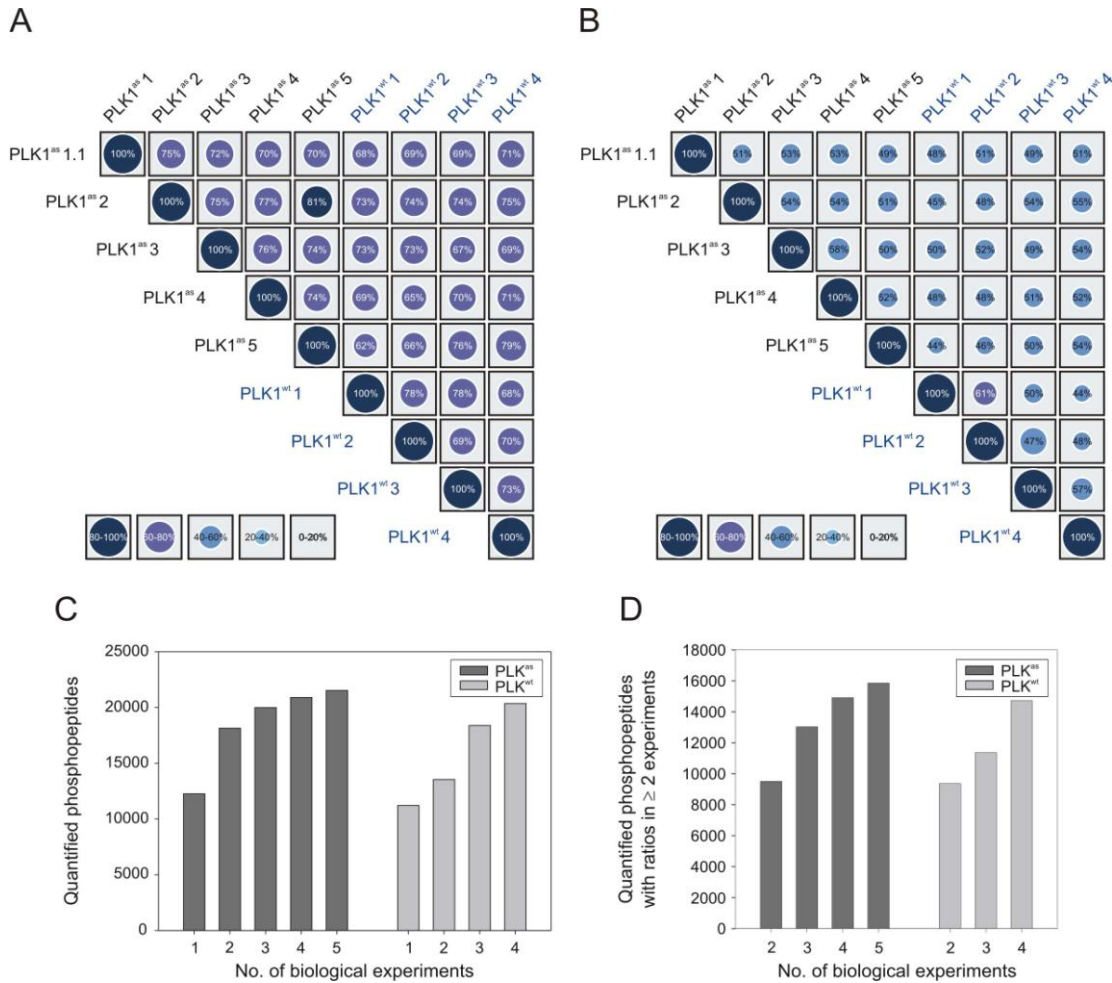


Figure 34: Comparison of the biological replicate experiments. All quantified phosphopeptides carrying class I phosphosites in the nine individual biological experiments were compared in ‘one versus all’ comparisons. (A) Overlap between all datasets in relation to the smaller one. (B) Jaccard similarity coefficient showing the overlap of two datasets in relation to their union, as described in the materials and methods section. (C) Total number of quantified phosphopeptides as a function of the number of combined biological experiments. (D) Total number of phosphopeptides that were quantified in two or more experiments in the *PLK1^{as}* or *PLK1^{wt}* cells as a function of the number of combined biological experiments.

Initially, we aimed to determine the minimal requirements needed to eliminate false-positives among identified, regulated phosphorylation events. Therefore, we analyzed all pair-wise combinations of reciprocal SILAC experiments in the *PLK1^{as}* cells as well as the corresponding combinations of *PLK1^{wt}* experiments with respect to phosphorylation ratios quantified in both compared experiments. First, we calculated for each individual ratio a ratio similarity coefficient (RSC) defined by the absolute value of the difference between two ratios divided by the mean of the ratios determined in biological duplicates. As cut-off

criteria for regulated phosphorylation events we choose a minimum of twofold regulation. For different RSC thresholds we then calculated the number of regulated phosphopeptides derived from either the *PLK1^{as}* or *PLK1^{wt}* cells that were not identified as regulated in the other cell system. We determined the number of phosphorylation events that were either considered as regulated or as not regulated in both cell systems according to the different RSC thresholds (Table A. 5). In addition, we performed a combined RSC analysis comprising all nine biological experiments. The resulting numbers of this comparative analysis are plotted in Figure 35A. In the *PLK1^{wt}* cells we found less than one exclusively regulated phosphopeptide, even with a RSC of as high as 0.5. Compared to the more than 400 phosphopeptides exclusively regulated in *PLK1^{as}* cells, this corresponds to a false-discovery rate of less than 1 % (Figure 35A). In contrast, when we compared single biological experiments of *PLK1^{as}* and *PLK1^{wt}* cells the estimated false-positive rates associated with Plk1^{as}-mediated changes greater than twofold were as high as 10 % (Table A. 4). Notably, although the requirement to be independently quantified in two biological experiments results in the identification of less regulated phosphopeptides, the number of congruently regulated phosphopeptides increases to a larger extent than the actual phosphopeptide identifications with an increasing number of combined biological experiments (Figure 35C). Collectively, this approach enabled us to identify more than 400 distinct phosphopeptides in *PLK1^{as}* cells, which are derived from 284 distinct proteins, and that were regulated by at least twofold upon inhibitor wash-out with a RSC of < 0.4 (Figure 35B, C; Table 8; and Table A. 6). In marked contrast to this, only one phosphopeptide with consistent regulation in *PLK1^{wt}* cells was identified. This casein kinase 1 δ -derived peptide is regulated in both *PLK1^{as}* and *PLK1^{wt}* cell lines and therefore represents a off-target effect that is not specifically linked to analog-sensitive kinase inhibition. Remarkably, despite the more than 100 events that exhibit more than twofold regulation upon 3-MB-PP1 wash-out in the *PLK1^{wt}* cells in individual experiments, we did not identify a single phosphopeptide that showed consistent regulation solely in this cell line across biological replicates (Figure 35A, B).

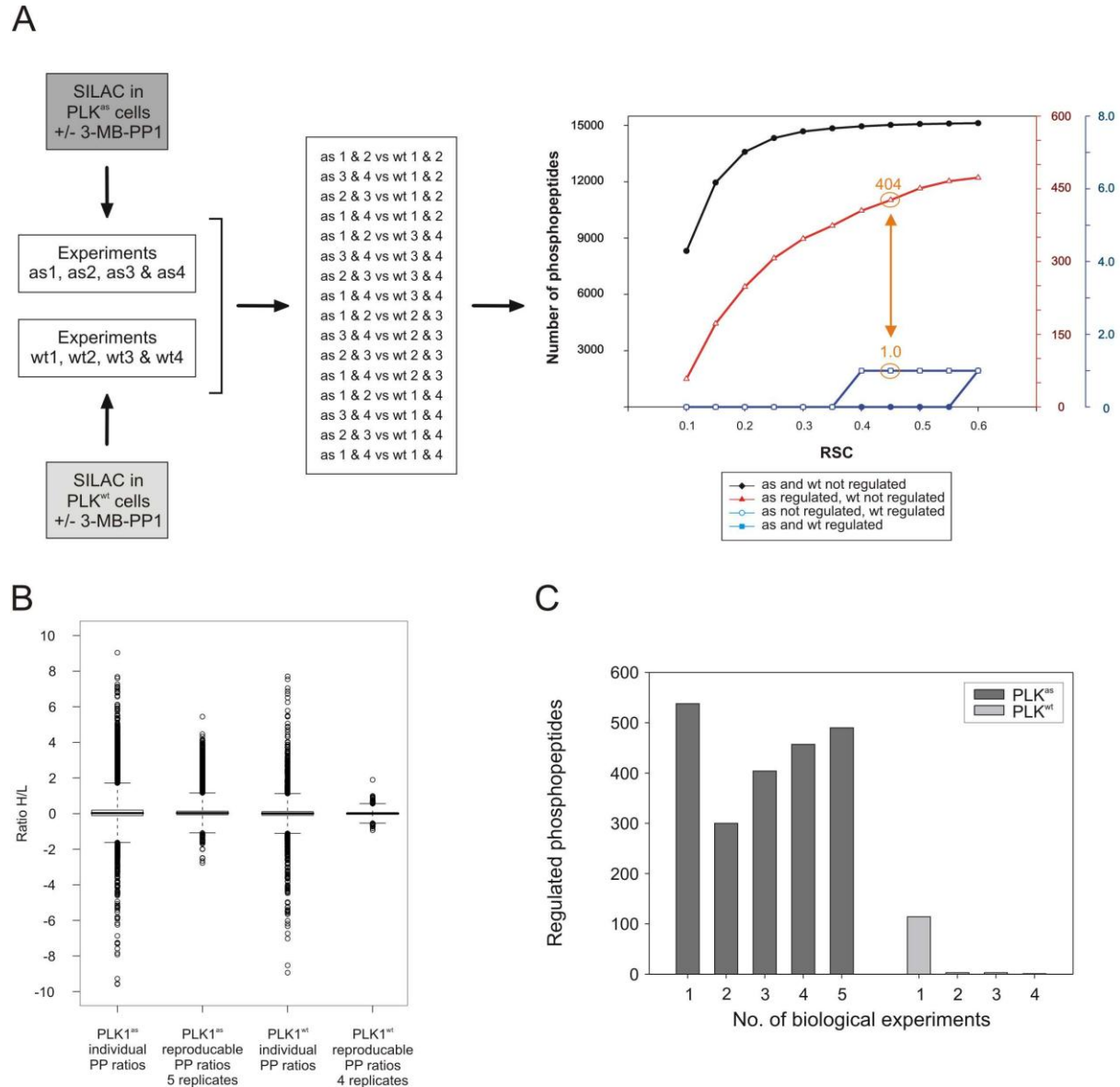


Figure 35: Comparison of reproducibly regulated phosphopeptides in PLK1^{as} and PLK1^{wt} cells. (A) Total number of quantified and regulated phosphopeptides in the RPE-PLK1as/wt cells as a function of the ratio of similarity coefficient (RSC). (B) Boxplot analysis of quantified phosphosite ratios in PLK1^{as} and PLK1^{wt} cells. Depicted are either all ratios or all mean ratios with a RSC < 0.4. (C) Regulated phosphopeptides with a RSC < 0.4 identified with increasing number of biological experiments with PLK1^{as} - and PLK1^{wt} cells.

4.3.3 Characterization of the identified cellular substrates of Plk1

In the following, we aimed to analyze our set of cellular Plk1 downstream signal transducers with respect to possible cellular functions and potentially direct kinase-substrate relationships. Therefore, we initially performed enrichment analysis for the gene ontology

(GO) cellular component, molecular function and biological process categories. In case of the cellular component category this revealed known and well-studied sites of Plk1 action to be highly overrepresented, such as the centrosome, kinetochore and spindle apparatus (Figure 36A). In addition, this pointed to potential Plk1 functions on multiple components of the nuclear envelope. Moreover, compared to all identified phosphoproteins or the entire human IPI database, we found Plk1-regulated phosphoproteins highly enriched in key mitotic processes such as the establishment and/or maintenance of chromatin architecture and microtubule based processes (Figure 35C). Interestingly, terms relating to DNA-dependent transcription and transcriptional cofactor activity were also overrepresented (Figure 36B).

Next, we performed multiple enrichment analyses for reported amino acid motifs connected to Plk1 activity and function. These revealed the reported consensus motif for Plk1 (*E/D-X-pS/pT-F/L/I/Y/W/V/M*)¹⁰² to be highly enriched in the set of identified Plk1 substrate proteins compared to all other identified proteins (Figure 36D). In addition, we found a less stringent consensus motif for Plk1 displaying an aspartate, glutamate or asparagine residue in the -2 position enriched by more than twofold. Notably, more than 85 % of all 284 identified Plk1 substrate proteins contained this motif. Besides, a simplified PBD binding motif (*S-pS/pT*) was also enriched in Plk1-regulated compared to all identified phosphoproteins (Figure 36D). This simplified PBD binding motif does not contain the proline residue at the +1 position as described by Elia *et al.*⁸⁷.

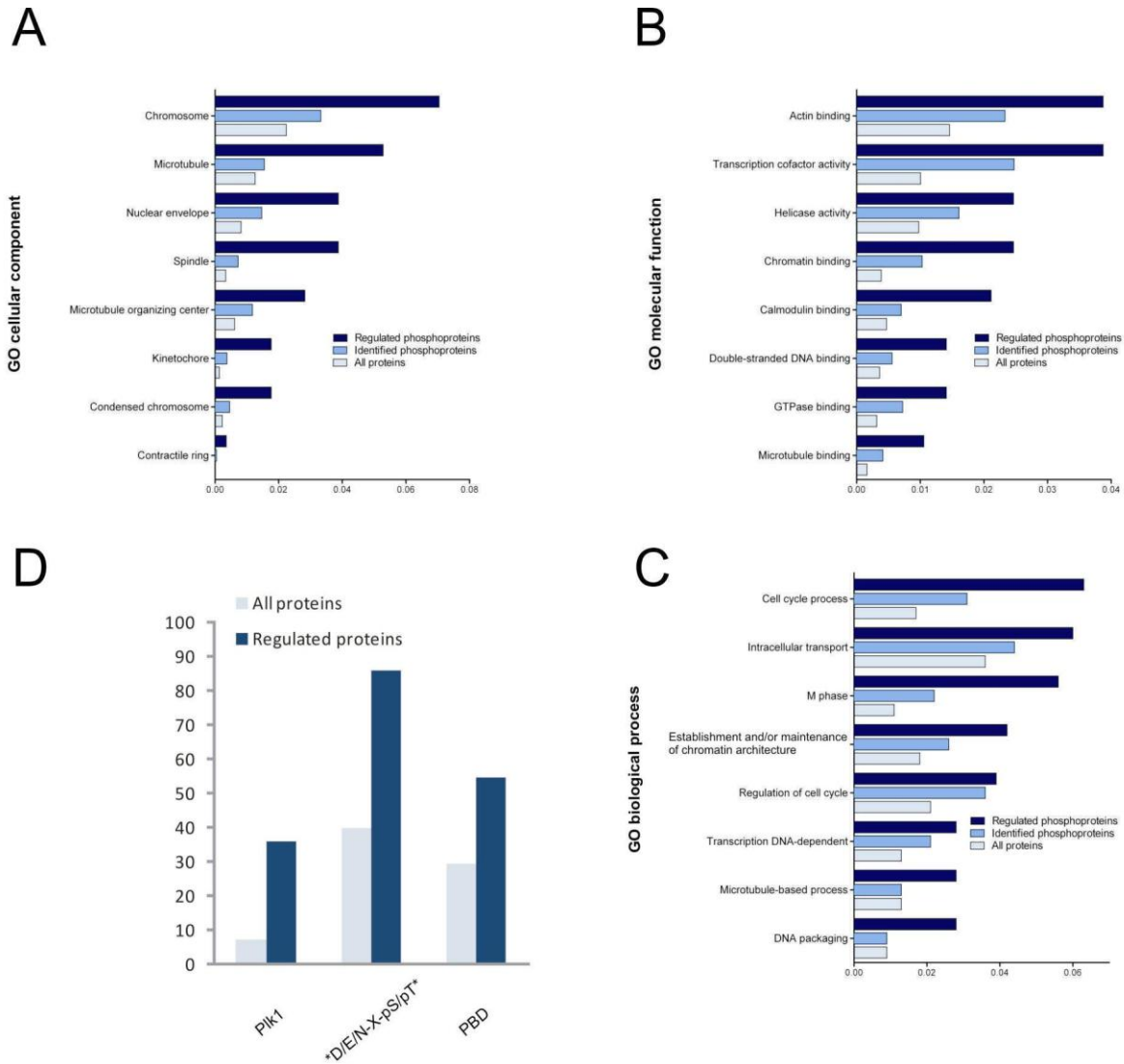


Figure 36: Gene ontology- and motif enrichment analysis. Selected overrepresented ($p < 0.05$) terms after Gene ontology enrichment analysis in the (A) cellular component-, (B) molecular function- and (C) biological process categories. Proteins that were identified with at least one phosphopeptide as a cellular Plk1 substrate based on the CSI-technology results were compared to all other identified phosphoproteins and the entire list of IPI entries. (D) Percentage of all identified and Plk1-regulated phosphoproteins matching the reported Plk1 consensus sequence (*E/D-X-pS/pT-F/L/I/Y/W/V/M*), a less stringent version of the Plk1 motif or harboring the PBD motif (*S-pS/pT*).

V. Discussion

5.1. Large-scale proteomics analysis of the human kinome

Protein kinases (PK) represent central proteins in phosphorylation-based signal transduction. Aberrant PK expression or activity has been associated with multiple pathological processes eventually leading to malignant transformation and tumor development¹⁸. Therefore, PKs have emerged as a major class of drug targets for therapeutic intervention²⁴⁻²⁶.

*5.1.1 Pyrido[2,3-*d*]pyrimidin-based affinity resins are efficient protein kinase pre-fractionation tools*

The often low cellular expression levels of PKs require specific enrichment techniques for their analysis. Immunoprecipitation with specific antibodies is a commonly applied strategy to enrich and detect specific PKs and their post translational modifications (PTMs). These studies, however, are restricted to available high affinity antibodies and not applicable for the global analysis of PK modification. Therefore, pre-fractionation techniques that permit the concomitant enrichment of large numbers of PKs have been developed. A rather unbiased strategy is based on affinity pre-fractionation methods that utilize immobilized small molecule inhibitors which are selective for PKs^{175, 206-207}. Recently, our group and others have demonstrated the high efficiency of such pre-fractionation strategies that employ multiple PK-selective affinity resins, in particular when combined with subsequent phosphopeptide enrichment techniques^{57, 166, 180}. In general, PK-selective affinity resins have to meet two important criteria: First, they have to exhibit rather promiscuous affinity towards distinct PKs. And second, they have to show strong selectivity for PKs compared to other cellular proteins.

In this study we established a generic strategy for the comprehensive comparison of structurally related small molecule inhibitors from the pyrido[2,3-*d*]pyrimidine class of compounds¹⁹¹. Pair-wise comparisons of the relative amount of either captured PKs or non-PK proteins allowed for a differential assessment of affinity resin performance. We demonstrated that the affinity resins VI16743 and VI16832 are particular efficient as PK pre-fractionation tools, as they both were

capable of retaining more than 130 distinct PKs from single cellline extracts. In addition, we could demonstrate that our batch-wise PK pre-fractionation approach enabled accurate and reproducible SILAC-based quantification. Notably, these comparisons showed that even in case of structurally highly related small molecule inhibitors the overall number of interactors and affinities of the individual targets are differentially affected upon chemical modifications of the inhibitor core structure.

Even in large-scale proteomics analyses rather little information about the relative cellular expression levels of PKs or their modification states is obtained in case unfractionated cell extracts are analyzed^{150, 222-223}. For example, this is exemplified by the total lysate analysis from Olsen *et al.* who quantified only 270 phosphorylations on PKs in their assessment of 6,000 phosphorylation sites upon EGF stimulation in HeLa cells¹⁵⁰. Therefore, in case the antibody-based analysis of a PK is not an option for selective enrichment, small molecule-based PK-selective affinity resins can provide a straightforward alternative for targeted PK biochemistry, for example by separating a small molecule-enriched PK mix by gel electrophoresis and the subsequent restriction to the molecular weight region that comprises the kinase-of-interest. Therefore, the dataset generated in this study provides a wealth of information on PKs amenable to such focused signal transduction approaches, and these might involve quantitative MS to monitor PTM regulation upon different types of cell treatment.

Another approach to enrich for tyrosine phosphorylated PKs utilizes high affinity antibodies directed against tyrosine phosphorylated proteins²²⁴. However, for the global analysis of PKs, these approaches are not applicable as such an analysis is inherently restricted to tyrosine phosphorylated proteins and therefore does not cover the vast majority of Ser/Thr kinases. Therefore, for unrestricted kinase-centric analysis from total cell extracts affinity purification strategies utilizing multiple immobilized compounds with distinct kinase selectivity profiles have been developed^{57, 166}. However, even if these approaches already cover a major fraction of the expressed cellular kinome, they have not been systematically optimized. This can be achieved by the comparative assessment of new enrichment compounds predicted to be rather unselective across the expressed kinome. The quantitative MS-based experimental strategy described for the comparison of pyrido[2,3-*d*]pyrimidine derivatives in this study represents a generic approach for such optimization efforts. In particular, future applications might characterize other kinase-

selective capture molecules retaining subsets of the expressed kinome that are not accessible by VI16743 and VI16832 affinity resins.

5.1.2 Comparative analysis of kinase expression in three cancer cell lines

The goal of PK-centric proteomics analyses is the unbiased evaluation of this cellular sub-proteome. In this study, we implemented a compact and straightforward experimental strategy for the quantitative analysis of relative PK expression levels in different cancer cell lines utilizing the previously characterized VI16832 affinity resin. This allowed the analysis of more than 170 distinct PKs and a multitude of other nucleotide-utilizing enzymes. As mammalian cells are estimated to express about 300 PKs²²⁵, this number indicates substantial kinome coverage by a single PK-selective affinity resin.

In addition, our VI16832 affinity resin-based kinase pre-fractionation strategy enabled the quantitative analysis of more than twice the number of protein kinases previously reported in a different approach based on reactive acyl phosphate-containing nucleotides for kinase expression profiling²²⁶. Moreover, compared to recent studies that combined several distinct affinity resins for PK enrichment – such as the ‘kinobeads’ approach described by Bantscheff and colleagues comprising seven different molecules - the VI16832 affinity resin as a single reagent allowed for the analysis of a comparable number of PKs^{57, 166}.

Quantitative MS by means of SILAC allows the comparative analysis of up to three different cell populations in a single experiment¹⁴⁸. However, more complex studies are possible by utilizing a shared reference sample across multiple triple-SILAC experiments. Thus, two or more SILAC experiments can be multiplexed^{150, 168}. In addition to time-course analysis or comparison of cell cycle stages this approach could also be applied for comprehensive kinase profiling across a large collection of cancer cell lines. Such analyses might reveal disease-associated PK expression patterns of PKs and thereby point to possible new targets for drug development activities. Moreover, such PK analyses are not necessarily restricted to cancer cell lines but could also be performed on primary tumor samples. Such applications might either use SILAC-encoded material from cell culture extracts as reference for PK quantitation²²⁷ or alternative quantification approaches based on isobaric tagging for relative and absolute quantification (iTRAQ)¹⁵³ or tandem mass tag (TMT)¹⁵⁴ reagents.

Recently, Rikova and colleagues performed a large scale proteomics analysis of phosphotyrosine-containing proteomes in more than 40 non-small cell lung cancer cell lines (NSCLC) and about 150 NSCLC tumors²¹¹. Subsequent clustering analysis revealed known oncogenic kinases like the EGFR and c-Met as well as novel PK fusion-proteins of ALK and ROS to be implicated in NSCLC. Furthermore, another important finding was that tumors and cell lines often differed in the set of expressed and activated PKs. In comparison to such phosphotyrosine-directed approaches, proteomics analysis of PK pre-fractionated sub-proteomes is expected to provide overlapping information with respect to tyrosine-phosphorylated PKs. On the other hand, the latter approach is expected to provide complementary data about serine/threonine kinases. In addition, expression data for the majority of the expressed members of the about 400 serine/threonine kinases of the human kinome will most likely reveal further insights into cancer cell biology. The importance of controlling serine/threonine kinase activity in terms of maintaining cellular integrity was exemplified by studies that revealed an association between the overexpression of mitotic kinases (like Aurora A/B, Plk1 and NEK2) and chromosomal instability which has been implicated in the emergence of human cancer^{129, 228}. The pyrido[2,3-*d*]pyrimidine inhibitor resins described in this study are particularly useful for such surveys, due to their ability to capture the majority of tyrosine-directed PKs as well as up to 100 additional serine/threonine kinases from individual cell extracts.

5.1.3 Benchmark analysis for the precision in automated phosphorylation site localization

For the automated site-specific analysis of phosphorylation events an algorithm called PTM scoring has been developed by Olsen *et al.*¹⁵⁰. This algorithm is implemented in the two software packages utilized for MS data analysis in this study (MSQuant and MaxQuant). In total, our benchmark analysis comprised a set of almost forty phosphorylation sites. For the first time, we systematically addressed the important question of how precisely this algorithm pinpoints actual modification sites. Notably, we observed no false assignments in case of phosphorylation sites that were identified with a *p*-value of 1. In addition, we still detected 94 % precision for sites assigned with a *p*-value of 0.75 or higher, which are commonly referred to as class I phosphorylation sites and are localized with high confidence. These findings were confirmed by

a further assessment of the PTM scoring algorithm that utilized a previous large-scale phosphoproteomics study of manually assigned phosphorylation sites as a reference dataset¹⁶⁶. In summary, we demonstrated the overall high accuracy of the PTM scoring algorithm and confirmed it as a valuable tool for the site-specific localization of phosphorylated residues.

5.1.4 In-depth survey of kinase phosphorylations

Phosphorylations can regulate protein function, either by direct allosteric effects or by modifying protein-protein interactions. Many proteins are phosphorylated on multiple sites²²⁹ and some human proteins have been shown to contain up to 150 phosphorylation sites²⁰⁰. In addition to catalyzing phosphorylations on their cellular substrate proteins, PKs are themselves modified by phosphorylations and knowledge of their actual phosphorylation state can provide information on their cellular catalytic activity¹². Therefore, strategies which combine initial PK enrichment with subsequent phosphopeptide enrichment methods for the comprehensive analysis of phosphorylations on PKs have been developed^{57, 166, 180}. In this study we further exploited the capability of the pyrido[2,3-*d*]pyrimidine-based VI16832 affinity resin to pre-fractionate PKs for an extensive site-specific analysis of phosphorylation sites. The more than 1,200 distinct phosphorylation sites that were identified presented the hitherto largest dataset of this PTM on PKs. Notably, different phosphorylation sites were often identified on commonly expressed PKs pointing towards potential cell type specific phosphoregulation of kinase functions. However, PK-enriched fractions were analyzed in individual qualitative MS experiments derived from different cell lines. Therefore, the lack of phosphopeptides for a certain PK cannot be regarded as definite proof for cell-type specific differences. This could also be due to run-to-run differences, which are inherent to LC-MS/MS analyses performed in the data-dependent acquisition mode. Nevertheless, our large-scale analysis provides a plethora of new starting points for further functional studies on cellular kinase regulation. The efficiency of our PK enrichment is further underscored by the higher overall phosphopeptide intensities for PKs compared to all other non-PK-derived phosphopeptide intensities. Importantly, these are not caused by a few high abundant and highly phosphorylated PKs but appear evenly distributed. However, some protein kinases accounted for particular high phosphopeptide intensities which likely reflected their high cellular abundance.

One important question, which has not been addressed in our study, is the functionality of the observed phosphorylations or alterations in the phosphorylation level. It is conceivable that not all phosphorylations possess regulatory function²³⁰. This might particularly be true for phosphorylation sites with low stoichiometry. Recently, our group has reported a strategy to gain information about the stoichiometry of site-specific phosphorylations¹⁶⁶. However, in case of phosphorylation-dependent regulation of enzymatic activity, even a comparatively small percentage of altered protein function can result in a cellular effect. As most proteins harbor phosphorylations on multiple sites^{229, 231}, the picture gets even more complicated.

In conclusion, this study underscored the enormous potential of approaches that integrate kinase pre-fractionation, phosphopeptide enrichment and high-resolution and high-accuracy MS. Moreover, this strategy exhibits considerable potential for future studies across different cancer cell lines or tumor samples. Further, kinome-wide comparisons on both the protein- as well as their state of post-translational modification might significantly expand our knowledge about kinase drug targets and their oncogenic activities on a systems-wide level.

5.2 Identification of cellular kinase inhibitor targets and interconnected mediators of downstream signaling cascades

Detailed knowledge about all direct cellular targets of a small molecule kinase inhibitor is of importance in selecting the appropriate inhibitor for the right indication and unveiling targets mediating potentially harmful side-effects. Furthermore, the comprehensive identification of essential mediators in downstream signalling cascades can reveal potential alternative proteins for therapeutic intervention.

5.2.1 Identification of direct kinase inhibitor targets without prior compound immobilization

Until recently, experimental strategies for the MS-based identification of direct targets of small molecule kinase inhibitors were commonly based on the generation of affinity resins displaying an immobilized variant of the drug-of-interest¹⁷⁵. These strategies allow employing total cellular

extracts thus enabling the profiling of the respective compound against a complete cellular proteome with proteins in their naturally occurring PTM states. However, for immobilization of the small molecule the presence of a functional group is a prerequisite. In some cases, available structural data of protein-drug complexes facilitates the synthetic design of such linker-containing derivatives. Nevertheless, introduction of a linker can result in altered protein binding affinities²³². Moreover, the linker itself can affect protein binding²³³. Thus, the synthesized derivative has ideally to be tested and compared against the genuine compound regarding its *in vitro* and *in vivo* bioactivity¹⁷⁵. To overcome these impediments we implemented an approach that detects the competitive binding of target proteins of small molecule inhibitors to a mix of PK-selective affinity resins. In theory, the amount of a retained protein that presents a direct target of the tested inhibitor should be markedly reduced upon prior inhibitor incubation of the respective cell population.

Especially in case of highly sensitive MS-based quantitative experiments individual sample processing is susceptible for the introduction of quantitative variations. Quantitative proteomics analyses utilizing SILAC-based labeling allow combining total cell extracts of differentially treated cell populations, thereby eliminating the risk to introduce any variances in subsequent sample processing steps. In our initial approach we combined cell lysates of differentially treated cell lines prior to multi-column PK-selective affinity chromatography. This strategy resulted in the quantification of about 130 distinct PKs and more than 1,100 phosphosites. However, as shown in Table 4, no protein ratio could be determined for the Bcr-Abl fusion protein. Besides, the determined protein ratio of the Bcr-Abl interacting protein Grb2 that reflected the amount of captured protein derived from imatinib-treated cells in respect to control cells was unchanged. Moreover, no competitive binding of quinone reductase 2 (NQO2), which is a known non-PK target of imatinib, was monitored⁵⁷. An explanation for these findings might be an excess of free imatinib in the imatinib-treated cells which can upon cell lysis also bind to its targets derived from untreated control proteins. Thus, this might reflect the dynamic equilibrium of the interaction between imatinib and its target proteins. During the course of the PK pre-fractionation this most probably resulted in an equivalent binding of imatinib to target proteins in all three SILAC-conditions. In case of Bcr-Abl, the high affinity of imatinib²³⁴ therefore apparently resulted in the complete abolishment of protein retention by the PK-selective affinity resins. In conclusion, and to avoid these disadvantages, we decided to modify our experimental

strategy. We therefore conceived a parallel batch-wise PK pre-fractionation and pooled the distinct eluates after affinity enrichment. At the time of these experiments were done such a strategy had not been reported in the literature. However, in the meantime a similar strategy was published by Bantscheff and colleagues who studied the competitive retention of proteins by a mix of seven PK-selective affinity resins for the small molecule inhibitors imatinib, dasatinib and nilotinib⁵⁷.

Moreover, we aimed to re-use the PK-affinity resins in one of our experiments. However, effective and convenient protein elution by simple incubation with a LDS-buffer at 70°C, as utilized in the comparison of three different kinase-affinity resins, was not possible as this might cause the inhibitor beads to clump. As a consequence, the surface area of the beads gets reduced resulting in lower binding capacities. Initially, we established an elution protocol utilizing an SDS-buffer at a lower temperature of 50 °C. The efficiency of this elution was similar to an elution with a LDS-buffer at 70°C. Moreover, upon protein elution and subsequent regeneration of the affinity resins they preserved their binding capacity in a succeeding second incubation (data not shown). Thus, these results indicate a viable strategy to re-use inhibitor affinity resins, which is important in case of limited compound availability.

The quantitative MS-based analysis of two biological replicate experiments resulted in the quantification of more than 170 PKs. As this accounts for more than half of the expressed cellular kinome this demonstrates high PK enrichment efficiency. Moreover, these results were highly reproducible and allowed for identifying proteins that exhibited the expected binding characteristics of direct cellular imatinib targets and their interacting proteins, as shown for Bcr-Abl and its associated signal transducers Grb2 and SHIP2^{50, 235}. However, we did not detect all of the recently identified Bcr-Abl interacting proteins²³⁶. In agreement with the reported high affinity of imatinib towards Bcr-Abl the binding of Bcr-Abl to the multi-inhibitor affinity resins was almost completely prevented upon prior exposure of K562 cells to 1 μM imatinib. Furthermore, we detected similar binding characteristics for discoidin domain receptor 1 (DDR1), which was previously identified as high affinity target of imatinib⁵⁷. In addition, we confirmed the findings by Bantscheff and colleagues, who reported NQO2 as the first direct target of imatinib representing a non-PK protein⁵⁷. The reported high affinities of imatinib towards DDR1 and NQO2 correlated with the marked reduction of the captured protein amount, which were already evident when incubated with 1 μM imatinib. Furthermore, we found the

capture of the tyrosine kinase Syk to be competed by imatinib in a dose-dependent manner. Syk has previously been identified as imatinib target which exhibits a K_i value of 5 μM , indicating comparatively low-affinity towards imatinib compared to a K_i value of about 100 nM for c-Abl^{207, 218, 234}. Our study revealed Syk binding to be reduced by about two third at 10 μM imatinib, which is consistent with the reported lower affinity of imatinib. Thus, our described approach provides a means to distinguish high- and low-affinity binders.

It has to be noted that during the course of this thesis also two other laboratories developed and published similar strategies^{57, 237}. Notably, the study by Shao-En Ong *et al.* demonstrated that such strategies are not limited to protein kinase inhibitors but can be applied also to other small molecule-based compounds such as immunophilin binders. Moreover, as already mentioned, Bantscheff *et al.* measured competitive protein binding to their ‘kinobeads’ at different inhibitor concentrations and presented an approximation to derive IC_{50} values. Notably, this strategy has been considerably improved with respect to quantitative kinase affinity determinations¹⁸¹. Therefore, it is now possible to not only identify potential direct targets of a small molecule inhibitor but in addition also to calculate rather accurate dissociation constants (K_d values), thus providing valuable information on the respective target affinities.

5.2.2 Identification of mediators in Bcr-Abl signaling cascades

In addition to the identification of direct cellular imatinib targets we also identified imatinib-sensitive downstream mediators in CML cell signaling. In total, almost 2,000 site-specific phosphorylation events were quantified. Approximately 1,000 such events were quantified in biological replicate experiments and revealed good concordance of the quantified phosphopeptide ratios. Thus, compared to a previous study we quantified almost five times as many phosphorylation sites in K562 cells upon imatinib treatment⁵⁷. Notably, we applied stringent cut-off criteria that had to be met to classify phosphorylation site as imatinib-sensitive. For example, we detected as many as 15 distinct down-regulated tyrosine phosphorylated residues mapping to the Bcr-Abl oncoprotein. All these sites were found at very low ratios upon cellular imatinib treatment, which likely reflects a combined effect of cellular dephosphorylation and near complete prevention of Bcr-Abl protein binding upon imatinib treatment. Therefore, we did not consider phosphorylation sites on direct, high-affinity, imatinib targets any further.

However, in case of the low-affinity imatinib target Syk we detected three tyrosine phosphorylated sites, Tyr-323, Tyr-348 and Tyr-352, which were markedly stronger down-regulated upon 10 μ M imatinib treatment compared to Syk protein binding. As these sites have been reported to increase Syk kinase activity²³⁸ our results suggest cellular inactivation of Syk kinase activity upon high-dose imatinib treatment.

In addition, we also identified a multitude of new down-regulated phosphorylation sites on proteins that were shown to be no direct targets of imatinib such as Tyr-551 on BTK and Tyr-771 on EphB4. Both PKs underwent selective dephosphorylation on tyrosine residues while their protein binding to the kinase inhibitor resins was unchanged. Therefore, these kinases were classified as downstream signaling elements of direct imatinib targets. Notably, these events comprised sites with reported regulatory functions that have not previously been linked to Bcr-Abl signaling. In addition, these sites are located at a conserved position in the activation loop that stabilizes the active kinase conformation in a phosphorylation-dependent manner¹². For pTyr-551 on the cytoplasmic tyrosine kinase BTK, 10 μ M imatinib treatment resulted in an about threefold decrease in tyrosine phosphorylation. This site was previously reported to be phosphorylated by the tyrosine kinases Lyn and Syk²³⁹. Therefore, our results suggest that reduced tyrosine phosphorylation levels on Syk resulting in reduced Syk kinase activity eventually affect the phosphorylation level of Tyr-551 on BTK. Moreover, BTK has been reported as a major target of the small molecule inhibitor dasatinib²⁴⁰, which gained FDA approved as second-line treatment for CML patients upon imatinib failure. Based on these findings, BTK presents an interesting candidate for further analysis of the potential therapeutic value of its targeted inhibition in CML. However, it has to be noted that earlier data revealed that inactivation of BTK in Bcr-Abl-transformed murine cells has no effect on viability and cell proliferation, thus arguing against an essential function of BTK in Bcr-Abl mediated signaling²⁴¹. Nevertheless, despite this data, cell-type specific requirements for BTK might exist. Endogenous expression levels of Bcr-Abl for example might be considerably lower when compared to ectopic overexpression in murine cells of the lymphoid or myeloid lineage.

Moreover, imatinib treatment resulted in about 75 % reduction of the Tyr-883 phosphorylation of focal adhesion kinase (FAK). This numbering is based on the IPI database identifier and corresponds to Tyr-861 based on the UniProtKB/Swiss-Prot-identifier (Q05397, FAK1_HUMAN). Notably, increased phosphorylation on Tyr-861 of FAK was reported in

metastatic breast cancer cells ²⁴². Moreover, Tyr-861 phosphorylation is important for the association of FAK and the breast cancer anti-estrogen resistance 1 (BCAR1) protein and plays a crucial role in rat sarcoma (Ras)-mediated cell transformation of fibroblast cells ²⁴³. The activation of Ras presents a hallmark in Bcr-Abl mediated cell transformation by promoting cell proliferation and survival ²⁴⁴. Thus, our data suggests a previously unknown function of FAK in Bcr-Abl mediated signaling in CML cells. Together, the about 70 down-regulated distinct phosphorylation sites add a considerable amount of new information on phosphorylation-based modification in K562 cells upon imatinib-treatment compared to a previous study that revealed only eight substantially down-regulated sites ⁵⁷.

Interestingly, imatinib treatment also caused the reproducible up-regulation of phosphorylation sites on 24 proteins. Notably, in contrast to the set of down-regulated sites, these were found on proteins like Myt1, Plk1 and Wee1 which are key promoters mitotic progression. Plk1 is overexpressed in many human tumors and has therefore emerged as a potential drug target ¹²⁹. Moreover, abundant Plk1 expression levels were detected in a variety of human leukemia cell lines and have been reported to act synergistically in combination with the tubulin depolymerizing drug vincristine, resulting in growth inhibition and apoptosis of leukemia cells ²⁴⁵. The increased phosphorylation on Thr-210, which resides in the activation loop of Plk1, is crucial for Plk1 activity control ⁸⁹ and points towards an induction of Plk1 kinase activity upon imatinib treatment. Thus, one might speculate that increased Plk1 activity is a possible cellular escape mechanism to compensate for Bcr-Abl suppression. However, it remains open to further investigations whether a combined inhibition of Plk1- and Bcr-Abl kinase activities in CML cells elicits synergistic effects in regard to inhibit cellular proliferation and inducing apoptosis.

In addition, we performed a complementary analysis of imatinib-regulated tyrosine phosphorylations. This study was rather straightforward as it dealt with samples of comparable low complexity. Upon immunoprecipitation of tyrosine-phosphorylated proteins quantification of more than 400 distinct phosphorylation sites comprising more than 150 phosphorylations on tyrosine residues was possible. Compared to our integrated analysis of direct imatinib targets and their downstream mediators, which contained about 6 % of all phosphorylations on tyrosine, this corresponded to a more than sixfold enrichment. This indicated highly efficient enrichment of tyrosine-phosphorylated proteins by the utilized anti-phosphotyrosine antibody. Compared to a similar study published by Goss *et al.* ⁵⁶ our study included biological replicate experiments, thus

increasing the trustworthiness of reported imatinib-sensitive phosphorylation sites. Notably, as demonstrated by the scatter plot analysis of the quantitative changes in the two individual experiments, our approach was highly reproducible. In total, 48 tyrosine residues were sensitive to imatinib treatment. These included the majority of sites that have been previously reported as responsive to imatinib in the analysis by Goss *et al.* and comprised phosphorylation sites on the Bcr-Abl interacting proteins like Abi-1, Gab1 and Shc as well as downstream mediators of Bcr-Abl signaling such as Erk2, SHIP-2 and STAT5A. This concordance confirmed the trustworthiness of our approach in general. Moreover, in addition to novel phosphorylation sites on proteins previously reported as imatinib-sensitive our study also revealed novel proteins that we identified to contain imatinib-sensitive phosphorylation sites. The adaptor protein CRKL, a member of the Crk-associated substrate (CAS)- family, is known to bind Bcr-Abl via its SH3 domain²⁴⁶ which likely explains the marked reduction on pTyr-251 upon imatinib treatment. The importance of this and other Bcr-Abl adaptor proteins for the induction of leukemia in mice has recently been highlighted²⁴⁷. Moreover, members of the CAS-family have been associated with lymphomas and leukemias²⁴⁸⁻²⁴⁹. Interestingly, we revealed two imatinib-sensitive tyrosine phosphorylation sites (Tyr-195 and Tyr-350) on Cas scaffolding protein family member 4 (CASS4/HEPL). These have not been previously connected to Bcr-Abl signaling. However, HEPL has recently been identified as a novel member of the CAS-family and its overexpression caused cell spreading and activation of FAK²⁵⁰. As altered cellular adhesion is a major transforming principle in Bcr-Abl-driven malignancies, functional studies might reveal the potential role of HEPL in these processes. Moreover, we found pTyr-555 on the targeting protein for Xklp2 (TPX2) to be significantly down-regulated. TPX2 is involved in mitotic spindle formation and chromosome segregation²⁵¹ and has not yet been connected to leukemia. However, overexpression of TPX2 has been associated with various malignancies²⁵²⁻²⁵³ and siRNA-mediated depletion causes cell cycle arrest and apoptosis in pancreatic cancer cell lines²⁵⁴. Therefore, it will be interesting to examine possible synergistic effects in CML cells with regard to reduced proliferation rates and increased apoptosis after imatinib treatment in combination with inhibition of TPX2.

5.3 New strategy for the analysis of cellular kinase-substrate relationships

Detailed knowledge of cellular kinase-substrate relationships is essential to chart the information flow within cellular signaling cascades. However, until now no systematic approaches for the *in vivo* identification of cellular substrates of a PK have been developed. Polo-like-kinase 1 (Plk1) is known as a key regulatory protein involved in multiple processes involved in progression through mitosis^{97, 255}. Moreover, overexpression of Plk1 has been reported in various human cancers¹²⁹.

5.3.1 Establishment of an optimized phosphoproteomics workflow

Comprehensive phosphoproteomics analysis critically depends on highly efficient phosphopeptide separation and enrichment strategies. One commonly applied strategy is based on the separation of complex phosphopeptide-containing total cell lysates by strong cation exchange chromatography (SCX)¹⁴⁴. Recently, Stephen Gygi and coworkers presented a protocol that combines SCX with phosphopeptide enrichment by immobilized metal affinity chromatography by which they obtained an impressive high coverage of the cellular phosphoproteome¹⁹⁵. Compared to the SCX-based phosphoproteomics we used in previous studies¹⁶⁶ this protocol appeared to be far more efficient. Based on that protocol, we established a modified strategy and demonstrated high separation power of the utilized SCX column and efficient subsequent IMAC-based phosphopeptide enrichment. Notably, this resulted in an about fivefold increase of identified phosphopeptides when compared to the number of quantified phosphopeptides upon SCX and phosphopeptide enrichment by TiO₂ microspheres, which were conducted in the identification of imatinib-sensitive phosphorylation sites.

When we employed this strategy for the identification of the cellular substrates of Plk1 we analyzed technical replicates of individual biological experiments. As expected, this resulted in a further increased total number of phosphopeptide quantifications. It will be interesting to test whether a recently launched larger SCX column containing about four times more resin material

can be employed to further increase SCX resolving power and thereby phosphoproteome coverage.

Based on this, we conceived a strategy that combined chemical genetics with state-of-the-art phosphoproteomics. This integrated approach was evaluated to identify cellular PK substrates. In addition, we studied the specificity of the chemical genetics strategy on the molecular level, an issue that has not been previously addressed by unbiased approaches. So far, chemical genetics has mostly been applied in targeted, hypothesis-driven studies of protein function¹²²⁻¹²³.

5.3.2 Identification of cellular substrates of Plk1

Typically, the ratios generated in quantitative MS experiments will follow a Gaussian distribution and even in an unperturbed cell system automated SILAC quantification reports a significant number of peptide ratios distinct from one due to their inaccurate quantification. This is of importance as in phosphoproteomics analyses quantitative data will comprise a certain amount of false-positive regulated phosphorylation events, even if a cut-off threshold of twofold change is applied. To avoid such artefacts it is essential to repeatedly measure regulated events in reproducible ratios in at least two biological replicate experiments.

An inherent advantage of the applied inhibitor wash-out strategy is that all detected changes in cellular phosphorylations are a direct consequence of specifically altered Plk1 activity. In contrast, the more commonly applied strategy involving the addition of kinase inhibitors to cells, would have required cellular phosphatase activity to remove phosphate groups from existing Plk1 phosphorylation sites. In our hands, when we monitored the known Plk1 substrate BubR1²²¹, this strategy proved rather inefficient and required considerably higher concentrations of 3-MB-PP1 (data not shown). In this study, we could demonstrate the feasibility of a genetically engineered cell system to meet all the above mentioned requirements by applying altered SILAC labeling regimes in both cell lines. Collectively, we quantified more than 23,000 distinct phosphorylation sites. Thus, to the best of our knowledge this study comprises the hitherto largest phosphoproteomics dataset, even surpassing the recently reported 20,443 phosphorylation sites by Olsen *et al.*¹⁶⁸. Importantly, we quantified a large fraction of all identified phosphopeptides in at least two biological replicate experiments, thus enabling us to filter for reproducible ratios across biological replicate analyses. Notably, we applied straightforward

filtering criteria based on ratio-similarity-coefficient (RSC) analysis. This enabled us to calculate, for the first time in a phosphoproteomics analysis, an experimentally validated, false-discovery rate (FDR) for the observed regulated phosphorylation events.

Altogether, we identified 284 candidate substrate proteins for Plk1 comprising more than 400 distinct phosphorylation sites. For example, our data not only recapitulated previously reported *in vitro* Plk1 phosphorylation sites on centrosomal proteins such as Cep55 and Cep170²⁵⁶⁻²⁵⁷, but unveiled additional Plk1-mediated phosphorylation events on proteins with fundamental roles in centrosome function including the pericentriolar material 1 protein (PCM1)²⁵⁸ and nuclear distribution protein nudeE homolog 1 (NDE1) (Table A. 6). These proteins have been implicated in essential mitotic processes. For example NDE1 is supposed to be involved in the translocation of Bub1 from the kinetochores to the spindle poles²⁵⁹. Such rearrangements have been reported to regulate the initiation of chromosome segregation and the exit from mitosis²⁶⁰. Our results provide the first evidence for their phosphoregulation by Plk1. We further identified site-specific modifications within Plk1 consensus motifs on kinesin-like microtubule motor proteins with both plus-end (Kif4A and Kif20A) and minus-end (CenpE) directed activities, pointing to a coordinated Plk1 control of spindle elongation and chromosome movement. In addition to CenpE, our data indicated direct Plk1 phosphorylation of several other proteins localizing to the centromere-kinetochore region such as the peripheral CenpF, which was shown to be required for microtubule attachment and spindle checkpoint function²⁶¹. Interestingly, we also identified extensive Plk1 regulation on various members of the nuclear pore complex such as Nup98, Nup107 and Nup153. These regulatory phosphorylations might not only contribute to nuclear envelope breakdown during prometaphase, but could moreover have mitotic functions as it has been described for RanBP2/Nup358²⁶². Very recently, these conclusions gained additional support by a study that revealed the multi-protein complex Nup107-160 to control the localization of the chromosome passenger complex (CPC) to the centromere²⁶³. The CPC consists of aurora kinase B, INCENP, surviving and borealin, which possess crucial functions during mitosis²⁶⁴. Notably, we also identified regulated phosphorylation events on INCENP. Moreover, the Nup107-160 complex was shown to recruit the γ -tubulin ring complex (γ -TuRC), a key protein in microtubule nucleation, to unattached kinetochores²⁶⁵. The overall concordance with previously reported Plk1 substrate requirements^{87, 102} indicates that a large fraction of these phosphorylation changes are due to direct cellular modifications by Plk1. This was further

affirmed by gene ontology analyses that revealed well-studied sites of cellular Plk1 function to be highly enriched in our set of potential Plk1 substrates. As the vast majority of these proteins have not previously been reported as Plk1 substrates, our study adds a considerable amount of new information on cellular Plk1 substrates and provides a multitude of valuable candidates for further functional analysis. Moreover, it will be highly interesting to apply our presented cellular substrate identification strategy to PKs whose function and substrates are still elusive. Importantly, with identified sets of cellular PK substrates one could also assign corresponding linear phosphorylation site motifs by utilizing software programs like MotifX²⁶⁶ or Dilimot²⁶⁷.

An advantage of the conducted RSC analysis is that, in addition to the calculation of an experimentally validated FDR, it enabled the identification of inherent effects of the utilized inhibitor due to the comparative analysis of cells expressing either a 3-MB-PP1-sensitive Plk1 mutant or the inhibitor-resistant wild-type enzyme. Notably, our comprehensive phosphoproteomics analysis revealed only one protein, casein kinase 1 delta (CK1 δ), as a likely off-target of the utilized small molecule inhibitor 3-MB-PP1. This observation is supported by the reported inhibition of CK1 δ by the structurally related purine analog 1-NM-PP1¹⁸⁴, which has been shown to be less potent in inhibiting analog-sensitive variants of Plk1¹²³. Given that this Plk1-independent inhibition was identified against a background of more than 10,000 quantified phosphorylation sites our results for the first time demonstrated the impressive cellular selectivity of 3-MB-PP1 for analog-sensitive kinase mutants

It has to be mentioned that Stephen Gygi and coworkers combined a similar chemical genetics approach with phosphoproteomics analysis and reported 308 *in vivo* substrates for the cyclin-dependent kinase (Cdk1) in *Saccharomyces cerevisiae*²⁶⁸. However, the approach reported by Holt *et al.* differs from our approach in multiple ways. First to mention is that no control experiments were done in yeast cells expressing the Cdk1 wild-type enzyme despite the use of a twofold higher inhibitor dose. Thus, possible off-target effects of the utilized inhibitor 1-NM-PP1 have not been evaluated. Second, they add the inhibitor to previously synchronized cell populations and therefore measure cellular phosphatase activity against already existing Cdk1 phosphorylations which might, as shown in our experiments for the Plk1 substrate BubR1, be limited in mitotic cells. And third, they analyze three distinct cell states and report all individual phosphorylation events that are at least twofold down-regulated and match the minimal Cdk1 consensus sequence as specific Cdk1 substrates. However, as they do not require reproducible

regulation, the reported Cdk1 substrates might contain an undefined number of false-positive identifications. Therefore our analysis extended the approach of Holt *et al.* and has essential advantages. In conclusion, our strategy defines a generic approach for the global analyses and high-confidence identification of cellular kinase substrates and includes the determination of an experimentally validated FDR. Furthermore, as the generation of genetically engineered cell systems is time consuming and not applicable for all proteins, we propose that in such cases the control experiments could be substituted by parallel control SILAC experiments in which different SILAC populations of identically treated cells are quantitatively analyzed as a reference to measure workflow-inherent quantification inaccuracies. This could also be generally applied in SILAC-based phosphoproteomics, for example when cellular effects of growth-factor stimulation or treatment with a therapeutic drug are monitored. Such an experimental design would be identical to the one implemented in our Plk1 wild-type/mutant comparisons with the only difference that the control set of SILAC cells remains untreated. This would enable subsequent RSC analysis and thus enable calculating an experimentally validated FDR for the observed cellular alterations on the level of phosphorylation changes or, more generally, of the regulation of protein expression or other types of PTMs.

VI. Summary

In the first part of this thesis an in-depth, mass spectrometry-based characterization of three inhibitor affinity resins for protein kinase prefractionation from cell extracts was performed. Quantitative comparisons of kinase binding behavior identified the pyrido[2,3-*d*]pyrimidine-based compound VI16832 as highly efficient capture molecule for broad kinase enrichment. The VI16832 affinity resin was further established as a valuable tool for the comparative analysis of relative kinase expression levels across different cancer cell lines and further applied for phosphorylation site mapping that generated the so far largest dataset for protein kinases.

In the second part kinase enrichment with immobilized small molecules was further used to identify both direct targets and downstream signal transducers affected by the clinical kinase inhibitor imatinib. Competitive binding analyses revealed both known and previously unreported imatinib targets. Furthermore, quantitative phosphoproteomics analyses of kinase-enriched fractions upon imatinib treatment of CML cells identified more than 70 drug-regulated phosphorylation sites, most of which were not described previously. These data pointed to various additional mediators in Bcr-Abl-driven leukemogenic signaling, which are candidate proteins for further functional studies to unveil alternative targets for therapeutic intervention.

Finally, in the third part, a highly efficient workflow was established for strong cation exchange chromatography-based phosphoproteomics analysis. This enabled the development of an experimental approach which, by integrating chemical genetics of protein kinases and MS-based phosphoproteomics, allowed for the systematic *in vivo* analysis of kinase-substrate relationships. In total, 284 proteins were identified as substrates of Plk1. Most of these have not been reported as Plk1 substrates but reflect known sites of cellular Plk1 function, however, in a yet unprecedented molecular complexity. Notably, identified Plk1 phosphorylation sites on cellular substrates correlated well with previously reported Plk1 substrate requirements. Therefore, our study provides a multitude of valuable candidates for further functional analysis. Moreover, an experimental design was developed that ensured the detection of biologically reproducible regulation events with very high confidence and can in principle be applied to any type of quantitative proteomics analysis.

VII. Literature

1. Sutherland EW, Jr., Wosilait WD. Inactivation and activation of liver phosphorylase. *Nature* 1955;175:169-70.
2. Fischer EH, Krebs EG. Conversion of phosphorylase b to phosphorylase a in muscle extracts. *J Biol Chem* 1955;216:121-32.
3. Eckhart W, Hutchinson MA, Hunter T. An activity phosphorylating tyrosine in polyoma T antigen immunoprecipitates. *Cell* 1979;18:925-33.
4. Hunter T, Sefton BM. Transforming gene product of Rous sarcoma virus phosphorylates tyrosine. *Proc Natl Acad Sci U S A* 1980;77:1311-5.
5. Witte ON, Dasgupta A, Baltimore D. Abelson murine leukaemia virus protein is phosphorylated in vitro to form phosphotyrosine. *Nature* 1980;283:826-31.
6. Ullrich A, Coussens L, Hayflick JS, et al. Human epidermal growth factor receptor cDNA sequence and aberrant expression of the amplified gene in A431 epidermoid carcinoma cells. *Nature* 1984;309:418-25.
7. Manning G, Plowman GD, Hunter T, Sudarsanam S. Evolution of protein kinase signaling from yeast to man. *Trends Biochem Sci* 2002;27:514-20.
8. Manning G, Whyte DB, Martinez R, Hunter T, Sudarsanam S. The protein kinase complement of the human genome. *Science (New York, NY)* 2002;298:1912-34.
9. Cohen P. The role of protein phosphorylation in human health and disease. The Sir Hans Krebs Medal Lecture. *Eur J Biochem* 2001;268:5001-10.
10. Ubersax JA, Ferrell JE, Jr. Mechanisms of specificity in protein phosphorylation. *Nat Rev Mol Cell Biol* 2007;8:530-41.
11. Zheng J, Knighton DR, ten Eyck LF, et al. Crystal structure of the catalytic subunit of cAMP-dependent protein kinase complexed with MgATP and peptide inhibitor. *Biochemistry* 1993;32:2154-61.
12. Nolen B, Taylor S, Ghosh G. Regulation of protein kinases; controlling activity through activation segment conformation. *Molecular cell* 2004;15:661-75.
13. Seet BT, Dikic I, Zhou MM, Pawson T. Reading protein modifications with interaction domains. *Nat Rev Mol Cell Biol* 2006;7:473-83.
14. Pawson T. Dynamic control of signaling by modular adaptor proteins. *Curr Opin Cell Biol* 2007;19:112-6.
15. Yang XJ. Multisite protein modification and intramolecular signaling. *Oncogene* 2005;24:1653-62.
16. Stehelin D, Varmus HE, Bishop JM, Vogt PK. DNA related to the transforming gene(s) of avian sarcoma viruses is present in normal avian DNA. *Nature* 1976;260:170-3.
17. Slamon DJ, Clark GM, Wong SG, Levin WJ, Ullrich A, McGuire WL. Human breast cancer: correlation of relapse and survival with amplification of the HER-2/neu oncogene. *Science* 1987;235:177-82.
18. Blume-Jensen P, Hunter T. Oncogenic kinase signalling. *Nature* 2001;411:355-65.
19. Bardelli A, Parsons DW, Silliman N, et al. Mutational analysis of the tyrosine kinome in colorectal cancers. *Science* 2003;300:949.

20. Notarangelo LD, Mella P, Jones A, et al. Mutations in severe combined immune deficiency (SCID) due to JAK3 deficiency. *Hum Mutat* 2001;18:255-63.
21. Malecki MT. Genetics of type 2 diabetes mellitus. *Diabetes Res Clin Pract* 2005;68 Suppl1:S10-21.
22. Lugo TG, Pendergast AM, Muller AJ, Witte ON. Tyrosine kinase activity and transformation potency of bcr-abl oncogene products. *Science* 1990;247:1079-82.
23. Stratton MR, Campbell PJ, Futreal PA. The cancer genome. *Nature* 2009;458:719-24.
24. Strebhardt K, Ullrich A. Paul Ehrlich's magic bullet concept: 100 years of progress. *Nat Rev Cancer* 2008.
25. Krause DS, Van Etten RA. Tyrosine kinases as targets for cancer therapy. *The New England journal of medicine* 2005;353:172-87.
26. Faivre S, Demetri G, Sargent W, Raymond E. Molecular basis for sunitinib efficacy and future clinical development. *Nature reviews* 2007;6:734-45.
27. Omura S, Iwai Y, Hirano A, et al. A new alkaloid AM-2282 OF *Streptomyces* origin. Taxonomy, fermentation, isolation and preliminary characterization. *J Antibiot (Tokyo)* 1977;30:275-82.
28. Tamaoki T, Nomoto H, Takahashi I, Kato Y, Morimoto M, Tomita F. Staurosporine, a potent inhibitor of phospholipid/Ca⁺⁺dependent protein kinase. *Biochem Biophys Res Commun* 1986;135:397-402.
29. Graziani Y, Erikson E, Erikson RL. The effect of quercetin on the phosphorylation activity of the Rous sarcoma virus transforming gene product in vitro and in vivo. *Eur J Biochem* 1983;135:583-9.
30. Hidaka H, Inagaki M, Kawamoto S, Sasaki Y. Isoquinolinesulfonamides, novel and potent inhibitors of cyclic nucleotide dependent protein kinase and protein kinase C. *Biochemistry* 1984;23:5036-41.
31. Yaish P, Gazit A, Gilon C, Levitzki A. Blocking of EGF-dependent cell proliferation by EGF receptor kinase inhibitors. *Science* 1988;242:933-5.
32. Bennett JH. Case of hypertrophy of the spleen and liver in which death took place from suppuration of the blood. *Edinburgh Medical and Surgical Journal* 1845;64:413-23.
33. Virchow R. Weisses Blut. *Frorieps Notizen* 1845;36:151-6.
34. Melo JV, Barnes DJ. Chronic myeloid leukaemia as a model of disease evolution in human cancer. *Nat Rev Cancer* 2007;7:441-53.
35. Nowell PC, Hungerford DA. A minute chromosome in human chronic granulocytic leukemia. *Science* 1960;132:1497.
36. Rowley JD. Letter: A new consistent chromosomal abnormality in chronic myelogenous leukaemia identified by quinacrine fluorescence and Giemsa staining. *Nature* 1973;243:290-3.
37. Ben-Neriah Y, Daley GQ, Mes-Masson AM, Witte ON, Baltimore D. The chronic myelogenous leukemia-specific P210 protein is the product of the bcr/abl hybrid gene. *Science* 1986;233:212-4.
38. Kurzrock R, Shtalrid M, Romero P, et al. A novel c-abl protein product in Philadelphia-positive acute lymphoblastic leukaemia. *Nature* 1987;325:631-5.
39. Pane F, Frigeri F, Sindona M, et al. Neutrophilic-chronic myeloid leukemia: a distinct disease with a specific molecular marker (BCR/ABL with C3/A2 junction). *Blood* 1996;88:2410-4.
40. Hanahan D, Weinberg RA. The hallmarks of cancer. *Cell* 2000;100:57-70.

41. Fialkow PJ, Martin PJ, Najfeld V, Penfold GK, Jacobson RJ, Hansen JA. Evidence for a multistep pathogenesis of chronic myelogenous leukemia. *Blood* 1981;58:158-63.
42. McLaughlin J, Chianese E, Witte ON. In vitro transformation of immature hematopoietic cells by the P210 BCR/ABL oncogene product of the Philadelphia chromosome. *Proc Natl Acad Sci U S A* 1987;84:6558-62.
43. Daley GQ, Van Etten RA, Baltimore D. Induction of chronic myelogenous leukemia in mice by the P210bcr/abl gene of the Philadelphia chromosome. *Science* 1990;247:824-30.
44. Deininger MW, Goldman JM, Melo JV. The molecular biology of chronic myeloid leukemia. *Blood* 2000;96:3343-56.
45. Nagar B, Hantschel O, Young MA, et al. Structural basis for the autoinhibition of c-Abl tyrosine kinase. *Cell* 2003;112:859-71.
46. Hantschel O, Nagar B, Guettler S, et al. A myristoyl/phosphotyrosine switch regulates c-Abl. *Cell* 2003;112:845-57.
47. McWhirter JR, Wang JY. Activation of tyrosinase kinase and microfilament-binding functions of c-abl by bcr sequences in bcr/abl fusion proteins. *Mol Cell Biol* 1991;11:1553-65.
48. Muller AJ, Young JC, Pendergast AM, et al. BCR first exon sequences specifically activate the BCR/ABL tyrosine kinase oncogene of Philadelphia chromosome-positive human leukemias. *Mol Cell Biol* 1991;11:1785-92.
49. Smith KM, Yacobi R, Van Etten RA. Autoinhibition of Bcr-Abl through its SH3 domain. *Mol Cell* 2003;12:27-37.
50. Pendergast AM, Quilliam LA, Cripe LD, et al. BCR-ABL-induced oncogenesis is mediated by direct interaction with the SH2 domain of the GRB-2 adaptor protein. *Cell* 1993;75:175-85.
51. Puil L, Liu J, Gish G, et al. Bcr-Abl oncoproteins bind directly to activators of the Ras signalling pathway. *EMBO J* 1994;13:764-73.
52. Oda T, Heaney C, Hagopian JR, Okuda K, Griffin JD, Druker BJ. Crkl is the major tyrosine-phosphorylated protein in neutrophils from patients with chronic myelogenous leukemia. *J Biol Chem* 1994;269:22925-8.
53. Pelicci G, Lanfrancone L, Salcini AE, et al. Constitutive phosphorylation of Shc proteins in human tumors. *Oncogene* 1995;11:899-907.
54. Sattler M, Mohi MG, Pride YB, et al. Critical role for Gab2 in transformation by BCR/ABL. *Cancer Cell* 2002;1:479-92.
55. Franke TF, Kaplan DR, Cantley LC. PI3K: downstream AKTion blocks apoptosis. *Cell* 1997;88:435-7.
56. Goss VL, Lee KA, Moritz A, et al. A common phosphotyrosine signature for the Bcr-Abl kinase. *Blood* 2006;107:4888-97.
57. Bantscheff M, Eberhard D, Abraham Y, et al. Quantitative chemical proteomics reveals mechanisms of action of clinical ABL kinase inhibitors. *Nat Biotechnol* 2007;25:1035-44.
58. Kujawski LA, Talpaz M. The role of interferon-alpha in the treatment of chronic myeloid leukemia. *Cytokine Growth Factor Rev* 2007;18:459-71.
59. Graziani Y, Chayoth R, Karny N, Feldman B, Levy J. Regulation of protein kinases activity by quercetin in Ehrlich ascites tumor cells. *Biochim Biophys Acta* 1982;714:415-21.
60. Akiyama T, Ishida J, Nakagawa S, et al. Genistein, a specific inhibitor of tyrosine-specific protein kinases. *J Biol Chem* 1987;262:5592-5.

61. Anafi M, Gazit A, Gilon C, Ben-Neriah Y, Levitzki A. Selective interactions of transforming and normal abl proteins with ATP, tyrosine-copolymer substrates, and tyrphostins. *J Biol Chem* 1992;267:4518-23.
62. Anafi M, Gazit A, Zehavi A, Ben-Neriah Y, Levitzki A. Tyrphostin-induced inhibition of p210bcr-abl tyrosine kinase activity induces K562 to differentiate. *Blood* 1993;82:3524-9.
63. Buchdunger E, Zimmermann J, Mett H, et al. Inhibition of the Abl protein-tyrosine kinase in vitro and in vivo by a 2-phenylaminopyrimidine derivative. *Cancer Res* 1996;56:100-4.
64. Heinrich MC, Griffith DJ, Druker BJ, Wait CL, Ott KA, Zigler AJ. Inhibition of c-kit receptor tyrosine kinase activity by STI 571, a selective tyrosine kinase inhibitor. *Blood* 2000;96:925-32.
65. Okuda K, Weisberg E, Gilliland DG, Griffin JD. ARG tyrosine kinase activity is inhibited by STI571. *Blood* 2001;97:2440-8.
66. Druker BJ, Tamura S, Buchdunger E, et al. Effects of a selective inhibitor of the Abl tyrosine kinase on the growth of Bcr-Abl positive cells. *Nat Med* 1996;2:561-6.
67. Carroll M, Ohno-Jones S, Tamura S, et al. CGP 57148, a tyrosine kinase inhibitor, inhibits the growth of cells expressing BCR-ABL, TEL-ABL, and TEL-PDGFR fusion proteins. *Blood* 1997;90:4947-52.
68. Druker BJ, Talpaz M, Resta DJ, et al. Efficacy and safety of a specific inhibitor of the BCR-ABL tyrosine kinase in chronic myeloid leukemia. *N Engl J Med* 2001;344:1031-7.
69. Kantarjian H, Sawyers C, Hochhaus A, et al. Hematologic and cytogenetic responses to imatinib mesylate in chronic myelogenous leukemia. *N Engl J Med* 2002;346:645-52.
70. Daub H, Specht K, Ullrich A. Strategies to overcome resistance to targeted protein kinase inhibitors. *Nat Rev Drug Discov* 2004;3:1001-10.
71. Gorre ME, Mohammed M, Ellwood K, et al. Clinical resistance to STI-571 cancer therapy caused by BCR-ABL gene mutation or amplification. *Science* 2001;293:876-80.
72. Druker BJ, Guilhot F, O'Brien SG, et al. Five-year follow-up of patients receiving imatinib for chronic myeloid leukemia. *N Engl J Med* 2006;355:2408-17.
73. Shah NP, Nicoll JM, Nagar B, et al. Multiple BCR-ABL kinase domain mutations confer polyclonal resistance to the tyrosine kinase inhibitor imatinib (STI571) in chronic phase and blast crisis chronic myeloid leukemia. *Cancer Cell* 2002;2:117-25.
74. Weisberg E, Manley PW, Cowan-Jacob SW, Hochhaus A, Griffin JD. Second generation inhibitors of BCR-ABL for the treatment of imatinib-resistant chronic myeloid leukaemia. *Nat Rev Cancer* 2007;7:345-56.
75. Schindler T, Bornmann W, Pellicena P, Miller WT, Clarkson B, Kuriyan J. Structural mechanism for STI-571 inhibition of abelson tyrosine kinase. *Science* 2000;289:1938-42.
76. Nagar B, Bornmann WG, Pellicena P, et al. Crystal structures of the kinase domain of c-Abl in complex with the small molecule inhibitors PD173955 and imatinib (STI-571). *Cancer Res* 2002;62:4236-43.
77. Weisberg E, Manley PW, Breitenstein W, et al. Characterization of AMN107, a selective inhibitor of native and mutant Bcr-Abl. *Cancer Cell* 2005;7:129-41.
78. Shah NP, Tran C, Lee FY, Chen P, Norris D, Sawyers CL. Overriding imatinib resistance with a novel ABL kinase inhibitor. *Science* 2004;305:399-401.
79. Carter TA, Wodicka LM, Shah NP, et al. Inhibition of drug-resistant mutants of ABL, KIT, and EGF receptor kinases. *Proc Natl Acad Sci U S A* 2005;102:11011-6.

80. Giles FJ, Cortes J, Jones D, Bergstrom D, Kantarjian H, Freedman SJ. MK-0457, a novel kinase inhibitor, is active in patients with chronic myeloid leukemia or acute lymphocytic leukemia with the T315I BCR-ABL mutation. *Blood* 2007;109:500-2.
81. Zhang J, Adrian FJ, Jahnke W, et al. Targeting Bcr-Abl by combining allosteric with ATP-binding-site inhibitors. *Nature* 2010.
82. Cortes J, Jabbour E, Kantarjian H, et al. Dynamics of BCR-ABL kinase domain mutations in chronic myeloid leukemia after sequential treatment with multiple tyrosine kinase inhibitors. *Blood* 2007;110:4005-11.
83. Lapenna S, Giordano A. Cell cycle kinases as therapeutic targets for cancer. *Nat Rev Drug Discov* 2009;8:547-66.
84. Lowery DM, Lim D, Yaffe MB. Structure and function of Polo-like kinases. *Oncogene* 2005;24:248-59.
85. Archambault V, Glover DM. Polo-like kinases: conservation and divergence in their functions and regulation. *Nat Rev Mol Cell Biol* 2009;10:265-75.
86. Lindon C, Pines J. Ordered proteolysis in anaphase inactivates Plk1 to contribute to proper mitotic exit in human cells. *J Cell Biol* 2004;164:233-41.
87. Elia AE, Cantley LC, Yaffe MB. Proteomic screen finds pSer/pThr-binding domain localizing Plk1 to mitotic substrates. *Science* 2003;299:1228-31.
88. Lake RJ, Jelinek WR. Cell cycle- and terminal differentiation-associated regulation of the mouse mRNA encoding a conserved mitotic protein kinase. *Mol Cell Biol* 1993;13:7793-801.
89. Jang YJ, Ma S, Terada Y, Erikson RL. Phosphorylation of threonine 210 and the role of serine 137 in the regulation of mammalian polo-like kinase. *J Biol Chem* 2002;277:44115-20.
90. Qian YW, Erikson E, Maller JL. Purification and cloning of a protein kinase that phosphorylates and activates the polo-like kinase Plx1. *Science* 1998;282:1701-4.
91. Macurek L, Lindqvist A, Lim D, et al. Polo-like kinase-1 is activated by aurora A to promote checkpoint recovery. *Nature* 2008;455:119-23.
92. Seki A, Coppinger JA, Jang CY, Yates JR, Fang G. Bora and the kinase Aurora a cooperatively activate the kinase Plk1 and control mitotic entry. *Science* 2008;320:1655-8.
93. Elia AE, Rellos P, Haire LF, et al. The molecular basis for phosphodependent substrate targeting and regulation of Plks by the Polo-box domain. *Cell* 2003;115:83-95.
94. Lee KS, Grenfell TZ, Yarm FR, Erikson RL. Mutation of the polo-box disrupts localization and mitotic functions of the mammalian polo kinase Plk. *Proc Natl Acad Sci U S A* 1998;95:9301-6.
95. Golsteyn RM, Mundt KE, Fry AM, Nigg EA. Cell cycle regulation of the activity and subcellular localization of Plk1, a human protein kinase implicated in mitotic spindle function. *J Cell Biol* 1995;129:1617-28.
96. Lane HA, Nigg EA. Antibody microinjection reveals an essential role for human polo-like kinase 1 (Plk1) in the functional maturation of mitotic centrosomes. *J Cell Biol* 1996;135:1701-13.
97. Barr FA, Sillje HH, Nigg EA. Polo-like kinases and the orchestration of cell division. *Nat Rev Mol Cell Biol* 2004;5:429-40.
98. Kumagai A, Dunphy WG. Purification and molecular cloning of Plx1, a Cdc25-regulatory kinase from *Xenopus* egg extracts. *Science* 1996;273:1377-80.
99. Toyoshima-Morimoto F, Taniguchi E, Nishida E. Plk1 promotes nuclear translocation of human Cdc25C during prophase. *EMBO Rep* 2002;3:341-8.

100. Nigg EA. Mitotic kinases as regulators of cell division and its checkpoints. *Nat Rev Mol Cell Biol* 2001;2:21-32.
101. Toyoshima-Morimoto F, Taniguchi E, Shinya N, Iwamatsu A, Nishida E. Polo-like kinase 1 phosphorylates cyclin B1 and targets it to the nucleus during prophase. *Nature* 2001;410:215-20.
102. Nakajima H, Toyoshima-Morimoto F, Taniguchi E, Nishida E. Identification of a consensus motif for Plk (Polo-like kinase) phosphorylation reveals Myt1 as a Plk1 substrate. *J Biol Chem* 2003;278:25277-80.
103. Watanabe N, Arai H, Nishihara Y, Taniguchi M, Hunter T, Osada H. M-phase kinases induce phospho-dependent ubiquitination of somatic Wee1 by SCFbeta-TrCP. *Proc Natl Acad Sci U S A* 2004;101:4419-24.
104. Sunkel CE, Glover DM. polo, a mitotic mutant of *Drosophila* displaying abnormal spindle poles. *J Cell Sci* 1988;89 (Pt 1):25-38.
105. Varmark H. Functional role of centrosomes in spindle assembly and organization. *J Cell Biochem* 2004;91:904-14.
106. Casenghi M, Barr FA, Nigg EA. Phosphorylation of Nlp by Plk1 negatively regulates its dynein-dynactin-dependent targeting to the centrosome. *J Cell Sci* 2005;118:5101-8.
107. Casenghi M, Meraldi P, Weinhart U, Duncan PI, Korner R, Nigg EA. Polo-like kinase 1 regulates Nlp, a centrosome protein involved in microtubule nucleation. *Dev Cell* 2003;5:113-25.
108. Hanisch A, Wehner A, Nigg EA, Sillje HH. Different Plk1 functions show distinct dependencies on Polo-Box domain-mediated targeting. *Mol Biol Cell* 2006;17:448-59.
109. Sumara I, Gimenez-Abian JF, Gerlich D, et al. Roles of polo-like kinase 1 in the assembly of functional mitotic spindles. *Curr Biol* 2004;14:1712-22.
110. Ahonen LJ, Kallio MJ, Daum JR, et al. Polo-like kinase 1 creates the tension-sensing 3F3/2 phosphoepitope and modulates the association of spindle-checkpoint proteins at kinetochores. *Curr Biol* 2005;15:1078-89.
111. Wong OK, Fang G. Plx1 is the 3F3/2 kinase responsible for targeting spindle checkpoint proteins to kinetochores. *J Cell Biol* 2005;170:709-19.
112. Wong OK, Fang G. Cdk1 phosphorylation of BubR1 controls spindle checkpoint arrest and Plk1-mediated formation of the 3F3/2 epitope. *J Cell Biol* 2007;179:611-7.
113. Peters JM. The anaphase-promoting complex: proteolysis in mitosis and beyond. *Mol Cell* 2002;9:931-43.
114. Hansen DV, Tung JJ, Jackson PK. CaMKII and polo-like kinase 1 sequentially phosphorylate the cytostatic factor Emi2/XErp1 to trigger its destruction and meiotic exit. *Proc Natl Acad Sci U S A* 2006;103:608-13.
115. Schmidt A, Duncan PI, Rauh NR, et al. *Xenopus* polo-like kinase Plx1 regulates XErp1, a novel inhibitor of APC/C activity. *Genes Dev* 2005;19:502-13.
116. Nasmyth K. How do so few control so many? *Cell* 2005;120:739-46.
117. Hauf S, Roitinger E, Koch B, Dittrich CM, Mechtler K, Peters JM. Dissociation of cohesin from chromosome arms and loss of arm cohesion during early mitosis depends on phosphorylation of SA2. *PLoS Biol* 2005;3:e69.
118. Tsou MF, Wang WJ, George KA, Uryu K, Stearns T, Jallepalli PV. Polo kinase and separase regulate the mitotic licensing of centriole duplication in human cells. *Dev Cell* 2009;17:344-54.
119. Neef R, Preisinger C, Sutcliffe J, et al. Phosphorylation of mitotic kinesin-like protein 2 by polo-like kinase 1 is required for cytokinesis. *J Cell Biol* 2003;162:863-75.

120. Zhou T, Aumais JP, Liu X, Yu-Lee LY, Erikson RL. A role for Plk1 phosphorylation of NudC in cytokinesis. *Dev Cell* 2003;5:127-38.
121. Litvak V, Argov R, Dahan N, et al. Mitotic phosphorylation of the peripheral Golgi protein Nir2 by Cdk1 provides a docking mechanism for Plk1 and affects cytokinesis completion. *Mol Cell* 2004;14:319-30.
122. Bishop AC, Ubersax JA, Petsch DT, et al. A chemical switch for inhibitor-sensitive alleles of any protein kinase. *Nature* 2000;407:395-401.
123. Burkard ME, Randall CL, Larochelle S, et al. Chemical genetics reveals the requirement for Polo-like kinase 1 activity in positioning RhoA and triggering cytokinesis in human cells. *Proc Natl Acad Sci U S A* 2007;104:4383-8.
124. Burkard ME, Maciejowski J, Rodriguez-Bravo V, et al. Plk1 self-organization and priming phosphorylation of HsCYK-4 at the spindle midzone regulate the onset of division in human cells. *PLoS Biol* 2009;7:e1000111.
125. Thompson SL, Compton DA. Examining the link between chromosomal instability and aneuploidy in human cells. *J Cell Biol* 2008;180:665-72.
126. Greene DR, Taylor SR, Wheeler TM, Scardino PT. DNA ploidy by image analysis of individual foci of prostate cancer: a preliminary report. *Cancer Res* 1991;51:4084-9.
127. Bartos JD, Stoler DL, Matsui S, et al. Genomic heterogeneity and instability in colorectal cancer: spectral karyotyping, glutathione transferase-M1 and ras. *Mutat Res* 2004;568:283-92.
128. Eckerdt F, Yuan J, Strebhardt K. Polo-like kinases and oncogenesis. *Oncogene* 2005;24:267-76.
129. Strebhardt K, Ullrich A. Targeting polo-like kinase 1 for cancer therapy. *Nat Rev Cancer* 2006;6:321-30.
130. Sherr CJ, McCormick F. The RB and p53 pathways in cancer. *Cancer Cell* 2002;2:103-12.
131. Smits VA, Klompaker R, Arnaud L, Rijksen G, Nigg EA, Medema RH. Polo-like kinase-1 is a target of the DNA damage checkpoint. *Nat Cell Biol* 2000;2:672-6.
132. van Vugt MA, Bras A, Medema RH. Polo-like kinase-1 controls recovery from a G2 DNA damage-induced arrest in mammalian cells. *Mol Cell* 2004;15:799-811.
133. Ando K, Ozaki T, Yamamoto H, et al. Polo-like kinase 1 (Plk1) inhibits p53 function by physical interaction and phosphorylation. *J Biol Chem* 2004;279:25549-61.
134. Guan R, Tapang P, Levenson JD, Albert D, Giranda VL, Luo Y. Small interfering RNA-mediated Polo-like kinase 1 depletion preferentially reduces the survival of p53-defective, oncogenic transformed cells and inhibits tumor growth in animals. *Cancer Res* 2005;65:2698-704.
135. Liu X, Lei M, Erikson RL. Normal cells, but not cancer cells, survive severe Plk1 depletion. *Mol Cell Biol* 2006;26:2093-108.
136. Lenart P, Petronczki M, Steegmaier M, et al. The small-molecule inhibitor BI 2536 reveals novel insights into mitotic roles of polo-like kinase 1. *Curr Biol* 2007;17:304-15.
137. Steegmaier M, Hoffmann M, Baum A, et al. BI 2536, a potent and selective inhibitor of polo-like kinase 1, inhibits tumor growth in vivo. *Curr Biol* 2007;17:316-22.
138. Reindl W, Yuan J, Kramer A, Strebhardt K, Berg T. Inhibition of polo-like kinase 1 by blocking polo-box domain-dependent protein-protein interactions. *Chem Biol* 2008;15:459-66.
139. Aebersold R, Mann M. Mass spectrometry-based proteomics. *Nature* 2003;422:198-207.
140. de Godoy LM, Olsen JV, Cox J, et al. Comprehensive mass-spectrometry-based proteome quantification of haploid versus diploid yeast. *Nature* 2008;455:1251-4.

141. Mann M. Can proteomics retire the western blot? *J Proteome Res* 2008;7:3065.
142. Scigelova M, Makarov A. Orbitrap mass analyzer--overview and applications in proteomics. *Proteomics* 2006;6 Suppl 2:16-21.
143. Olsen JV, Ong SE, Mann M. Trypsin cleaves exclusively C-terminal to arginine and lysine residues. *Mol Cell Proteomics* 2004;3:608-14.
144. Beausoleil SA, Jedrychowski M, Schwartz D, et al. Large-scale characterization of HeLa cell nuclear phosphoproteins. *Proc Natl Acad Sci U S A* 2004;101:12130-5.
145. Florens L, Washburn MP, Raine JD, et al. A proteomic view of the *Plasmodium falciparum* life cycle. *Nature* 2002;419:520-6.
146. Liu H, Sadygov RG, Yates JR, 3rd. A model for random sampling and estimation of relative protein abundance in shotgun proteomics. *Anal Chem* 2004;76:4193-201.
147. Ong SE, Mann M. Mass spectrometry-based proteomics turns quantitative. *Nat Chem Biol* 2005;1:252-62.
148. Ong SE, Blagoev B, Kratchmarova I, et al. Stable isotope labeling by amino acids in cell culture, SILAC, as a simple and accurate approach to expression proteomics. *Mol Cell Proteomics* 2002;1:376-86.
149. Mann M. Functional and quantitative proteomics using SILAC. *Nat Rev Mol Cell Biol* 2006;7:952-8.
150. Olsen JV, Blagoev B, Gnad F, et al. Global, in vivo, and site-specific phosphorylation dynamics in signaling networks. *Cell* 2006;127:635-48.
151. Kruger M, Moser M, Ussar S, et al. SILAC mouse for quantitative proteomics uncovers kindlin-3 as an essential factor for red blood cell function. *Cell* 2008;134:353-64.
152. Gygi SP, Rist B, Gerber SA, Turecek F, Gelb MH, Aebersold R. Quantitative analysis of complex protein mixtures using isotope-coded affinity tags. *Nat Biotechnol* 1999;17:994-9.
153. Ross PL, Huang YN, Marchese JN, et al. Multiplexed protein quantitation in *Saccharomyces cerevisiae* using amine-reactive isobaric tagging reagents. *Mol Cell Proteomics* 2004;3:1154-69.
154. Thompson A, Schafer J, Kuhn K, et al. Tandem mass tags: a novel quantification strategy for comparative analysis of complex protein mixtures by MS/MS. *Anal Chem* 2003;75:1895-904.
155. Gerber SA, Rush J, Stemman O, Kirschner MW, Gygi SP. Absolute quantification of proteins and phosphoproteins from cell lysates by tandem MS. *Proc Natl Acad Sci U S A* 2003;100:6940-5.
156. Hunter T, Cooper JA. Protein-tyrosine kinases. *Annu Rev Biochem* 1985;54:897-930.
157. Johnson SA, Hunter T. Kinomics: methods for deciphering the kinome. *Nat Methods* 2005;2:17-25.
158. Mertins P, Eberl HC, Renkawitz J, et al. Investigation of protein-tyrosine phosphatase 1B function by quantitative proteomics. *Mol Cell Proteomics* 2008;7:1763-77.
159. Macek B, Mann M, Olsen JV. Global and Site-Specific Quantitative Phosphoproteomics: Principles and Applications. *Annu Rev Pharmacol Toxicol* 2008.
160. Schreiber TB, Mausbacher N, Breitkopf SB, Grundner-Culemann K, Daub H. Quantitative phosphoproteomics--an emerging key technology in signal-transduction research. *Proteomics* 2008;8:4416-32.
161. Andersson L, Porath J. Isolation of phosphoproteins by immobilized metal (Fe³⁺) affinity chromatography. *Anal Biochem* 1986;154:250-4.

162. Posewitz MC, Tempst P. Immobilized gallium(III) affinity chromatography of phosphopeptides. *Anal Chem* 1999;71:2883-92.
163. Larsen MR, Thingholm TE, Jensen ON, Roepstorff P, Jorgensen TJ. Highly selective enrichment of phosphorylated peptides from peptide mixtures using titanium dioxide microcolumns. *Mol Cell Proteomics* 2005;4:873-86.
164. Pinkse MW, Uitto PM, Hilhorst MJ, Ooms B, Heck AJ. Selective isolation at the femtomole level of phosphopeptides from proteolytic digests using 2D-NanoLC-ESI-MS/MS and titanium oxide precolumns. *Anal Chem* 2004;76:3935-43.
165. Zhai B, Villen J, Beausoleil SA, Mintseris J, Gygi SP. Phosphoproteome analysis of *Drosophila melanogaster* embryos. *J Proteome Res* 2008;7:1675-82.
166. Daub H, Olsen JV, Bairlein M, et al. Kinase-selective enrichment enables quantitative phosphoproteomics of the kinome across the cell cycle. *Molecular cell* 2008;31:438-48.
167. Dephoure N, Zhou C, Villen J, et al. A quantitative atlas of mitotic phosphorylation. *Proc Natl Acad Sci U S A* 2008;105:10762-7.
168. Olsen JV, Vermeulen M, Santamaria A, et al. Quantitative phosphoproteomics reveals widespread full phosphorylation site occupancy during mitosis. *Sci Signal* 2010;3:ra3.
169. Rix U, Superti-Furga G. Target profiling of small molecules by chemical proteomics. *Nat Chem Biol* 2009;5:616-24.
170. Bantscheff M, Scholten A, Heck AJ. Revealing promiscuous drug-target interactions by chemical proteomics. *Drug Discov Today* 2009;14:1021-9.
171. Cuatrecasas P, Wilchek M, Anfinsen CB. Selective enzyme purification by affinity chromatography. *Proc Natl Acad Sci U S A* 1968;61:636-43.
172. Karaman MW, Herrgard S, Treiber DK, et al. A quantitative analysis of kinase inhibitor selectivity. *Nat Biotechnol* 2008;26:127-32.
173. Knockaert M, Gray N, Damiens E, et al. Intracellular targets of cyclin-dependent kinase inhibitors: identification by affinity chromatography using immobilised inhibitors. *Chem Biol* 2000;7:411-22.
174. Knockaert M, Lenormand P, Gray N, Schultz P, Pouyssegur J, Meijer L. p42/p44 MAPKs are intracellular targets of the CDK inhibitor purvalanol. *Oncogene* 2002;21:6413-24.
175. Godl K, Wissing J, Kurtenbach A, et al. An efficient proteomics method to identify the cellular targets of protein kinase inhibitors. *Proceedings of the National Academy of Sciences of the United States of America* 2003;100:15434-9.
176. Brehmer D, Godl K, Zech B, Wissing J, Daub H. Proteome-wide identification of cellular targets affected by bisindolylmaleimide-type protein kinase C inhibitors. *Mol Cell Proteomics* 2004;3:490-500.
177. Wissing J, Godl K, Brehmer D, et al. Chemical proteomic analysis reveals alternative modes of action for pyrido[2,3-d]pyrimidine kinase inhibitors. *Mol Cell Proteomics* 2004;3:1181-93.
178. Brehmer D, Greff Z, Godl K, et al. Cellular targets of gefitinib. *Cancer Res* 2005;65:379-82.
179. Godl K, Gruss OJ, Eickhoff J, et al. Proteomic characterization of the angiogenesis inhibitor SU6668 reveals multiple impacts on cellular kinase signaling. *Cancer Res* 2005;65:6919-26.
180. Wissing J, Jansch L, Nimtz M, et al. Proteomics analysis of protein kinases by target class-selective prefractionation and tandem mass spectrometry. *Mol Cell Proteomics* 2007;6:537-47.

181. Sharma K, Weber C, Bairlein M, et al. Proteomics strategy for quantitative protein interaction profiling in cell extracts. *Nat Methods* 2009;6:741-4.
182. Shah K, Liu Y, Deirmengian C, Shokat KM. Engineering unnatural nucleotide specificity for Rous sarcoma virus tyrosine kinase to uniquely label its direct substrates. *Proc Natl Acad Sci U S A* 1997;94:3565-70.
183. Taylor S, Peters JM. Polo and Aurora kinases: lessons derived from chemical biology. *Curr Opin Cell Biol* 2008;20:77-84.
184. Bain J, Plater L, Elliott M, et al. The selectivity of protein kinase inhibitors: a further update. *Biochem J* 2007;408:297-315.
185. Knight ZA, Shokat KM. Features of selective kinase inhibitors. *Chem Biol* 2005;12:621-37.
186. Bishop AC, Shah K, Liu Y, Witucki L, Kung C, Shokat KM. Design of allele-specific inhibitors to probe protein kinase signaling. *Curr Biol* 1998;8:257-66.
187. Rae JM, Creighton CJ, Meck JM, Haddad BR, Johnson MD. MDA-MB-435 cells are derived from M14 melanoma cells--a loss for breast cancer, but a boon for melanoma research. *Breast cancer research and treatment* 2007;104:13-9.
188. Senis YA, Craig AW, Greer PA. Fps/Fes and Fer protein-tyrosinekinases play redundant roles in regulating hematopoiesis. *Exp Hematol* 2003;31:673-81.
189. Sambrook J, Fritsch, E. & Maniatis, T. *Molecular Cloning: A Laboratory Manual*. Cold Spring Harbor Laboratory Press: New York 1990.
190. Gershoni JM, Palade GE. Protein blotting: principles and applications. *Anal Biochem* 1983;131:1-15.
191. Barvian M, Boschelli DH, Cossrow J, et al. Pyrido[2,3-d]pyrimidin-7-one inhibitors of cyclin-dependent kinases. *Journal of medicinal chemistry* 2000;43:4606-16.
192. Wessel D, Flugge UI. A method for the quantitative recovery of protein in dilute solution in the presence of detergents and lipids. *Anal Biochem* 1984;138:141-3.
193. Shevchenko A, Tomas H, Havlis J, Olsen JV, Mann M. In-gel digestion for mass spectrometric characterization of proteins and proteomes. *Nat Protoc* 2006;1:2856-60.
194. Rappsilber J, Mann M, Ishihama Y. Protocol for micro-purification, enrichment, pre-fractionation and storage of peptides for proteomics using StageTips. *Nature protocols* 2007;2:1896-906.
195. Villen J, Gygi SP. The SCX/IMAC enrichment approach for global phosphorylation analysis by mass spectrometry. *Nat Protoc* 2008;3:1630-8.
196. Gruhler A, Olsen JV, Mohammed S, et al. Quantitative phosphoproteomics applied to the yeast pheromone signaling pathway. *Mol Cell Proteomics* 2005;4:310-27.
197. Schroeder MJ, Shabanowitz J, Schwartz JC, Hunt DF, Coon JJ. A neutral loss activation method for improved phosphopeptide sequence analysis by quadrupole ion trap mass spectrometry. *Analytical chemistry* 2004;76:3590-8.
198. Olsen JV, de Godoy LM, Li G, et al. Parts per million mass accuracy on an Orbitrap mass spectrometer via lock mass injection into a C-trap. *Mol Cell Proteomics* 2005;4:2010-21.
199. Schulze WX, Mann M. A novel proteomic screen for peptide-protein interactions. *J Biol Chem* 2004;279:10756-64.
200. Gnad F, Ren S, Cox J, et al. PHOSIDA (phosphorylation site database): management, structural and evolutionary investigation, and prediction of phosphosites. *Genome Biol* 2007;8:R250.

201. Cox J, Mann M. MaxQuant enables high peptide identification rates, individualized p.p.b.-range mass accuracies and proteome-wide protein quantification. *Nat Biotech* 2008;26:1367-72.
202. Maere S, Heymans K, Kuiper M. BiNGO: a Cytoscape plugin to assess overrepresentation of gene ontology categories in biological networks. *Bioinformatics* 2005;21:3448-9.
203. Shannon P, Markiel A, Ozier O, et al. Cytoscape: a software environment for integrated models of biomolecular interaction networks. *Genome research* 2003;13:2498-504.
204. Adachi J, Kumar C, Zhang Y, Olsen JV, Mann M. The human urinary proteome contains more than 1500 proteins, including a large proportion of membrane proteins. *Genome Biol* 2006;7:R80.
205. Choudhary C, Kumar C, Gnad F, et al. Lysine acetylation targets protein complexes and co-regulates major cellular functions. *Science* 2009;325:834-40.
206. Daub H. Characterisation of kinase-selective inhibitors by chemical proteomics. *Biochimica et biophysica acta* 2005;1754:183-90.
207. Rix U, Hantschel O, Durnberger G, et al. Chemical proteomic profiles of the BCR-ABL inhibitors imatinib, nilotinib, and dasatinib reveal novel kinase and nonkinase targets. *Blood* 2007;110:4055-63.
208. Blencke S, Zech B, Engkvist O, et al. Characterization of a conserved structural determinant controlling protein kinase sensitivity to selective inhibitors. *Chemistry & biology* 2004;11:691-701.
209. Elias JE, Haas W, Faherty BK, Gygi SP. Comparative evaluation of mass spectrometry platforms used in large-scale proteomics investigations. *Nat Methods* 2005;2:667-75.
210. Gilliland DG, Griffin JD. The roles of FLT3 in hematopoiesis and leukemia. *Blood* 2002;100:1532-42.
211. Rikova K, Guo A, Zeng Q, et al. Global survey of phosphotyrosine signaling identifies oncogenic kinases in lung cancer. *Cell* 2007;131:1190-203.
212. Olsen JV, Mann M. Improved peptide identification in proteomics by two consecutive stages of mass spectrometric fragmentation. *Proc Natl Acad Sci U S A* 2004;101:13417-22.
213. Thingholm TE, Jensen ON, Robinson PJ, Larsen MR. SIMAC (sequential elution from IMAC), a phosphoproteomics strategy for the rapid separation of monophosphorylated from multiply phosphorylated peptides. *Mol Cell Proteomics* 2008;7:661-71.
214. Cohen P. Protein kinases--the major drug targets of the twenty-first century? *Nat Rev Drug Discov* 2002;1:309-15.
215. Lozzio CB, Lozzio BB. Human chronic myelogenous leukemia cell-line with positive Philadelphia chromosome. *Blood* 1975;45:321-34.
216. Cox J, Mann M. MaxQuant enables high peptide identification rates, individualized p.p.b.-range mass accuracies and proteome-wide protein quantification. *Nat Biotechnol* 2008;26:1367-72.
217. Goga A, McLaughlin J, Afar DE, Saffran DC, Witte ON. Alternative signals to RAS for hematopoietic transformation by the BCR-ABL oncogene. *Cell* 1995;82:981-8.
218. Atwell S, Adams JM, Badger J, et al. A novel mode of Gleevec binding is revealed by the structure of spleen tyrosine kinase. *J Biol Chem* 2004;279:55827-32.
219. Petronczki M, Lenart P, Peters JM. Polo on the Rise--from Mitotic Entry to Cytokinesis with Plk1. *Dev Cell* 2008;14:646-59.

220. van Vugt MA, Medema RH. Getting in and out of mitosis with Polo-like kinase-1. *Oncogene* 2005;24:2844-59.
221. Elowe S, Hummer S, Uldschmid A, Li X, Nigg EA. Tension-sensitive Plk1 phosphorylation on BubR1 regulates the stability of kinetochore microtubule interactions. *Genes Dev* 2007;21:2205-19.
222. Bodenmiller B, Mueller LN, Mueller M, Domon B, Aebersold R. Reproducible isolation of distinct, overlapping segments of the phosphoproteome. *Nat Methods* 2007;4:231-7.
223. Villen J, Beausoleil SA, Gerber SA, Gygi SP. Large-scale phosphorylation analysis of mouse liver. *Proc Natl Acad Sci U S A* 2007;104:1488-93.
224. Kratchmarova I, Blagoev B, Haack-Sorensen M, Kassem M, Mann M. Mechanism of divergent growth factor effects in mesenchymal stem cell differentiation. *Science* 2005;308:1472-7.
225. Su AI, Cooke MP, Ching KA, et al. Large-scale analysis of the human and mouse transcriptomes. *Proc Natl Acad Sci U S A* 2002;99:4465-70.
226. Patricelli MP, Szardenings AK, Liyanage M, et al. Functional interrogation of the kinome using nucleotide acyl phosphates. *Biochemistry* 2007;46:350-8.
227. Geiger T, Cox J, Ostasiewicz P, Wisniewski JR, Mann M. Super-SILAC mix for quantitative proteomics of human tumor tissue. *Nat Methods* 2010;7:383-5.
228. Li JJ, Li SA. Mitotic kinases: the key to duplication, segregation, and cytokinesis errors, chromosomal instability, and oncogenesis. *Pharmacology & therapeutics* 2006;111:974-84.
229. Cohen P. The regulation of protein function by multisite phosphorylation--a 25 year update. *Trends Biochem Sci* 2000;25:596-601.
230. Lienhard GE. Non-functional phosphorylations? *Trends Biochem Sci* 2008;33:351-2.
231. Salazar C, Hofer T. Versatile regulation of multisite protein phosphorylation by the order of phosphate processing and protein-protein interactions. *FEBS J* 2007;274:1046-61.
232. Scholten A, Poh MK, van Veen TA, van Breukelen B, Vos MA, Heck AJ. Analysis of the cGMP/cAMP interactome using a chemical proteomics approach in mammalian heart tissue validates sphingosine kinase type 1-interacting protein as a genuine and highly abundant AKAP. *J Proteome Res* 2006;5:1435-47.
233. Shiyama T, Furuya M, Yamazaki A, Terada T, Tanaka A. Design and synthesis of novel hydrophilic spacers for the reduction of nonspecific binding proteins on affinity resins. *Bioorg Med Chem* 2004;12:2831-41.
234. Manley PW, Cowan-Jacob SW, Buchdunger E, et al. Imatinib: a selective tyrosine kinase inhibitor. *Eur J Cancer* 2002;38 Suppl 5:S19-27.
235. Wisniewski D, Strife A, Swendeman S, et al. A novel SH2-containing phosphatidylinositol 3,4,5-trisphosphate 5-phosphatase (SHIP2) is constitutively tyrosine phosphorylated and associated with src homologous and collagen gene (SHC) in chronic myelogenous leukemia progenitor cells. *Blood* 1999;93:2707-20.
236. Brehme M, Hantschel O, Colinge J, et al. Charting the molecular network of the drug target Bcr-Abl. *Proc Natl Acad Sci U S A* 2009;106:7414-9.
237. Ong SE, Schenone M, Margolin AA, et al. Identifying the proteins to which small-molecule probes and drugs bind in cells. *Proc Natl Acad Sci U S A* 2009;106:4617-22.
238. Geahlen RL. Syk and pTyr'd: Signaling through the B cell antigen receptor. *Biochim Biophys Acta* 2009;1793:1115-27.
239. Kurosaki T, Kurosaki M. Transphosphorylation of Bruton's tyrosine kinase on tyrosine 551 is critical for B cell antigen receptor function. *J Biol Chem* 1997;272:15595-8.

240. Hantschel O, Rix U, Schmidt U, et al. The Btk tyrosine kinase is a major target of the Bcr-Abl inhibitor dasatinib. *Proc Natl Acad Sci U S A* 2007;104:13283-8.
241. MacPartlin M, Smith AM, Druker BJ, Honigberg LA, Deininger MW. Bruton's tyrosine kinase is not essential for Bcr-Abl-mediated transformation of lymphoid or myeloid cells. *Leukemia* 2008;22:1354-60.
242. Vadlamudi RK, Sahin AA, Adam L, Wang RA, Kumar R. Heregulin and HER2 signaling selectively activates c-Src phosphorylation at tyrosine 215. *FEBS Lett* 2003;543:76-80.
243. Lim Y, Han I, Jeon J, Park H, Bahk YY, Oh ES. Phosphorylation of focal adhesion kinase at tyrosine 861 is crucial for Ras transformation of fibroblasts. *J Biol Chem* 2004;279:29060-5.
244. Ren R. Mechanisms of BCR-ABL in the pathogenesis of chronic myelogenous leukaemia. *Nat Rev Cancer* 2005;5:172-83.
245. Ikezoe T, Yang J, Nishioka C, et al. A novel treatment strategy targeting polo-like kinase 1 in hematological malignancies. *Leukemia* 2009;23:1564-76.
246. ten Hoeve J, Kaartinen V, Fioretos T, et al. Cellular interactions of CRKL, and SH2-SH3 adaptor protein. *Cancer Res* 1994;54:2563-7.
247. Johnson KJ, Griswold IJ, O'Hare T, et al. A BCR-ABL mutant lacking direct binding sites for the GRB2, CBL and CRKL adapter proteins fails to induce leukemia in mice. *PLoS One* 2009;4:e7439.
248. Seo S, Ichikawa M, Kurokawa M. Structure and function of cas-L and integrin-mediated signaling. *Crit Rev Immunol* 2006;26:391-406.
249. Defilippi P, Di Stefano P, Cabodi S. p130Cas: a versatile scaffold in signaling networks. *Trends Cell Biol* 2006;16:257-63.
250. Singh MK, Dadke D, Nicolas E, et al. A novel Cas family member, HEPL, regulates FAK and cell spreading. *Mol Biol Cell* 2008;19:1627-36.
251. Gruss OJ, Vernos I. The mechanism of spindle assembly: functions of Ran and its target TPX2. *J Cell Biol* 2004;166:949-55.
252. Harada T, Chelala C, Bhakta V, et al. Genome-wide DNA copy number analysis in pancreatic cancer using high-density single nucleotide polymorphism arrays. *Oncogene* 2008;27:1951-60.
253. Tonon G, Wong KK, Maulik G, et al. High-resolution genomic profiles of human lung cancer. *Proc Natl Acad Sci U S A* 2005;102:9625-30.
254. Warner SL, Stephens BJ, Nwokenkwo S, et al. Validation of TPX2 as a potential therapeutic target in pancreatic cancer cells. *Clin Cancer Res* 2009;15:6519-28.
255. van de Weerd BC, Medema RH. Polo-like kinases: a team in control of the division. *Cell Cycle* 2006;5:853-64.
256. Fabbro M, Zhou BB, Takahashi M, et al. Cdk1/Erk2- and Plk1-dependent phosphorylation of a centrosome protein, Cep55, is required for its recruitment to midbody and cytokinesis. *Dev Cell* 2005;9:477-88.
257. Guarguaglini G, Duncan PI, Stierhof YD, Holmstrom T, Duensing S, Nigg EA. The forkhead-associated domain protein Cep170 interacts with Polo-like kinase 1 and serves as a marker for mature centrioles. *Mol Biol Cell* 2005;16:1095-107.
258. Hames RS, Crookes RE, Straatman KR, et al. Dynamic recruitment of Nek2 kinase to the centrosome involves microtubules, PCM-1, and localized proteasomal degradation. *Mol Biol Cell* 2005;16:1711-24.

259. Yan X, Li F, Liang Y, et al. Human Nudel and NudE as regulators of cytoplasmic dynein in poleward protein transport along the mitotic spindle. *Mol Cell Biol* 2003;23:1239-50.
260. Howell BJ, Moree B, Farrar EM, Stewart S, Fang G, Salmon ED. Spindle checkpoint protein dynamics at kinetochores in living cells. *Curr Biol* 2004;14:953-64.
261. Vergnolle MA, Taylor SS. Cenp-F links kinetochores to Ndel1/Nde1/Lis1/dynein microtubule motor complexes. *Curr Biol* 2007;17:1173-9.
262. Salina D, Enarson P, Rattner JB, Burke B. Nup358 integrates nuclear envelope breakdown with kinetochore assembly. *J Cell Biol* 2003;162:991-1001.
263. Platani M, Santarella-Mellwig R, Posch M, Walczak R, Swedlow JR, Mattaj IW. The Nup107-160 nucleoporin complex promotes mitotic events via control of the localization state of the chromosome passenger complex. *Mol Biol Cell* 2009;20:5260-75.
264. Ruchaud S, Carmena M, Earnshaw WC. Chromosomal passengers: conducting cell division. *Nat Rev Mol Cell Biol* 2007;8:798-812.
265. Mishra RK, Chakraborty P, Arnaoutov A, Fontoura BM, Dasso M. The Nup107-160 complex and gamma-TuRC regulate microtubule polymerization at kinetochores. *Nat Cell Biol* 2010;12:164-9.
266. Schwartz D, Gygi SP. An iterative statistical approach to the identification of protein phosphorylation motifs from large-scale data sets. *Nat Biotechnol* 2005;23:1391-8.
267. Neduva V, Linding R, Su-Angrand I, et al. Systematic discovery of new recognition peptides mediating protein interaction networks. *PLoS Biol* 2005;3:e405.
268. Holt LJ, Tuch BB, Villen J, Johnson AD, Gygi SP, Morgan DO. Global analysis of Cdk1 substrate phosphorylation sites provides insights into evolution. *Science* 2009;325:1682-6.

VIII. Appendix

Abbreviations

Å	Ångström
ATP	Adenosintriphosphate
BSA	Bovine serum albumin
°C	Degree celsius
DMEM	Dulbecco's modified eagle medium
DMF	Dimethylformamide
DMSO	Dimethylsulfoxide
DTT	Dithiothreitol
ECL	Enhanced chemiluminescence
EDTA	Ethylenediaminetetraacetate
EGF	Epidermal growth factor
EGFR	Epidermal growth factor receptor
EGTA	Ethylene glycol-bis(2-aminoethyl)-N,N,N',N'-tetraacetic acid
EtOH	Ethanol
FCS	Fetal calf serum
FDR	False discovery rate
Grb2	Growth factor receptor-bound protein 2
H	Hour
HEPES	N-(2-Hydroxyethyl)-piperazin-N'-2-Ethansulfonic acid
IAA	Iodoacetamide
IMAC	Immobilized metal affinity chromatography
IP	Immunoprecipitation
IPI	International Protein Index
KCl	Potassium chloride
kDa	Kilodalton
μ	Micro
l	Liter
LC	Liquid chromatography
m	Milli
M	Molar
min	Minute
MS	Mass spectrometry
MS ²	tandem MS or MS/MS
NaCl	Sodium chloride
PAGE	Polyacrylamide gel electrophoresis
PBS	Phosphate-buffered saline
PDGFR	Platelet-derived growth factor receptor
PMSF	Phenylmethanesulfonyl fluoride
PKCδ	Protein kinase C δ
pSer	Phosphoserine

pThr	Phosphothreonine
pTyr	Phosphotyrosine
RSC	Ratio of similarity coefficient
rpm	Rotations per minute
RT	Room temperature
SCX	Strong cation exchange (SCX) chromatography
SDS	Sodium dodecyl sulfate
SH2	Src homology domain 2
siRNA	Short interfering RNA
SILAC	Stable isotope labeling by amino acids in cell culture
Src	Homologue to v-src (sarcoma viral oncogene)
STAGEtips	STopAndGoExtraction tips
TiO ₂	Titanium dioxide
Tris	Tris(hydroxymethyl)aminomethan
o.n.	Overnight
V	Volt
vol/vol	volume/volume
Vol	Volume
WT	Wild type
wt/wt	weight/weight

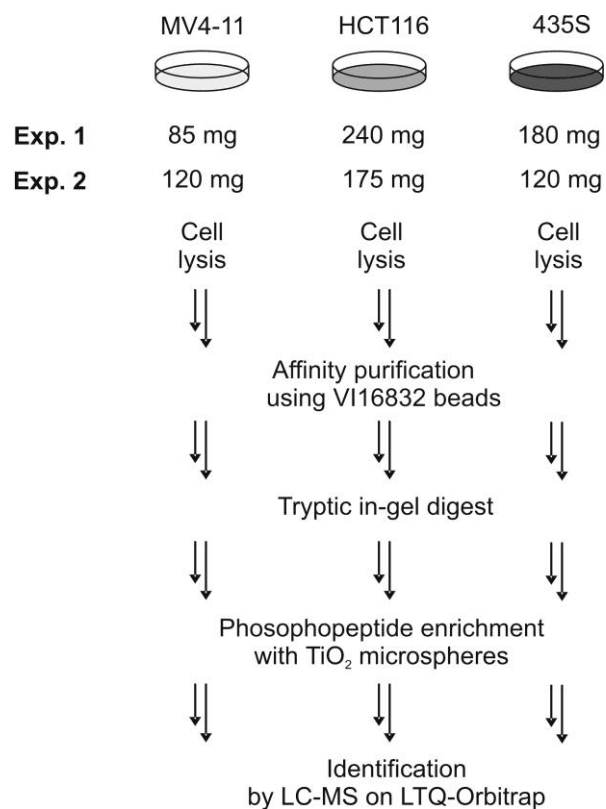


Figure A. 1: Schematic workflow for the phosphoproteomics analysis of three cancer cell lines. Experiments with the cancer cell lines MV4-11 (leukemia), HCT-116 (colon carcinoma) and 435S (melanoma-derived cells) were analyzed in two replicates. Phosphopeptides were enriched by means of titanium dioxide (TiO₂) prior to MS-based identification of VI16832-interacting sub-proteomes.

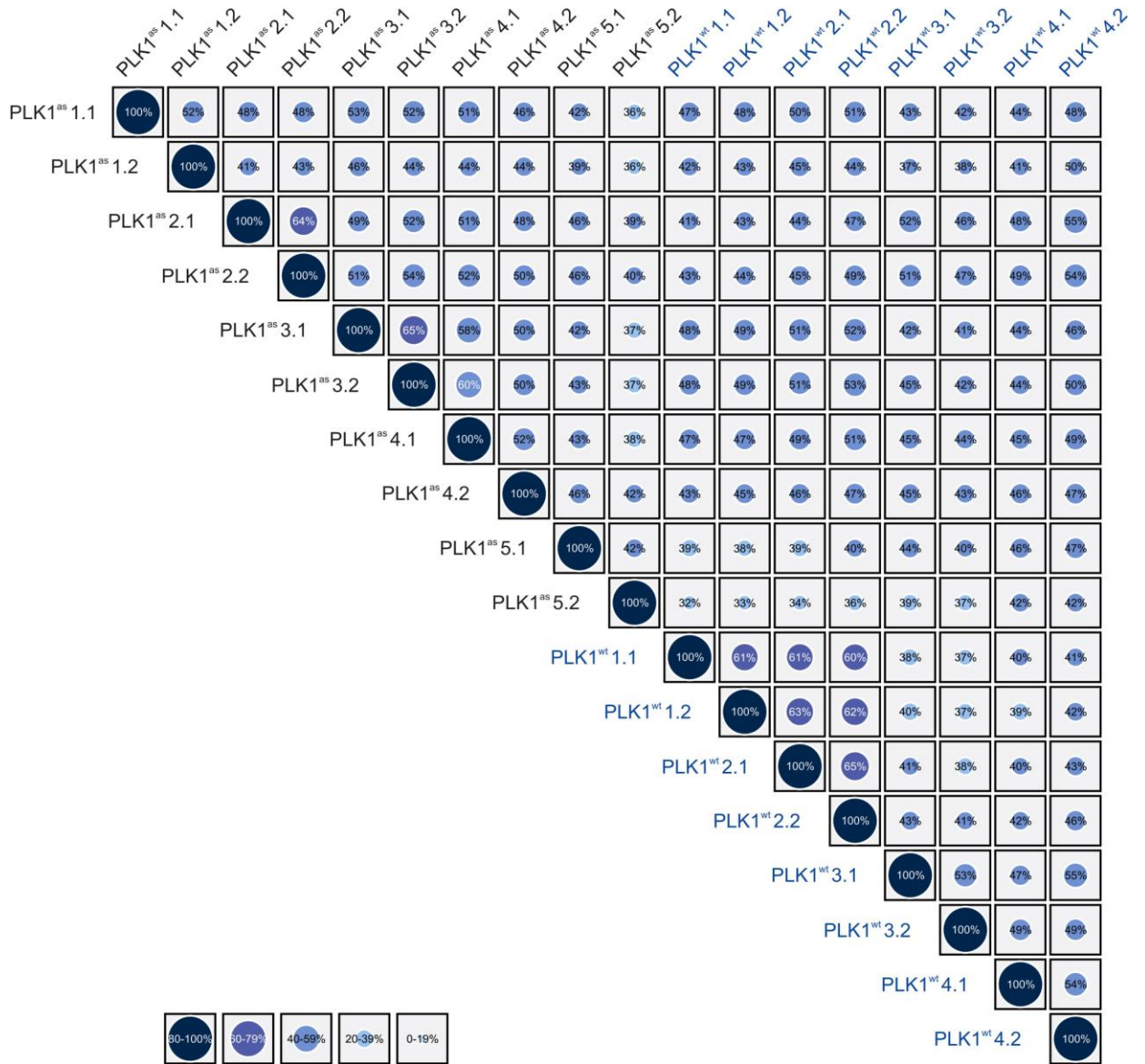


Figure A. 2: The phosphopeptides quantified in eighteen different technical replicates of the nine biological experiments were compared in ‘one versus all’ comparisons as the overlap between all datasets in relation to the smaller one.

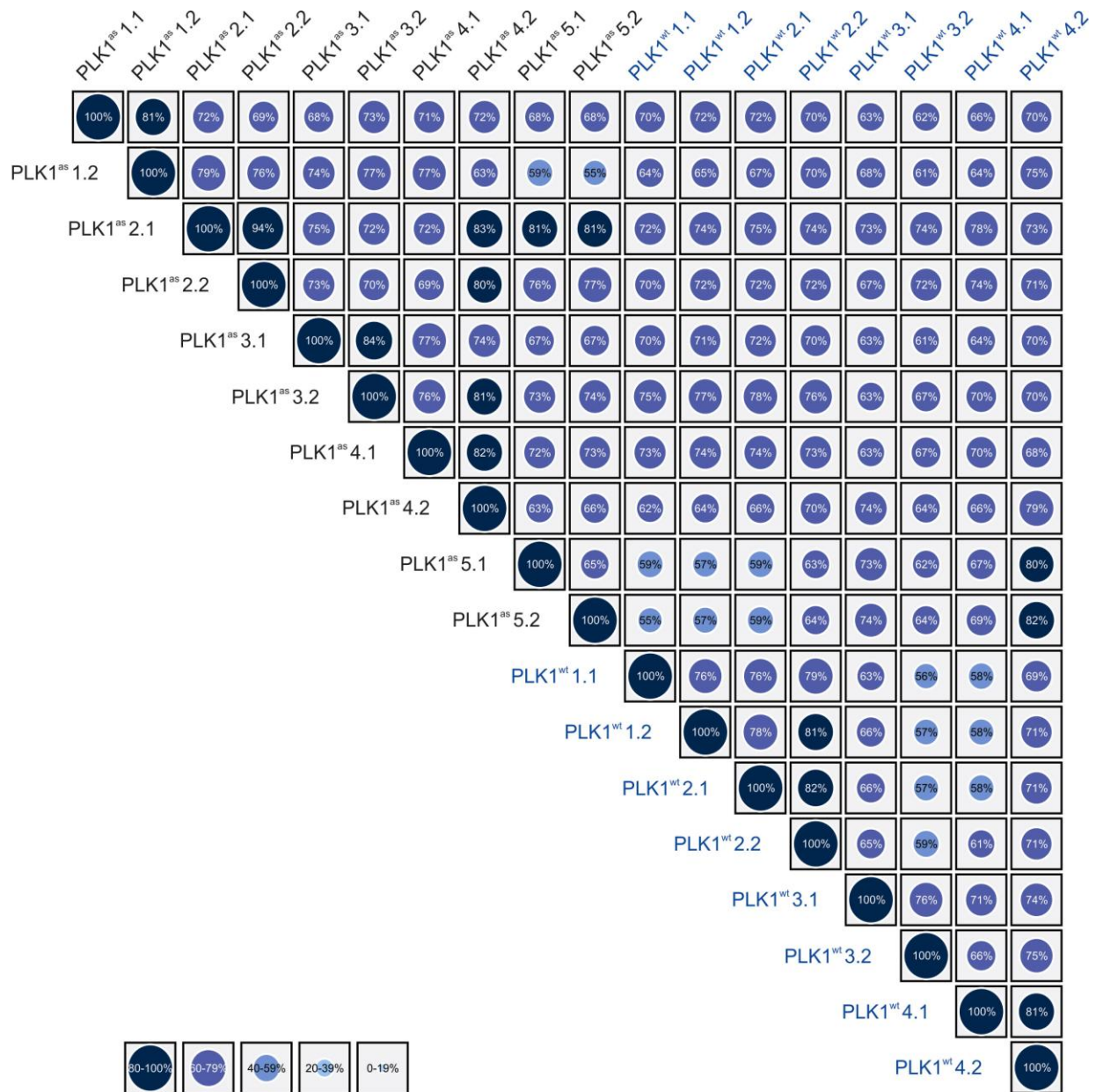


Figure A. 3: The phosphopeptides quantified in eighteen different technical replicates of the nine biological experiments were compared in ‘one versus all’ comparisons for the Jaccard similarity coefficient showing the overlap of two datasets in relation to their union, as described in the online methods.

Table A. 1 Overview of the three different projects performed to identify cellular target proteins of imatinib in K562 cells and imatinib-sensitive phosphorylation sites.

Experiment	SILA-labeling		Biological replicates	Volume per label	Total protein (mg) employed for enrichment
6-resin, multicolumn (chapter 5.2.1)	Arg0/Lys0, Arg6/Lys4, Arg10/Lys8 (cultured in P15 dishes)		no	400 ml	105
5-resin, batch-wise (chapter 5.2.2)	Arg0/Lys0, Arg6/Lys4, Arg10/Lys8 (cultured in P15 dishes, then spinner flasks)		yes	500 ml	165
anti-pTyr-IP (chapter 5.2.3)	Arg0/Lys0, Arg10/Lys8 (cultured in P15 dishes)		yes	100 ml	20

Experiment	Arg0/Lys0	Arg6/Lys4	Arg6/Lys4	MS-samples
6-resin, multicolumn (chapter 5.2.1)	DMSO, 16h	10 μ M imatinib, 90min	10 μ M imatinib, 16h	50%, in-solution digest, SCX, 7xTiO2 50%, in-gel digest, 6x TiO2, 6xST
5-resin, batch-wise (chapter 5.2.2)	DMSO, 90min	1 μ M imatinib, 90min	10 μ M imatinib, 16h	25%, in-solution digest, SCX, 7xTiO2 75%, in-gel digest, 8x TiO2, 16xST
anti-pTyr-IP (chapter 5.2.3)	DMSO, 90min	n.a.	10 μ M imatinib, 16h	100%, in-solution digste, 1xTiO2, 1xST

Table A. 2: Proteins comprising imatinib-sensitive phosphorylation sites. The shown phosphopeptide ratios reflect the averaged ratio from both biological replicate experiments that were normalized for the respective quantified protein ratio.

Accession	Protein Names	Phosphosite	Modified Sequence	Ratio 1 μ M/DMSO (Normalized by Protein)	Ratio 10 μ M/DMSO (Normalized by Protein)
IPI00029132	Tyrosine-protein kinase BTK	S553	YVLDDDEYTS(ph)SVGSKFPVR	0.67	0.38
IPI00029132	Tyrosine-protein kinase BTK	Y551	YVLDDDEY(ph)TSSVGSK	0.63	0.34
IPI00025830	Wee1-like protein kinase	T190	LFDTPTH(ph)PK	1.83	2.71
IPI00021248	Polo-like kinase 1	T210	KKT(ph)LCGTPNYIAPEVLSK	2.93	3.70
IPI00413961	Focal adhesion kinase 1	Y883	GSIDREDGSLQGPIGNQHIY(ph)QPVGKPDPAAPPK	0.52	0.25
IPI00289342	Ephrin type-B receptor 4	Y774	FLEENSSDPTY(ph)TSSLGGK	0.65	0.23
IPI00289342	Ephrin type-B receptor 4	S769	FLEENS(ph)SDPTYTSSLGGK	0.51	0.17
IPI00018597	Spleen tyrosine kinase	Y323	QESTVSFNPHY(ph)EPELAPWAADK	0.92	0.45
IPI00018597	Spleen tyrosine kinase	Y348	EALPMDTEVY(ph)ESPY(ph)ADPEEIRPK	0.68	0.18
IPI00018597	Spleen tyrosine kinase	Y352	EALPMDTEVYESPY(ph)ADPEEIRPK	0.93	0.29
IPI00384765	Myt1 kinase	S469	DALDLS(ph)DINSEPPR	3.80	3.52

Table A. 3: Overview of all performed experiments in the Plk1 project.

Experiment	SILAC labeling	Experimental condition (Arg0/Lys0)	Experimental condition (Arg10/Lys8)	Protein (mg) employed in SCX	No. of LC-MS/MS runs
as 1	normal	3-MB-PP1 wash-out negative	3-MB-PP1 wash-out positive	~ 5	24
as 2	inverted	3-MB-PP1 wash-out positive	3-MB-PP1 wash-out negative	~ 5	24
as 3	normal	3-MB-PP1 wash-out negative	3-MB-PP1 wash-out positive	~ 5	24
as 4	inverted	3-MB-PP1 wash-out positive	3-MB-PP1 wash-out negative	~ 8	24
as 5	normal	3-MB-PP1 wash-out negative	3-MB-PP1 wash-out positive	~ 8	24
wt 1	normal	3-MB-PP1 wash-out negative	3-MB-PP1 wash-out positive	~ 8	24
wt 2	inverted	3-MB-PP1 wash-out positive	3-MB-PP1 wash-out negative	~ 8	24
wt 3	normal	3-MB-PP1 wash-out negative	3-MB-PP1 wash-out positive	~ 8	24
wt 4	inverted	3-MB-PP1 wash-out positive	3-MB-PP1 wash-out negative	~ 8	24

Table A. 4: Mutational comparison of individual biological experiments in respect to the ratio of similarity coefficient (RSC). Total number of quantified and regulated phosphopeptides detected in all possible combinations of one *PLK1^{as}* (except experiment as5) and one *PLK1^{wt}* experiments as a function of the RSC.

	PLK1 ^{as} and PLK1 ^{wt} not regulated	PLK1 ^{as} regulated, PLK1 ^{wt} not regulated	PLK1 ^{as} not regulated, PLK1 ^{wt} regulated	PLK1 ^{as} and PLK1 ^{wt} regulated
as 1 vs wt 1	7785	280	44	14
as 2 vs wt 1	8216	362	45	12
as 3 vs wt 1	8378	294	54	10
as 4 vs wt 1	8128	284	47	8
as 1 vs wt 2	8134	312	37	12
as 2 vs wt 2	8721	399	39	10
as 3 vs wt 2	8872	324	53	11
as 4 vs wt 2	8552	312	44	9
as 1 vs wt 3	8194	387	49	10
as 2 vs wt 3	10192	583	54	25
as 3 vs wt 3	8921	355	57	9
as 4 vs wt 3	9049	375	56	9
as 1 vs wt 4	8635	388	51	10
as 2 vs wt 4	10507	613	43	16
as 3 vs wt 4	9335	375	55	11
as 4 vs wt 4	9364	378	54	10
Average	8811	376	49	12

Table A. 5: Mutational two-paired comparison of biological experiments in respect to the ratio of similarity coefficient (RSC) Total number of quantified and regulated phosphopeptides detected in all possible combinations of two *PLK1^{as}* (except experiment as5) and two *PLK1^{wt}* experiments as a function of the RSC.

Regulation of ratios	Combined experiments	Ratio similarity coefficient										
		0.1	0.15	0.2	0.25	0.3	0.35	0.4	0.45	0.5	0.55	0.6
PLK1 ^{as} and PLK1 ^{wt} not regulated	as 1 & 2 vs wt 1 & 2	3489	4957	5708	6015	6187	6267	6303	6327	6344	6356	6367
	as 3 & 4 vs wt 1 & 2	4557	5891	6398	6607	6711	6775	6805	6831	6845	6859	6868
	as 2 & 3 vs wt 1 & 2	4023	5585	6257	6515	6646	6721	6750	6780	6803	6814	6825
	as 1 & 4 vs wt 1 & 2	3956	5262	5860	6097	6220	6283	6302	6320	6336	6347	6358
	as 1 & 2 vs wt 3 & 4	3677	5267	6134	6521	6687	6777	6817	6851	6868	6886	6893
	as 3 & 4 vs wt 3 & 4	4407	5933	6597	6869	6980	7048	7095	7122	7137	7154	7164
	as 2 & 3 vs wt 3 & 4	4159	5891	6716	7059	7193	7282	7324	7368	7389	7401	7409
	as 1 & 4 vs wt 3 & 4	3834	5282	5981	6275	6392	6472	6504	6528	6549	6565	6576
	as 1 & 2 vs wt 2 & 3	3448	4816	5543	5850	5999	6074	6105	6130	6142	6154	6162
	as 3 & 4 vs wt 2 & 3	4307	5590	6087	6284	6380	6429	6461	6485	6498	6508	6516
	as 2 & 3 vs wt 2 & 3	3924	5403	6048	6318	6438	6501	6532	6559	6573	6580	6586
	as 1 & 4 vs wt 2 & 3	3778	4997	5570	5811	5919	5977	5996	6016	6033	6043	6053
	as 1 & 2 vs wt 1 & 4	3266	4671	5428	5739	5890	5958	5989	6011	6024	6037	6044
	as 3 & 4 vs wt 1 & 4	4137	5450	5970	6184	6272	6325	6353	6375	6389	6403	6408
	as 2 & 3 vs wt 1 & 4	3729	5249	5917	6182	6299	6363	6389	6418	6438	6450	6458
	as 1 & 4 vs wt 1 & 4	3626	4911	5507	5744	5844	5895	5914	5933	5948	5962	5970
	Average		3895	5322	5983	6254	6379	6447	6477	6503	6520	6532
PLK1 ^{as} regulated, PLK1 ^{wt} not regulated	as 1 & 2 vs wt 1 & 2	85	115	142	161	167	171	173	178	180	186	189
	as 3 & 4 vs wt 1 & 2	53	89	116	131	149	164	170	174	180	183	185
	as 2 & 3 vs wt 1 & 2	93	139	164	174	184	187	192	196	199	203	205
	as 1 & 4 vs wt 1 & 2	47	72	101	110	126	141	143	154	158	160	163
	as 1 & 2 vs wt 3 & 4	91	149	188	219	227	235	240	247	254	261	265
	as 3 & 4 vs wt 3 & 4	48	99	141	170	187	205	212	216	222	227	231
	as 2 & 3 vs wt 3 & 4	82	157	207	223	234	239	247	249	252	258	261
	as 1 & 4 vs wt 3 & 4	41	85	123	141	163	177	186	200	206	209	214
	as 1 & 2 vs wt 2 & 3	74	118	151	174	178	187	191	196	199	205	209
	as 3 & 4 vs wt 2 & 3	46	92	122	145	159	175	181	183	189	191	194
	as 2 & 3 vs wt 2 & 3	77	139	170	184	193	198	203	207	209	213	216
	as 1 & 4 vs wt 2 & 3	39	72	102	116	133	148	152	165	171	173	177
	as 1 & 2 vs wt 1 & 4	83	112	143	162	165	169	171	176	179	185	187
	as 3 & 4 vs wt 1 & 4	48	83	114	131	145	161	168	173	178	180	183
	as 2 & 3 vs wt 1 & 4	80	134	166	176	184	186	192	193	196	200	202
	as 1 & 4 vs wt 1 & 4	42	72	105	114	129	142	145	156	159	162	165
	Average		64.3	107.9	140.9	158.2	170.2	180.3	185.4	191.4	195.7	199.8
PLK1 ^{as} not regulated, PLK1 ^{wt} regulated	as 1 & 2 vs wt 1 & 2	1	1	1	1	1	1	1	1	1	1	1
	as 3 & 4 vs wt 1 & 2	0	0	0	0	0	0	0	0	0	0	0
	as 2 & 3 vs wt 1 & 2	0	0	0	0	0	0	0	0	0	0	0
	as 1 & 4 vs wt 1 & 2	0	0	0	0	1	1	1	1	1	1	1
	as 1 & 2 vs wt 3 & 4	0	0	0	0	0	0	0	0	0	0	2
	as 3 & 4 vs wt 3 & 4	0	0	0	0	0	0	0	0	0	0	1
	as 2 & 3 vs wt 3 & 4	0	0	0	0	0	0	0	0	0	0	2
	as 1 & 4 vs wt 3 & 4	0	0	0	0	0	0	0	0	0	0	1
	as 1 & 2 vs wt 2 & 3	1	1	1	1	1	1	1	1	1	1	2
	as 3 & 4 vs wt 2 & 3	0	0	0	0	0	0	0	0	0	0	1
	as 2 & 3 vs wt 2 & 3	1	1	1	1	1	1	1	1	1	1	2
	as 1 & 4 vs wt 2 & 3	0	0	0	0	0	0	0	0	0	0	1
	as 1 & 2 vs wt 1 & 4	0	0	0	0	0	0	0	0	0	0	1
	as 3 & 4 vs wt 1 & 4	0	0	0	0	0	0	0	0	1	1	2
	as 2 & 3 vs wt 1 & 4	0	0	0	0	0	0	0	0	1	1	2
	as 1 & 4 vs wt 1 & 4	0	0	0	0	0	0	0	0	0	0	1
	Average		0.188	0.188	0.188	0.188	0.250	0.250	0.250	0.250	0.375	0.375

Regulation of ratios	Combined experiments	Ratio similarity coefficient										
		0.1	0.15	0.2	0.25	0.3	0.35	0.4	0.45	0.5	0.55	0.6
PLK1 tm and PLK1 ^{fl} regulated	as 1 & 2 vs wt 1 & 2	0	0	0	0	1	1	1	1	1	1	1
	as 3 & 4 vs wt 1 & 2	0	0	0	0	0	0	0	0	0	0	0
	as 2 & 3 vs wt 1 & 2	0	0	0	0	0	0	0	0	0	0	0
	as 1 & 4 vs wt 1 & 2	0	0	0	0	0	0	1	1	1	1	1
	as 1 & 2 vs wt 3 & 4	1	1	1	1	1	1	1	1	1	1	1
	as 3 & 4 vs wt 3 & 4	0	0	0	0	0	0	0	0	0	0	0
	as 2 & 3 vs wt 3 & 4	0	0	0	0	0	0	0	0	0	0	0
	as 1 & 4 vs wt 3 & 4	0	0	0	0	0	0	1	1	1	1	1
	as 1 & 2 vs wt 2 & 3	0	0	1	1	1	1	1	1	1	1	1
	as 3 & 4 vs wt 2 & 3	0	1	1	1	1	1	1	1	1	1	1
	as 2 & 3 vs wt 2 & 3	0	0	0	0	0	0	0	0	0	0	0
	as 1 & 4 vs wt 2 & 3	0	1	1	1	1	1	2	2	2	2	2
	as 1 & 2 vs wt 1 & 4	1	1	1	1	1	1	1	1	1	1	1
	as 3 & 4 vs wt 1 & 4	0	0	0	0	0	0	0	0	0	0	0
	as 2 & 3 vs wt 1 & 4	0	0	0	0	0	0	0	0	0	0	0
	as 1 & 4 vs wt 1 & 4	0	0	0	0	0	0	1	1	1	1	1
	Average	0.125	0.250	0.313	0.313	0.375	0.375	0.625	0.625	0.625	0.625	0.625

Table A. 6: Plk1 cellular substrates revealed by the ratio of similarity coefficient (RSC) analysis.

Accession	Protein Name	Gene Name	Substrate reported in literature	Phosphorylation sites	Regulation of
IPI00550377	Acyl-CoA-binding domain-containing protein 5	ACBD5			up
IPI00004408	Gamma-adducin	ADD3		S618	up
IPI00876984	Uncharacterized protein AHCTF1P	AHCTF1P		S1118,S1321,T1407,S1571,T2125,S2127	up
IPI00021812	Neuroblast differentiation-associated protein AHNAK	AHNAK		S508,S511,S658,S793,S1286,S1298,S174 S2138,S3054,S3112,S4150,S4220,S4360 S4540,S4614,S4684,S4803,S4812,S5110 S5125,S5332	up
IPI00856045	Protein AHNAK2	AHNAK2		S4419,S4425	up
IPI00237884	A-kinase anchor protein 12	AKAP12		S1251	up
IPI00320664	A-kinase anchor protein 2	AKAP2		S696,T698,S704	up
IPI00033907	Anaphase-promoting complex subunit 1	ANAPC1	Kraft et al., 2003	T291,S313,S317,S355,S377,S686,S688	up & down
IPI00292914	Ankyrin repeat and IBR domain-containing protein 1	ANKIB1		S441	up
IPI00829741	Ankyrin repeat and LEM domain-containing protein 2	ANKLE2		S647	up
IPI00002286	Ankyrin repeat domain-containing protein 11	ANKRD11		S1583	up
IPI00784020	Ankyrin repeat domain-containing protein 17	ANKRD17		S1457	up
IPI00477505	Ankyrin repeat domain-containing protein 28	ANKRD28		S1044	up
IPI00444646	Uncharacterized protein AP1GBP1	AP1GBP1		S607,S854,S886,S890,S1070	up
IPI00013184	N-terminal acetyltransferase complex ARD1 subunit homolog A	ARD1A		S213,S216	up
IPI00299263	ADP-ribosylation factor GTPase-activating protein 3	ARFGAP3		S367,S370	up
IPI00020567	Rho GTPase-activating protein 1	ARHGAP1		S257	up
IPI00166301	Rho GTPase-activating protein 24	ARHGAP24		S415	up
IPI00646885	Rho GTPase-activating protein 5	ARHGAP5		S968,S1115	up & down
IPI00794402	Rho GDP-dissociation inhibitor 1	ARHGDIA		S24	up
IPI00296069	AT-rich interactive domain-containing protein 4A	ARID4A		S427	up
IPI00167074	ADP-ribosylation factor-like protein 6-interacting protein 6	ARL6IP6		S2,S10	up
IPI00292168	Histone chaperone ASF1A	ASF1A		S165	up
IPI00743813	Abnormal spindle-like microcephaly-associated protein	ASPM		S283,S367,S370	up
IPI00845355	Transcriptional regulator ATRX	ATRX		S1253	up
IPI00298940	Serine/threonine-protein kinase 6	AURKA			up
IPI00298883	5-azacytidine-induced protein 1	AZ1		S146,S150	up
IPI00011635	Bcl-2-like 13 protein	BCL2L13		S302,S303,S305,S420	up
IPI00006079	Bcl-2-associated transcription factor 1	BCLAF1		S198	up
IPI00004859	Bloom syndrome protein	BLM		S419,S422	up & down
IPI00218982	Breast cancer type 1 susceptibility protein	BRCA1		S1164	up
IPI00333014	Uncharacterized protein C13orf3	C13orf3			up
IPI00104907	Uncharacterized potential DNA-binding protein C14orf106	C14orf106		S172,S1104	up
IPI00029473	Protein Njmu-R1	C17orf75			up
IPI000791060	Uncharacterized protein C19orf62	C19orf62		S66	up
IPI00018786	WD repeat-containing protein C2orf44	C2orf44		S299	up
IPI00152082	Putative uncharacterized protein C7orf47	C7orf47		S45,S47,S52	up
IPI00395444	Calmodulin-regulated spectrin-associated protein 1	CAMSAP1		S1204	up
IPI00409607	Calmodulin-regulated spectrin-associated protein 1-like protein 1	CAMSAP1L1		S598,S599,S901	up
IPI00871979	Coiled-coil domain-containing protein 50	CCDC50		S137	up
IPI00302925	T-complex protein 1 subunit theta	CCT8		S271	up
IPI00005822	Cell division cycle protein 23 variant	CDC23		S588,T596	up
IPI00640320	M-phase inducer phosphatase 3 isoform 4	CDC25C	Toyoshima-Morimoto et al., 2002; Schmidt et al., 2006; Bonnet et al., 2008; Ikezoe et al., 2009		up & down
IPI00794278	Cell division cycle protein 27 homolog	CDC27	Kraft et al., 2003	T389,S390,S392,S393,S432,S441,T452	up
IPI00015894	Cdc42 effector protein 4	CDC42EP4		S344	up
IPI00014197	Protein CDV3 homolog	CDV3		S216	up
IPI00296365	Centromeric protein E	CENPE		S611	up
IPI00855998	Centromere protein F	CENPF		S275,S276,S773,S1747	up
IPI00186194	Centrosomal protein of 170 kDa	CEP170	Guarguaglini et al., 2005	S862,S879,S881,S887	up
IPI00456708	Centrosomal protein of 192 kDa	CEP192		S1502	up
IPI00103595	Centrosome-associated protein 350	CEP350		S2362	up
IPI00101532	Centrosomal protein of 55 kDa	CEP55	Fabbro et al., 2005	S425,S428,S436	up
IPI00383439	Centrosomal protein of 97 kDa	CEP97		S308,S314,S752	up
IPI00220289	Chromodomain-helicase-DNA-binding protein 6	CHD6			up
IPI00719073	Chromodomain-helicase-DNA-binding protein 8	CHD8		S1544	up
IPI00025974	Charged multivesicular body protein 4b	CHMP4B		S184	up
IPI00071824	Cytoskeleton-associated protein 2	CKAP2		S534	up
IPI00871686	CLIP-associating protein 2	CLASP2		S1186,S1189	up
IPI00006442	Coilin	COIL		S301,T303,S305	up
IPI00027996	Coronin-7	CORO7		S915	up
IPI00375652	Cytoplasmic polyadenylation element-binding protein 4	CPEB4			up
IPI00470891	Cold shock domain-containing protein E1	CSE1		T761	up
IPI00183400	Casein kinase I isoform alpha	CSNK1A1		T321	up
IPI00011102	Casein kinase I isoform delta	CSNK1D		S382	up
IPI00219868	Catenin delta-1	CTNND1		S4	up
IPI00029601	Src substrate cortactin	CTTN		S432	up
IPI00179438	Disabled homolog 2	DAB2			up
IPI00005904	Probable ATP-dependent RNA helicase DDX20	DDX20		S672	up
IPI00293078	Probable ATP-dependent RNA helicase DDX27	DDX27		S79	up
IPI00871695	Protein DEK	DEK		T62,S100	up
IPI00552796	Putative uncharacterized protein DKFZp564P1772	DKFZp564P1772			up

IPI00218729	Disks large homolog 1	DLG1		S571	up
IPI00290410	Deoxyribonucleotidyltransferase terminal-interacting protein 2	DNNTIP2		S330,S429,S434	up
IPI00016580	Kinetochore-associated protein DSN1 homolog	DSN1		S28,S30	up
IPI00642259	Dystonin	DST		S2551,S2919,S2933	up
IPI00787864	Protein ECT2	ECT2	Niyya et al., 2006	S38,Y41	up
IPI00018274	Epidermal growth factor receptor	EGFR		S1064,S1081	up
IPI00178187	EH domain-binding protein 1	EHPB1		S578	up
IPI00002569	Eukaryotic translation initiation factor 4E-binding protein 1	EIF4EBP1		S112	up
IPI00299254	Eukaryotic translation initiation factor 5B	EIF5B		S214	up
IPI00010105	Eukaryotic translation initiation factor 6	EIF6		S235,S239,S243,T245	up
IPI00292134	Epidermal growth factor receptor substrate 15	EPS15		S467,S470,S485	up
IPI00871411	Epidermal growth factor receptor substrate 15-like 1	EPS15L1		S708	up
IPI00438286	Protein LAP2	ERBB2IP		S715	up
IPI00552569	DNA excision repair protein ERCC-6-like	ERCC6L	Baumann et al., 2007	S790,S807,S810,T813,S1004	up
IPI00011919	Protein FADD	FADD		S190,S194	up
IPI00719210	Protein FAM29A	FAM29A		S943	up
IPI00017979	Protein FAM54A	FAM54A			up
IPI00071826	Protein FAM54B	FAM54B		S255,S261	up
IPI00827920	Extended synaptotagmin-2	FAM62B		S739,S743	up
IPI00290571	F-box only protein 30	FBXO30		S213	up
IPI00383500	Fermitin family homolog 2	FERMT2		S673	up
IPI00297578	Filamin A-interacting protein 1-like	FILIP1L		S953,T955	up
IPI00217686	Putative rRNA methyltransferase 3	FTSJ3		S688	up
IPI00001364	GC-rich sequence DNA-binding factor homolog	GCFC		S154,S155	up
IPI00795611	G protein-coupled receptor kinase interactor 1 variant	GIT1		S371,T373	down
IPI00743931	Golgi reassembly-stacking protein 2	GORASP2		S409,T415	up
IPI00397836	Serine/threonine-protein kinase haspin	GSG2		S287,S288,T289	up
IPI00293242	General transcription factor II-I	GTF2I			up
IPI00016861	General transcription factor 3C polypeptide 2	GTF3C2		S143	up
IPI00219037	Histone H2A.x	H2AFX			down
IPI00014938	Nuclear protein Hcc-1	HCC1			up
IPI00217442	Multiple ankyrin repeats single KH domain protein isoform 2	hCG_2045902			up
IPI00479069	HEAT repeat-containing protein 5B	HEATR5B			up
IPI00217560	Protein HIRA	HIRA		T555	up & down
IPI00179700	High mobility group protein HMG-I/HMG-Y	HMGGA1		S36,S44,T53	down
IPI00011274	Heterogeneous nuclear ribonucleoprotein D-like	HNRPDL		S127	up
IPI00031768	Protein Hook homolog 3	HOOK3		S238	up
IPI00642238	Heterochromatin protein 1-binding protein 3	HP1BP3		S6	up
IPI00382470	Heat shock protein HSP 90-alpha	HSP90AA1			up
IPI00456919	E3 ubiquitin-protein ligase HUWE1	HUWE1		S1368	up
IPI00024970	Inner centromere protein	INCENP		S235,T239	up
IPI00385328	Interleukin-1 receptor-associated kinase 1	IRAK1		S397	down
IPI00376199	Interferon regulatory factor 2-binding protein 2	IRF2BP2			up
IPI00014319	Influenza virus NS1A-binding protein	IVNS1ABP		S336,S338	up
IPI00384541	Uncharacterized protein KIAA0460	KIAA0460		S593,S597	up
IPI00412243	cDNA FLI75055	KIAA1609		S425	up
IPI00029422	Kinesin-like protein KIF20A	KIF20A	Neef et al., 2003	S49,S528,S532	up
IPI00178150	Chromosome-associated kinesin KIF4A	KIF4A		S1001,S1013,S1038	up & down
IPI00472303	Kinesin light chain 1	KLC1		S441	up
IPI00021634	Kinesin light chain 2	KLC2		S589	up
IPI00798034	Protein KRI1 homolog	KRI1		S628,S634,S645	up
IPI00554788	Keratin, type I cytoskeletal 18	KRT18		S405,S406	up
IPI00294742	La-related protein 7	LARP7		S254	up
IPI00000861	LIM and SH3 domain protein 1	LASP1		T68	up
IPI00032491	Inner nuclear membrane protein Man1	LEMED3		T365	down
IPI00013160	Ligatin	LGTN		S237	up
IPI00008918	LIM domain and actin-binding protein 1	LIMA1		S686,S692,S709,S741	up
IPI00177498	LIM and calponin homology domains-containing protein 1	LIMCH1		S362,S369	up
IPI00217975	Lamin-B1	LMNB1		S210	up
IPI00028369	Protein lunapark	LNP		S321	up
IPI00871815	Leucyl-cystinyl aminopeptidase	LNPEP		S147	up
IPI00396321	Leucine-rich repeat-containing protein 59	LRRCS9		S23	up
IPI00785113	Leucine-rich repeat flightless-interacting protein 1	LRRFIP1			up
IPI00007277	Leucine-rich repeat flightless-interacting protein 2	LRRFIP2		T317,S320	down
IPI00296830	Leucine zipper protein 1	LUZP1		T679,S956	up & down
IPI00006108	Mastermind-like protein 1	MAML1		S261	up
IPI00008868	Microtubule-associated protein 1B	MAP1B		S828,S831,S832,S1276,T1282,S1396 S1400,S1415,S1438,S1443,S1915,S1917 T1932,S1939,T1949,S1988,S2016,S2024	up
IPI00871726	Microtubule-associated protein 4	MAP4		S693	up
IPI00167009	MAP7 domain-containing protein 1	MAP7D1			up
IPI00847637	MAP7 domain-containing protein 3	MAP7D3		S457,S461	up
IPI00641181	MARCKS-related protein	MARCKSL1		S104	up
IPI00074258	Microtubule-associated serine/threonine-protein kinase-like	MASTL		S512	up
IPI00020719	Mitochondrial antiviral-signaling protein	MAVS	Vitour et al., 2009	S152,S165,S253,S258	up & down
IPI00002374	Microcephalin	MCPH1		S548	up
IPI00033036	Methionine aminopeptidase 2	METAP2		S74	up
IPI00004233	Antigen Ki-67	MKI67		T1111,S1118,T1120,T1323,T2406	up
IPI00002828	Centromere protein U	MLF1IP	Kang et al., 2006		up
IPI00015980	Multiple PDZ domain protein	MPDZ		S483,S488	up

IPI00827503	M-phase phosphoprotein 1	MPHOSPH1	T560,S1621	up
IPI00030408	M-phase phosphoprotein 8	MPHOSPH8	S189	up
IPI00646857	Metaxin-3	MTX3	S306,S311	up
IPI00555833	Myelin expression factor 2	MYEF2		up
IPI00019502	Myosin-9	MYH9	T1151	up
IPI00017763	Nucleosome assembly protein 1-like 4	NAP1L4	S5,S7,S12	up
IPI00747787	Condensin-2 complex subunit D3	NCAPD3	S1370,S1384	down
IPI00299507	Condensin complex subunit 2	NCAPH		up
IPI00761043	Nuclear receptor coactivator 7	NCOA7		up
IPI00872673	Nuclear distribution protein nudE homolog 1	NDE1	S271,T272,T275,T278	up
IPI00791509	neural cell expressed,developmentally down-regulated gene 1	NEDD1	S411,S418,S433	up & down
IPI00217710	Nuclear factor of activated T-cells 5	NFAT5		up
IPI00845373	Nuclear factor NF-kappa-B p100 subunit	NFKB2		up
IPI00216654	Nucleolar phosphoprotein p130	NOLC1	S653	up
IPI00220740	Nucleophosmin	NPM1	S4,S10,Y17	up
IPI00375682	Nik-related protein kinase	NRK	S719	up
IPI00292771	Nuclear mitotic apparatus protein 1	NUMA1	S1789,S1800,S1830,S1834	up & down
IPI00028005	Nuclear pore complex protein Nup107	NUP107	S4,S11	up
IPI00292059	Nuclear pore complex protein Nup153	NUP153	T202,S203,S209,S240	up
IPI00337397	Nuclear pore complex protein Nup98-Nup96	NUP98	S591,S595,S606,S664	up
IPI00006197	Nuclear valosin-containing protein-like	NVL	S185,S191	down
IPI00016405	OCIA domain-containing protein 1	OCIAD1	S108,S116	up
IPI00304189	Optineurin	OPTN	S170,S171,S174,S177	up
IPI00013216	Origin recognition complex subunit 2	ORC2L	S122	up
IPI00759749	Poly(ADP-ribose) glycohydrolase	PARG		up
IPI00294744	Poly(A)-specific ribonuclease PARN	PARN	S557	up
IPI00296909	Poly [ADP-ribose] polymerase 4	PARP4	T768	up
IPI00384176	Protein polybromo-1	PBRM1	S1405	up
IPI00001654	Pericentriolar material 1 protein	PCM1	S1030	up
IPI00479143	Pericentrin	PCNT	S2044	up
IPI00329338	Choline-phosphate cytidyltransferase A	PCYT1A	S233	up
IPI00010414	PDZ and LIM domain protein 1	PDLIM1	S215	up
IPI00643342	PEA15 protein	PEA15		up
IPI00867617	PHF2 protein	PHF2	S705	up
IPI00552149	PHD finger protein 6, isoform CRA_d	PHF6	S146,S156	up
IPI00395568	PHD finger protein 6	PHF6	T134,S145,S154,S155	up
IPI00480187	PHD finger protein 8	PHF8	S722	up
IPI00291916	PH-interacting protein	PHIP	S1560	up
IPI00216184	Phosphatidylinositol-binding clathrin assembly protein	PICALM		up
IPI00032304	Plastin-1	PLS1		up
IPI00789041	Pinin	PNN	S443,S450	up
IPI00001651	Pogo transposable element with KRAB domain	POGK	S11	up
IPI00219171	POU domain, class 2, transcription factor 1	POU2F1	S347	up
IPI00183002	Protein phosphatase 1 regulatory subunit 12A	PPP1R12A	S978	up
IPI00028077	Presenilin-1	PSEN1	S366,S367	up
IPI00455510	Prothymosin alpha	PTMA	S2,T8,S9,S10	up
IPI00018914	Tyrosine-protein phosphatase non-receptor type 14	PTPN14	S620	up
IPI00290328	Receptor-type tyrosine-protein phosphatase eta	PTPRJ		up
IPI00152946	Rac GTPase-activating protein 1	RACGAP1	S154,S157,S170	up
IPI00759532	Ankycorbin	RAI14	S317,S318,S358,S419	up
IPI00414127	Ran-specific GTPase-activating protein	RANBP1	T18	up
IPI00221325	E3 SUMO-protein ligase RanBP2	RANBP2	S1447,S2270	up
IPI00166044	Regulatory-associated protein of mTOR	RAPTOR	S859,S863	up
IPI00304023	retinoblastoma binding protein 8 (RBBP8)	RBBP8	S345,S347	up & down
IPI00001134	RNA-binding protein 7	RBM7		up
IPI00455500	Rapamycin-insensitive companion of mTOR	RICTOR	S1370,S1373,T1376	up
IPI00293845	Telomere-associated protein RIF1	RIF1	S1708,S1711,S1747,T1808,T1968,S1973 T1982,S2467,S2473	up
IPI00306406	Serine/threonine-protein kinase RIO2	RIOK2	S380	up
IPI00017203	Protein RMI1 homolog	RMI1	S225	up
IPI00465370	RING finger protein 219	RNF219	S526,S561,S592	up & down
IPI00743293	Reticulon-3	RTN3	S30	up
IPI00296594	RING1 and YY1-binding protein	RYBP		up
IPI00646058	Scaffold attachment factor B	SAB-B1		up
IPI00005648	Scaffold attachment factor B2	SAFB2	S207,S288	up
IPI00787162	SAPS domain family, member 2	SAPS2	S278	up
IPI00719725	SAPS domain family member 3	SAPS3	S722	up
IPI00026969	SEC23-interacting protein	SEC23IP	S134	up
IPI00852741	Protein transport protein Sec31A	SEC31A		up
IPI00784614	Septin-9 isoform 1	SEPT9	S30,T49	up
IPI00470498	Plasminogen activator inhibitor 1 RNA-binding protein	SERBP1	S237	up
IPI00646645	Probable helicase senataxin	SETX	S842	up
IPI00746412	SFRS2-interacting protein	SFRS2IP	S588	up
IPI00168691	SHC SH2 domain-binding protein 1	SHCBP1	S5	up
IPI00029822	SMARCA4 isoform 2	SMARCA4	S1382	up
IPI00008422	SWI/SNF-related matrix-associated actin-dependent regulator of chromatin subfamily A containing DEAD/H box 1	SMARCA41	S146,S152	up
IPI00411559	Structural maintenance of chromosomes protein 4	SMC4	S1056	up
IPI00290204	U1 small nuclear ribonucleoprotein 70 kDa	SNRNP70	S410	up

IPI00011675	Nuclear autoantigen Sp-100	SP100		S171,S180	up
IPI00328118	Sperm-associated antigen 5	SPAG5		S397,S401	up
IPI00745406	C-jun-amino-terminal kinase-interacting protein 4	SPAG9		S183,S185,S194,S265,S816	up
IPI00329583	Spermatogenesis-associated protein 5	SPATA5			up
IPI00005154	FACT complex subunit SSRP1	SSRP1		S659	up
IPI00014456	Striatin	STRN		S259	up
IPI00217200	Syntaxin-binding protein 4	STXBP4		S6,S10	up
IPI00828150	Suppressor of G2 allele of SKP1 homolog	SUGT1		S331	up
IPI00018370	Supervillin	SVIL		S238,S245	up
IPI00059242	Synapse-associated protein 1	SVAP1		S313	up
IPI00247295	Nesprin-1	SYNE1		S8277,T8312	up
IPI00012441	Synaptojanin-1	SYNJ1		S830	up
IPI00018111	Transcription initiation factor TFIID subunit 7	TAF7		S200,S201,S264	up
IPI00299166	TRAF family member-associated NF-kappa-B activator	TANK		S208,T213	up
IPI00164610	TBC1 domain family member 1	TBC1D1		S556,S558,S559	up
IPI00794613	TBC1 domain family member 15	TBC1D15		S201,S205	up
IPI00290452	Transmembrane BAX inhibitor motif-containing protein 1	TMBIM1		S83	up
IPI00853149	Transmembrane protein 131	TMEM131		S1630	up
IPI00386760	Nucleoporin NDC1	TMEM48			up
IPI00010586	TATA element modulatory factor	TMF1		S214,S217,S349,S542	up
IPI00005087	Tropomodulin-3	TMOD3		S25	up
IPI00030131	Lamina-associated polypeptide 2, isoforms beta/gamma	TMPO		S378	up
IPI00304589	182 kDa tankyrase 1-binding protein	TNKS1BP1		S882	up
IPI00307545	Tensin-1	TNS1			up
IPI00478232	DNA topoisomerase 2-alpha	TOP2A	Li et al., 2008	T1280,S1283	up
IPI00644766	Torsin-1A-interacting protein 1	TOR1AIP1		S184	up
IPI00742743	Tumor suppressor p53-binding protein 1	TP53BP1		S129,S132,S385,T399,S403,S528,S530 S776,S814,S835,S836,S839,S998,T1001 S1004,S1007,S1024,S1033,S1440,S1623	up & down
IPI00306825	Tumor protein D54	TPD52L2		S19,S21,T23	up
IPI00010779	Tropomyosin alpha-4 chain	TPM4		T216	up
IPI00742682	Nucleoprotein TPR	TPR		S1185,S2048	up
IPI00008477	Targeting protein for Xklp2	TPX2	Plx1 (Xenopus laevis): Eckerdt et al., 2009	S652	up
IPI00413160	TRIO and F-actin-binding protein	TRIOBP		S2362	up
IPI00003515	Thyroid receptor-interacting protein 11	TRIP11		S486	up
IPI00028493	Tuberin	TSC2		S1346	up
IPI00218343	Tubulin alpha-1C chain	TUBA1C		S48	up
IPI00005613	Splicing factor U2AF 35 kDa subunit	U2AF1		S19	up
IPI00005018	Upstream-binding protein 1	UBP1			up
IPI00026320	E3 ubiquitin-protein ligase UBR5	UBR5			up
IPI00607554	Ubiquitin carboxyl-terminal hydrolase 47	USP47		S876	up
IPI00107113	U3 small nucleolar RNA-associated protein 14 homolog A	UTP14A		S77	up
IPI00025160	Protein VAC14 homolog	VAC14		S509	up

Acknowledgements

This study was carried out in the Cell Signaling Group of PD. Dr. Henrik Daub that is embedded in the Department of Molecular Biology (Director: Prof. Dr. Axel Ullrich) at the Max-Planck Institute of Biochemistry (Martinsried, Germany). Many people have contributed to this work and have made the last three and a half years a fun and exciting time. Therefore, I'd like to thank you all!

In particular I would like to express my gratitude to:

My mentor, PD Dr. Henrik Daub, for giving me the chance to work on exciting projects in a stimulating scientific environment, and in particular, for his excellent supervision and always having time.

Prof. Dr. Axel Ullrich, for his generous support of my projects and funding of my PhD position.

Prof. Dr. Johannes Buchner for his kindness to review my PhD thesis.

Prof. Dr. Michael Groll for being the head of my thesis committee.

Our cooperation partners Prof. Dr. Matthias Mann, Prof. Dr. Jesper V. Olsen, Dr. Jürgen Cox and Dr. Florian Gnad for help and advice in fundamental MS techniques and early access to MaxQuant, Prof. Dr. Prasad Jallepalli for providing us the RPE-Plk1^{as/wt} cell lines.

My fellow PhD students and lab mates, not only for supporting me in scientific questions but also for always encouraging me and their friendship. Thank you Andreas, Christoph, Claus, Markus, Martin, Matthias, Michaela, Nina, Phil, Philipp, Renate, Stephan, Ute, Wolfgang...

I am also grateful to my diploma student Markus Grammel, it was a pleasure to supervise your thesis!

Finally, I especially want to thank my parents and my brothers for always supporting me.

